002122
ADA031914

MOST Project

Contract Number: N - 000 24 70 C 1137
TRACOR Project Number: 002 154 01

UNDERWATER SOUND TRANSMISSION

by

H. L. Saxton

Submitted to

Naval Ship Systems Command

Department of the Navy

Washington, D. C. 20360

Attn: Code 00V1B

Submitted on

10 April 1970

DDC
NOV 11 1976
A

DISTRIBUTION STATEMENT A
Approved for public release;
Distribution Unlimited

TRACOR

1601 RESEARCH BLVD. / ROCKVILLE, MARYLAND 20850 / 301-762-7070

002122

TRACOR Project Number: 002 154 01

(1)

(6) UNDERWATER SOUND TRANSMISSION

by

(10) H. L. Saxton

(15) N0001 24-70-C-1137

Submitted to

Naval Ship Systems Command

Department of the Navy

Washington, D. C. 20360

DDC
RECEIVED
NOV 11 1976
A

(12) 148p.

(11) Submitted on

10 Apr 70

Letter on File

A

AD400355

DISTRIBUTION STATEMENT A
Approved for public release;
Distribution Unlimited

TABLE OF CONTENTS:

TABLE OF CONTENTS

TABLE OF CONTENTS

ILLUSTRATIONS

ILLUSTRATIONS

UNDERWATER SOUND TRANSMISSION

GENERAL

Sound generated anywhere in the ocean is propagated in all directions, or in a beam or beams, to ocean volumes more or less remote from the source. It is important to know where sound that we generate goes and at what power level it arrives. This knowledge is necessary in the active functions of communication, echo ranging, and echo sounding, and in the passive functions of detecting noise of enemy ships and of avoiding the detection by the enemy of noise radiated from our own ships and submarines.

In the transmission of sound in the ocean, energy travels along directed lines that may be called rays. When energy strikes the bottom, the surface, or any other boundary, it is scattered. If sound rays were straight lines, and if reflection were specular and without loss, and if there were no attenuation of the sound, the calculation of levels at remote points would be quite simple. We would simply apply the inverse square law, which is nothing more than a statement to the effect that all energy contained in a spherical shell about the source at one instant is propagated outward and is contained in another shell of larger radius at a later instant. Since the volume of the shell for a given thickness is proportional to the square of the radius, the energy per unit volume must be inversely proportional to the square of the radius. Thus, if a comparison is made of the energy per unit volume, or of the intensity, at a radius r yards as compared to the same quantity at a radius of one yard, the level at the greater radius is simply that at one yard divided by r^2. Expressed in decibels, the loss is 20 log r.

Nature is not as simple as the picture of the last paragraph. As a rule, none of the foregoing conditions is satisfied. It is therefore necessary for us to know something about the ocean and how the transmission of sound is affected by ocean conditions. Logically, we now turn to a discussion of ocean conditions that exist and affect all of the characteristics of sound transmitted in the ocean that have been mentioned.

SOUND SPEED PROFILES

The principal ocean characteristics affecting sound speed are temperature, pressure, and salinity. Quite complicated formulas have been developed by Kuhawara[1], Del Grosso[2], and Wilson[3] while Mackenzie[4] and others have adjusted these to explain experimental data. Anyone engaged in very precise computations would do well to review the literature. For our purpose, a family of curves for the case of atmospheric pressure and a simple correction for depth will be given. The curves in Fig. 1a give sound speed as a function of temperature for 21, 31, and 41 $^{o}/_{oo}$ of NaCl. To the values given by these curves there may be added .018/sec. multiplied by depth, accounting for the increase in sound speed with increased depth.

As an example, suppose that we have a condition of temperature 40°F and salinity 31$^{o}/_{oo}$ at a depth of 1000 feet. From the curves we read the sound speed for zero depth as 4805 ft./sec. To this we must add (.018/sec.) x 1000 feet, giving 4823 ft./sec.

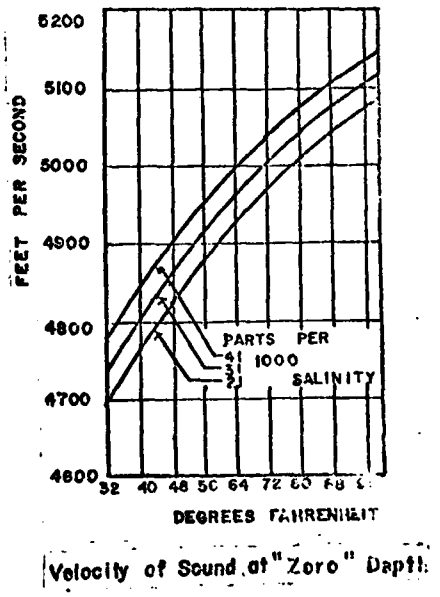

Velocity of Sound at "Zero" Depth

Fig. 1a

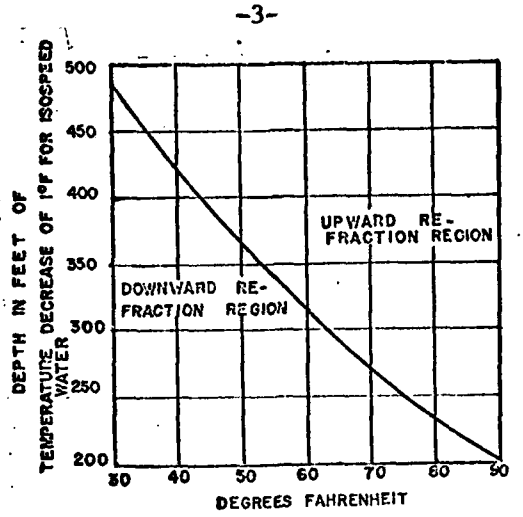

Conditions for isospeed

Fig. 1b

Figure 1b is the curve for a balance between pressure and temperature effects establishing an isospeed condition. In warm water, a negative temperature gradient of greater magnitude is required to balance pressure increase with depth than in cold water. Any combination of temperature and temperature gradient above the curve produces upward refraction. Any combination below the curve produces downward refraction.

In the mid North Atlantic and North Pacific the temperature falls off from a few hundred feet below the surface to about 4200 feet in the Atlantic and 3500 feet in the Pacific, and below these respective depths it remains nearly constant. Temperature is the prevalent variable controlling sound speed down to approximately the depth at which it becomes nearly constant at a value close to 32^{o}F. Consequently, the sound speed tends to decrease with depth down to approximately this critical depth. Below this depth at which the temperature becomes substantially constant, pressure controls changes in sound speed, and from this depth to the bottom the sound speed increases. A common situation in deep water at mid latitudes is one in which below the depth of minimum speed the sound speed increases with depth reaching at about 12,500 feet depth a value equal to that at the surface.

Surmounting the temperature structure described, there will generally

be a mixed layer in which the temperature is nearly constant or even increases slightly with depth. This layer is very unstable, and some peculiar temperature profiles are obtained in it. Figure 2 shows a few approximations to temperature variation with depth down to 500 feet, actual bathythermograms being replaced by a number of straight-line segments. At a in the figure we have no surface-bounded duct. If the same portion of the ocean were exposed for several hours to the mixing action of a high wind (and consequent high sea state), we would expect mixing of the water near the surface and the development of the BT such as approximated at b or c. The mixed layer as here represented constitutes a surface-bounded duct. We must keep in mind that the speed profile approximately parallels the temperature profile but will decrease less rapidly with depth or will increase slowly when temperature is constant and depth is increased. The approximation of speed profile by linear segments follows from that for temperature.

The type of straight-line approximation of a BT shown in Fig. 2 may be improved by the use of a larger number of shorter segments. Calculations of ray paths based on these approximations give good representations of the salient features. Limitations in accuracy occur mainly at layer boundaries involving sound speed maxima.

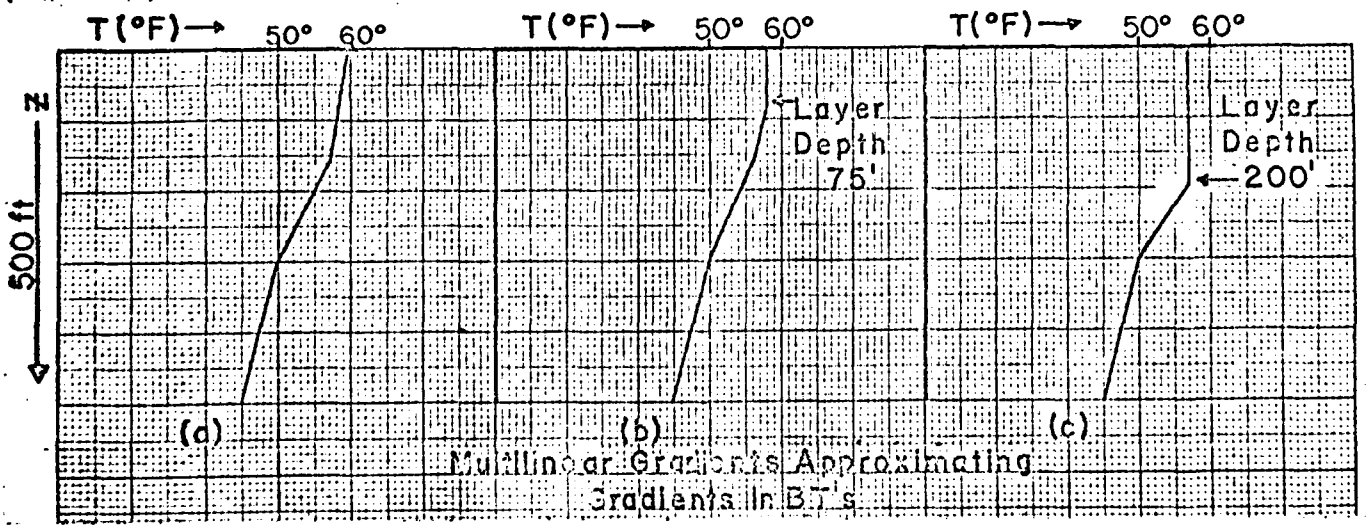

Fig. 2

REFRACTION

When we are faced with any speed profile, corresponding to Fig. 2 what sort of ray paths are anticipated? To answer this question, it is necessary to describe how speed gradients cause deviations from straight-line propagation. Actually, nearly all sound rays in the ocean follow refractive paths, that is curved paths.

Let us imagine a hypothetical case of a plane wave directed horizontally in a medium extending upward with a constant positive sound-speed gradient, g, until the sound speed falls to zero at some height h, say 90,000 yards. The condition would then be that since sound speed would be proportional to distance downward from this height, a plane wave front would pivot about a point at this height. Each ray normal to the wave front would describe the arc of a circle. The real, existing part of the wave front within the layer characterized by g does behave this way. We may write, then, that the vertical distance h of the center of curvature from any given reference point at which sound speed is c, in terms of sound speed and sound-speed gradient, is given by

$$h = \frac{-c}{dc/dy} = \frac{-c}{g}. \qquad (1)$$

The negative signs result from calling distances downward positive. The value h is positive for a negative g.

We shall follow the convention of labelling all variables at z_o with a zero subscript. The radius of curvature ρ_o is

$$\rho_o = \frac{h_o}{\cos \phi_o} = \frac{-c_o}{g \cos \phi_o} \qquad (2)$$

where ϕ_o is the angle of the ray below the horizontal and also the deviation of the radius of curvature clockwise from the vertical and g is the vertical

speed gradient. The value of ϕ at $z = 0$ is ϕ_o. The sign of ρ is herein conventional to agree with the sign of h. The geometry involved is depicted in Fig. 3.

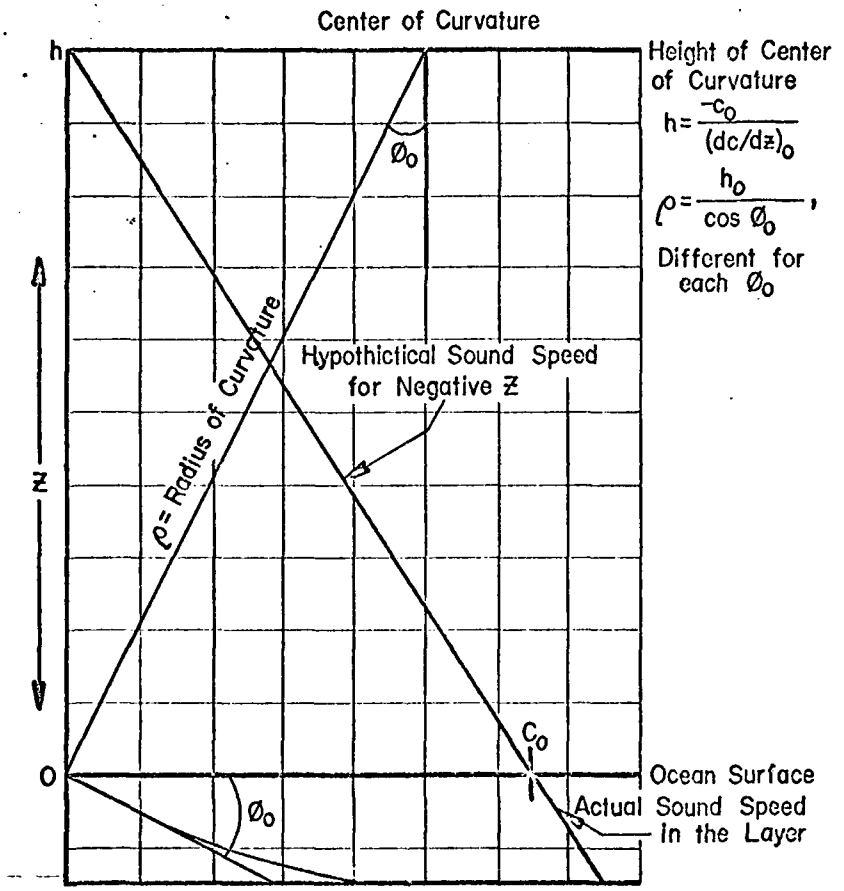

Geometry of Ray Path with Constant Speed Gradient

Fig. 3

If now the speed gradient actually existing is approximated by a succession of straight lines (constant gradients), each ray is approximated by the arc of a circle in passing through each depth segment assumed to have its own given gradient, with the appropriate radius of curvature for each depth segment. Eq. (2) is everywhere satisfied. Since ρ is constant along a single

ray in a medium of constant gradient, $\frac{c}{\cos \phi}$ is constant, an expression of Snell's law. Actually Snell's law is not restricted to a single medium even though g changes from one medium to the next. (We should perhaps comment here that Snell's law is expressed by some authors as a relation between the sines of the angles with the z axis.)

ACOUSTIC PATHS

Forming rays by the use of Eq. (2), we obtain the general characteristics of the ray paths shown in Fig. 4 from a source S near the surface to distant ranges; these are the path in the surface duct, the bottom-bounce path, and the convergence-zone path.

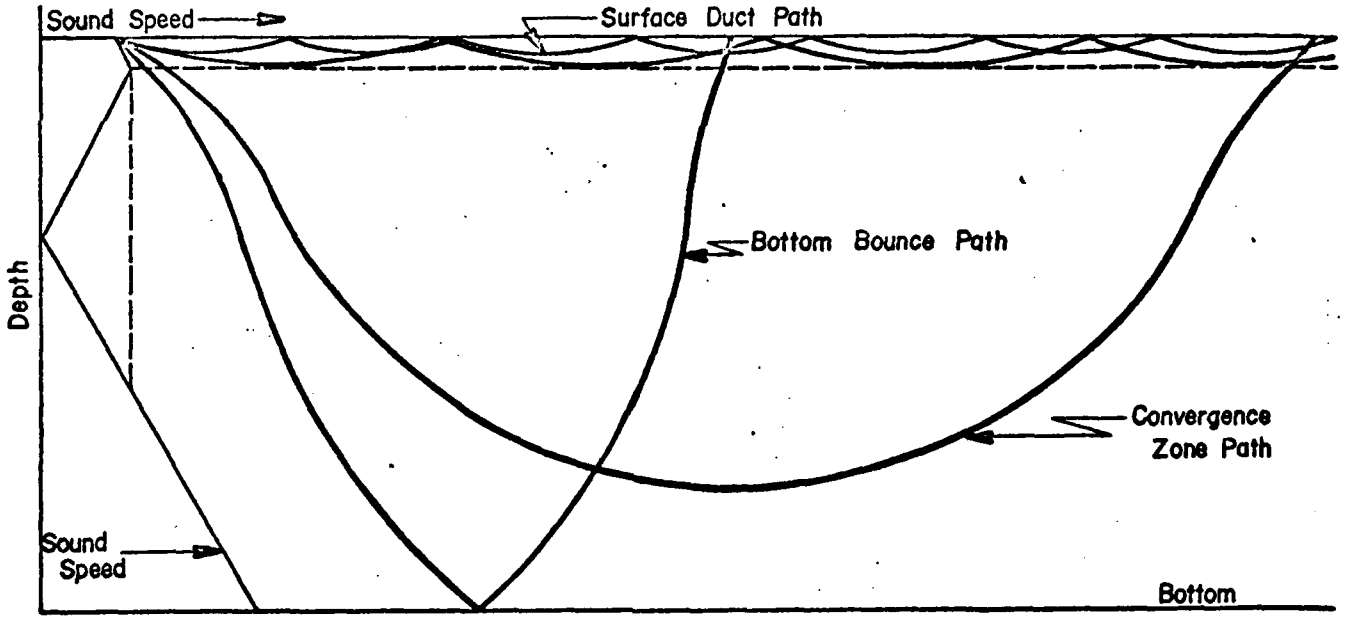

Major Paths to Long Range

Fig. 4

Besides the fundamental paths illustrated in Fig. 4 there are other near-surface to near-surface paths involving multiple bounces. For example, Fig. 5 shows four different paths of slightly different lengths incorporating

one bottom bounce and zero to two surface bounces in the outward transmission of sound from the source to target. There are for each of the outgoing paths four different return paths involved in echo ranging, making a total of sixteen different round-trip paths, not all of different lengths. Further combinations may arise from complicated reflection processes.

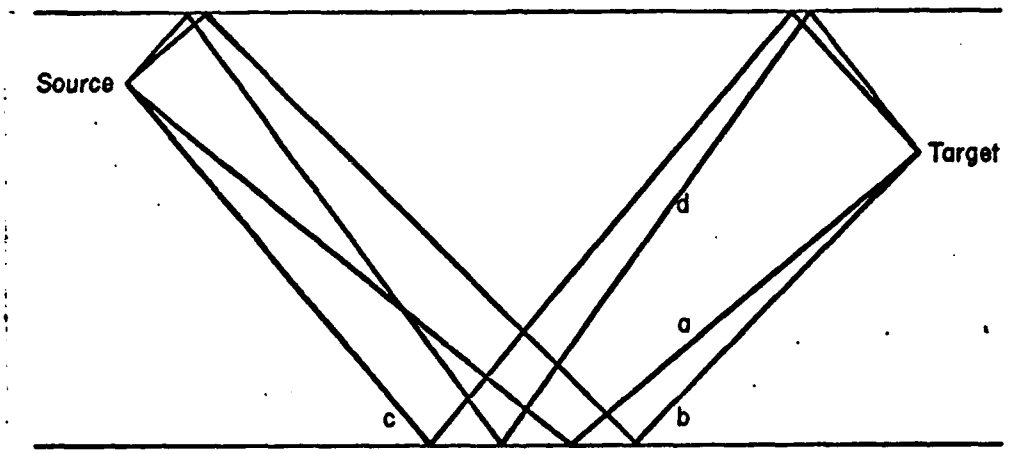

Acoustic Paths From Shallow Source To Shallow Target Using One Bottom Reflection

Fig. 5

In all cases shown so far, the source has been near the surface in the surface-bounded duct. We consider next the ray paths available from a relatively deep source. Fig. 6a shows ray paths from a source at a depth of 1400 yards to points near the surface. A ray starting out horizontally does not reach the surface since it is at the depth for which the sound-speed gradient is zero. Nearby rays will not reach the surface either since by Snell's law they become horizontal at a c only slightly greater than that at source depth. However, there is a limit ray of some elevation at the source that will just graze the surface and a second limit ray depressed an amount equal to the

elevation of the first that will just graze the surface after a downward excursion and ascent. Any steeper rays will insonify all the surface nearer to the source for the case of initially upward rays or points on the surface beyond the limiting ray for rays directed downward. But near the surface in between the upward and downward limiting rays there is a shadow zone.

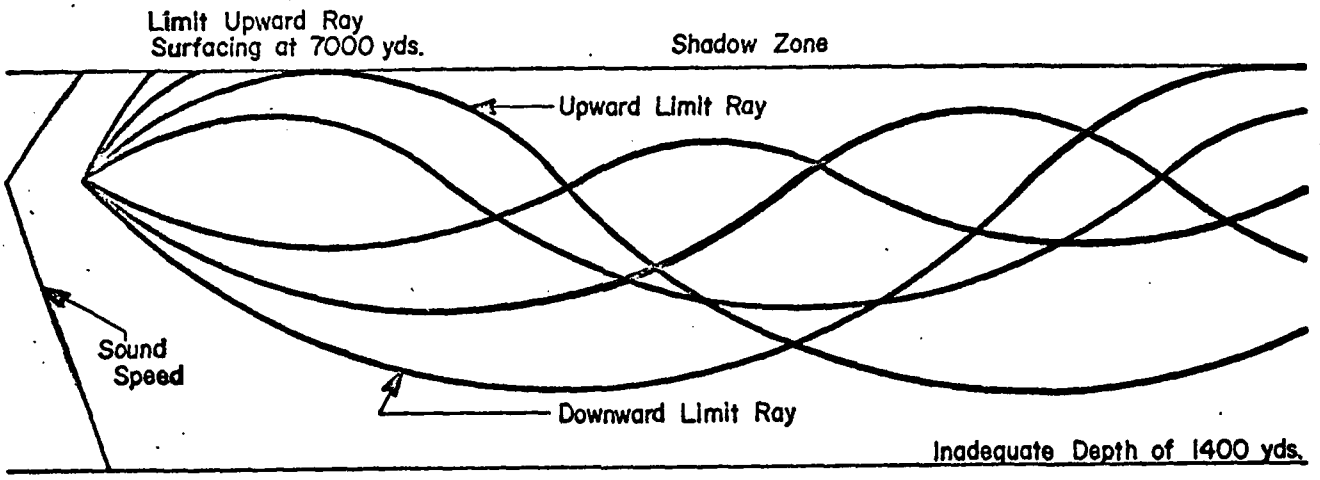

Upward Paths from Deep Sources

Fig. 6a

The way to get rid of the shadow zone is illustrated in Fig. 6b. This method is to locate the source at a depth where the sound speed is equal to or greater than that at the surface. When this is done, the horizontally directed ray at the source will again become horizontal or maintain an incident angle at the surface, and there will be no shadow zone of the form just described. All upward rays will fill in from the point of incidence of the initially horizontal ray to lesser ranges, and all rays directed downward will fill in from this point of incidence outward. The combination of ray paths available constitutes what is called "the reliable acoustic path." Our own preference is to limit the use of this terminology to the last example although this is not the most common practice. The path of the last example is reliable in the sense that there are direct rays to all ranges out to that range reached by a downward directed ray that just grazes the bottom.

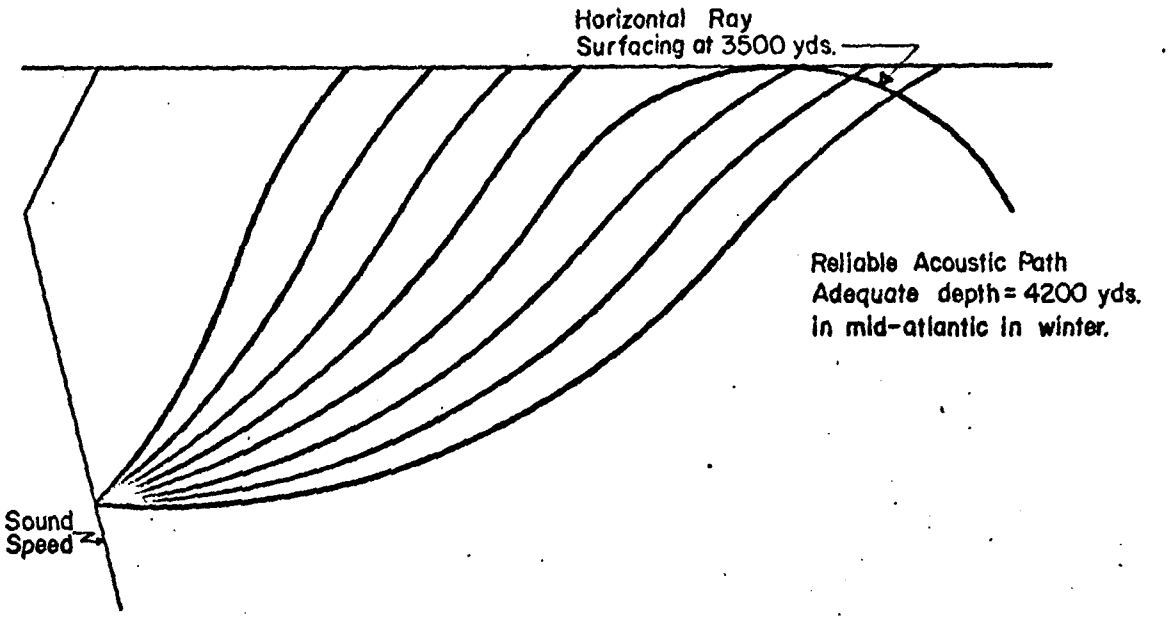

Upward Paths from Deep Sources

Fig. 6b

DIVERGENCE LOSS THEORY

To calculate divergence loss for curvilinear propagation, we start with a "tube" of sound rays and determine how its cross sectional area varies with distance from the source. The limitation in dimension implied by "tube" is necessary when the spreading rate is a function of the coordinates, as it is in curvilinear propagation, for then the spreading in different tubes is different. The divergence loss in decibels is $10 \log \frac{I_1}{I_2}$. This is just $10 \log \frac{\Delta A_2}{\Delta A_1}$, in which ΔA_1 is area of the reference cross section and ΔA_2 is that of the tube when it reaches the desired range. For rectilinear propagation the ratio of the areas is the same as the ratio of the square of the radial distances and the divergence loss is therefore always $10 \log \frac{r_2^2}{r_1^2}$. We shall ordinarily take the reference distance as 1 unit of length so that this may be written $20 \log r_2$. ΔA_2 may be considered to have two dimensions at right angles to each other and the loss in each dimension

may be considered as 10 log r_2. This will be convenient for physical insight into how loss in curvilinear propagation compares with that in rectilinear propagation.

We shall consider linear gradients only because any sound-speed gradient may be approximated by a number of linear segments so that a multiple-layer theory will approximate any actual case.

Single Sound-speed Gradient

Our interest is in deviation from the simple case of spherical divergence. The scope of our immediate inquiry is limited to divergence in a single medium of constant vertical sound-speed gradient, g, now assumed negative.

We consider a fountain of sound rays from a source S contained as they start out from the source between two cones having a common vertical axis and a common apex. We let the inner of these cones make an angle ϕ_o with the horizontal and let the outer of the two cones make an angle $\phi_o + \delta\phi_o$ with the horizontal. (Remember angles are positive clockwise from the x axis). Let us consider at first only the rays starting along the inner cone. As these rays are traced, they travel along arcs of circles since the medium is assumed to have a constant speed gradient within it. They thus bend outward as shown in Fig. 7. As these rays, which are initially lying in the conical surface and each in a vertical plane through the axis of the cone, advance, the locus of points reached simultaneously is always a circle in a horizontal plane of radius x given by

$$x = r \cos \theta. \qquad (3)$$

The circumference of this circle in a horizontal plane is the horizontal dimension of the advancing wave front. It is designated s_1 and is given by

$$s_1 = 2\pi r \cos \theta. \tag{4}$$

Fig. 7 illustrates the geometry involved.

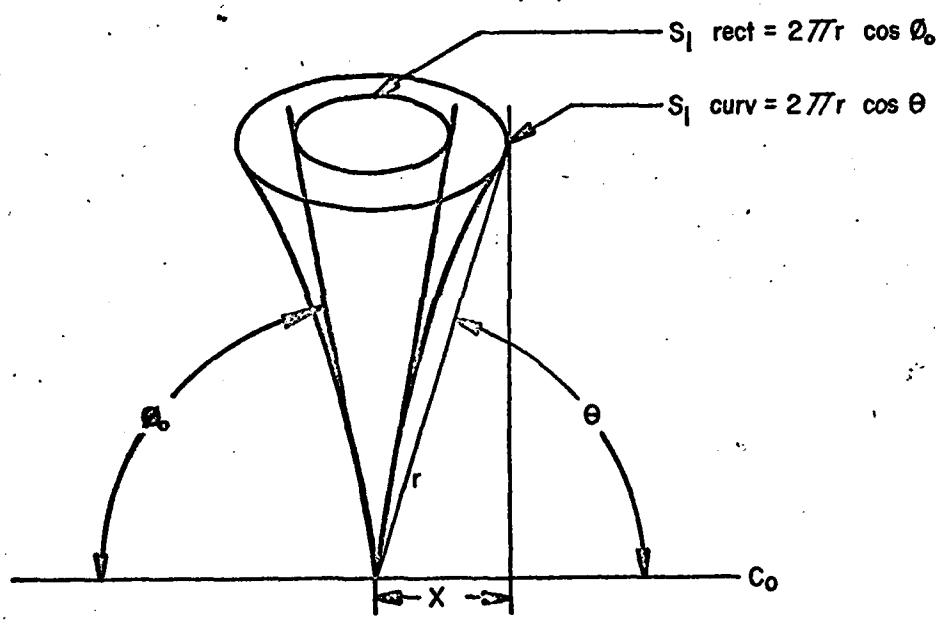

Geometry of Refracted Rays in Constant Gradient Medium in Horizontal Plane

Fig. 7

For rectilinear propagation θ is always ϕ_o and

$$x_{rect} = r \cos \phi_o, \tag{5}$$

the special case of Eq. (3) when $\theta = \phi_o$. Likewise,

$$s_{1\ rect} = 2\pi r \cos \phi_o. \tag{6}$$

From Eq. (4) and Eq. (6), we have

$$\frac{s_{1\ curv}}{s_{1\ rect}} = \frac{\cos \theta}{\cos \phi_o}. \tag{7}$$

To the reader who has a better feeling for calculations based on straight-line propagation to the identical horizontal circle, we point out that this approach would yield the same result, Eq. (7), because the circles compared at the reference range of 1 yard would introduce this relation.

In Fig. 7, with the rays starting upward and bending downward, the ratio of the s's is greater than 1 until $\cos \theta = \cos \phi_o$, which will occur when $\theta = -\phi_o$, if at all. It may also be noted that the ratio is maximum when $\theta = 0$, in other words, when the ray is at the same depth as the source.

Another point of interest is <u>rate</u> of spreading in the horizontal. The total angle around any cone with its vertex as center is $\alpha = 2\pi \cos \phi$. This α is rate of change of arc length in the horizontal with path length, or spreading rate in the horizontal. The following relationship holds:

$$\frac{\alpha}{\cos \phi} = \frac{\alpha_o}{\cos \phi_o}. \tag{8}$$

When ϕ tends toward the horizontal, α increases, and when ϕ tends away from the horizontal, α decreases. In Fig. 7, ϕ is tending toward the horizontal and spreading rate is increasing. Since spreading rate in rectilinear

propagation is α_o, Eq.(8) shows that, relatively, propagation over a refractive path has a greater rate of spread so long as $\cos \phi > \cos \phi_o$ in the case shown in Fig. 7, or, until $\phi = -\phi_o$, which takes place when the ray bends back to the depth at which it started. Therefore, over this range of ϕ the ratio of $\frac{s_1 curv}{s_1 rect}$ increases to the maximum given by Eq. (7) when $\theta = 0$.

For spreading in a vertical plane we compare the rays starting in the outer cone bounding the fountain of rays with those starting in the inner cone. A single pair of rays, as depicted in Fig. 8 will be adequate. $\delta\phi$ is the angle between rays at points reached at the same instant of time (not same depth) in this section.

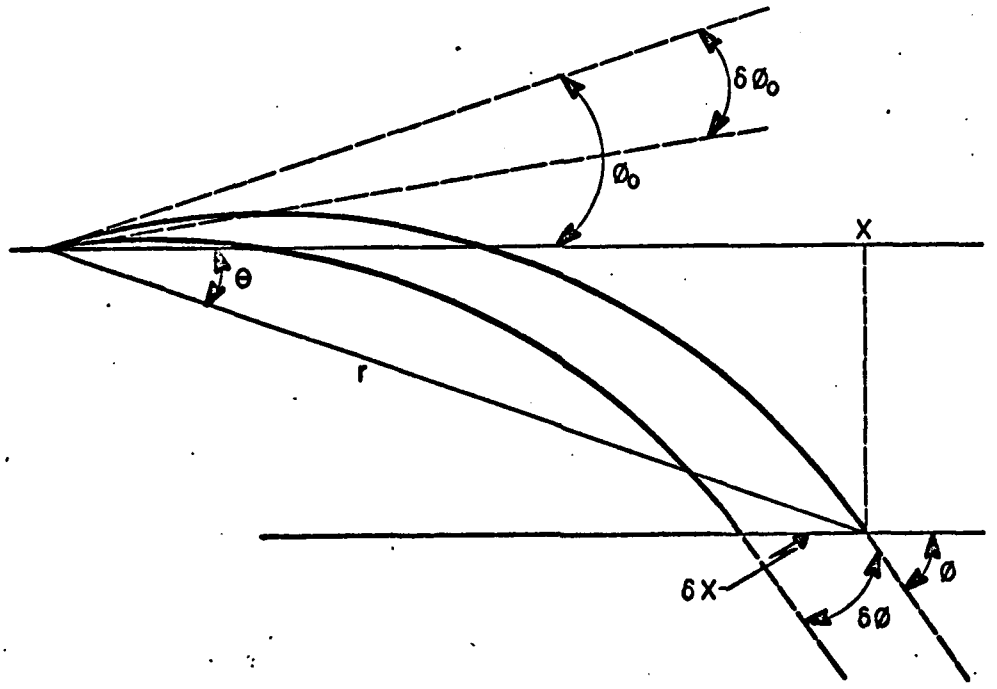

Spreading in Vertical Plane

Fig. 8

In Fig. 8 the reference ray depicted starts from the source at a negative angle ϕ_o above the horizontal. A nearby ray in the same vertical plane starts out at an angle $\delta\phi_1$ below the reference ray. As we follow these rays, ϕ continuously increases from its initial negative value ϕ_o, and $\delta\phi$ varies from its initial value $\delta\phi_o$ in a manner to be determined. The method of procedure toward an indication of ray spreading that follows is the most elegant approach, but not the simplest. (Another method will be used for the multi-layer case, and the results can be shown to agree.) In the immediate method we plan to derive δs_2, the arc subtended between neighboring rays, by finding the distance between points on these rays reached at the same time.

The following equation is fairly obvious as it relates speed along the circumference of a circle to rate of change of angular position:

$$\frac{d\phi}{dt} = \frac{c}{\rho} = -g \cos \phi \tag{9}$$

with the second equality in Eq. (9) resulting from Eq. (2). When g is negative, ϕ is increasing, and when g is positive, ϕ is decreasing. Separating variables and integrating, we obtain

$$\int_{\phi_o}^{\phi} \frac{d\phi}{\cos \phi} = -g \int_o^t dt \tag{10}$$

or

$$\ln \tan \left[\frac{\pi}{4} + \frac{\phi}{2}\right] = \ln \tan \left[\frac{\pi}{4} + \frac{\phi_o}{2}\right] - gt. \tag{11}$$

In deriving Eq. (11), we have integrated along a single ray allowing the time to vary. We shall now hold time constant and take the differentials of the two sides of Eq. (11) as we vary ϕ_o and thereby go from reference ray at angle ϕ_o to neighboring ray at angle $\phi_o + \delta\phi_o$. The differentials of both sides are similar and come out in rather simple form by the following steps:

$$\delta \ln \tan \left(\frac{\pi}{4} + \frac{\delta\phi}{2}\right) = \frac{1}{\tan \left(\frac{\pi}{4} + \frac{\phi}{2}\right)} \sec \left(\frac{\pi}{4} + \frac{\phi}{2}\right) \frac{\delta\phi}{2}$$

$$= \frac{\delta\phi}{2 \sin \left(\frac{\pi}{4} + \frac{\phi}{2}\right) \cos \left(\frac{\pi}{4} + \frac{\phi}{2}\right)}$$

$$= \frac{\delta\phi}{\sin \left(\frac{\pi}{2} + \phi\right)}$$

$$= \frac{\delta\phi}{\cos \phi}. \tag{12}$$

Applying Eq. (12) to the differentials of the two sides of Eq. (11), we obtain

$$\frac{\delta\phi_1}{\cos \phi_1} = \frac{\delta\phi_o}{\cos \phi_o}. \tag{13}$$

The angle between two rays as they pass through points reached at the same time is $\delta\phi$.

The quantity $\delta\phi$ is the spreading rate in the vertical $\frac{d(\delta s_2)}{dl}$. It corresponds to α in the horizontal given by Eq. (8). Since the spreading rates follow the same functional form, the accrued spreads must also, and we

may write for the ratio in the vertical plane of δs_2 to $\delta s_{2\ rect}$:

$$\frac{\delta s_{2\ curv}}{\delta s_{2\ rect}} = \frac{\cos\theta}{\cos\phi_o}. \tag{14}$$

This is analogous to Eq. (7). Finally, the ratio of the areas which are the products of s_1 and δs_2 for each of the cases, is

$$\frac{A_{curv}}{A_{rect}} = \left[\frac{\cos\theta}{\cos\phi_o}\right]^2, \tag{15}$$

The loss in excess of spherical will be 10 times the logarithm of the ratio of the areas. The total loss for the curvilinear case is then

$$\text{loss} = 20 \log r + 20 \log \frac{\cos\theta}{\cos\phi_o}. \tag{16}$$

We reiterate that the treatment is for a medium with one constant sound-speed gradient.

Multiple Layers without Sound-speed Discontinuities

The result of the last section in so far as divergence in the horizontal is concerned is extensible to multiple layers with horizontal boundaries. Eq. (7) is still applicable. The justification hinges on the fact that a fountain of rays experiences a spreading into the circumference of a circle of radius x regardless of the number of layers, and the expression for x remains r cos θ.

Divergence in the vertical is somewhat complicated by propagation through multiple layers with different sound-speed gradients. When sound passes through one or more layer boundaries, accounting in terms of points reached at the same time becomes impracticable. The complication which develops is depicted

in Fig. 9 which shows by solid lines the position of a wave front as neighboring ray reaches a boundary and again as the reference ray reaches the boundary. In between these positions, the two rays are in different layers and may experience quite different bending. In the figure the reference ray is bending up while the neighboring ray is bending down. This effect leads in the example to markedly increased spreading so that the single layer formula for loss in the vertical plane no longer applies.

While considering this phenomenon, it would be wise to note that a similar effect may occur in reflection from a boundary. Suppose that we start with the specification that $g_1 = -g_0$. The effect already described will hold. But now, let us replace the boundary by a perfect reflector. The reflected rays will then be the mirror image of the previously transmitted rays and therefore, will experience the same increased spread as shown by dotted lines in Fig. 9.

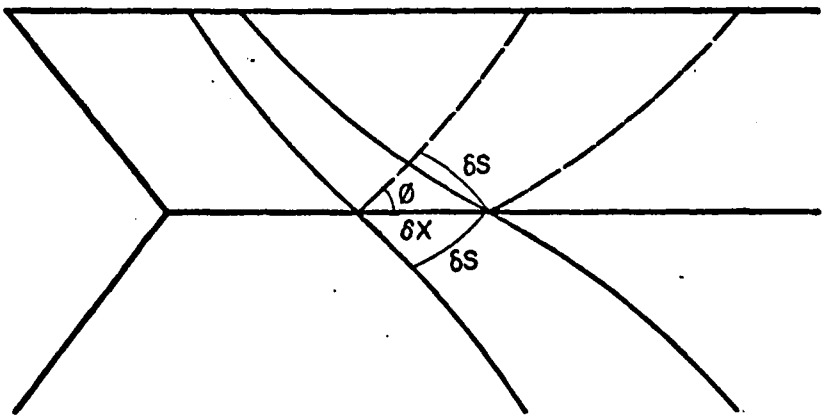

Mechanism Increasing Divergence Loss
At Reflection from Sound-speed Maximum

Fig. 9

Taking a further look at Fig. 9, we may be struck with the idea that the effect described becomes negligible in the limit of small $\delta\phi_i$. It is true that if we halve δx_i, we approximately halve the travel time in different media and therefore, approximately halve the distortion. However, this leaves the same change in angle per unit angle which is the important characteristic.

To handle the situation just described we hereafter compare pairs of rays at the same depth rather than at the same time. $\delta\phi$ takes on a new meaning becoming the angle between the rays at the same depth. δx_i is the horizontal spacing of the rays at the i^{th} boundary.

We shall reiterate and expand our conventions. Characteristics at the source or derived from characteristics at the source will carry the subscript zero. The quantities c_o, g_o, and ϕ_o are characteristics at the source, and derivable from these are h_o and ρ_o. Consecutive layer boundaries below the source will carry subscripts 1, 2, 3, etc. with corresponding subscripts for characteristics there and for new h's and ρ's established from these characteristics. In the negative direction (up) negative subscripts will be associated with successive layer boundaries. In examples to be presented later the source will be at the surface and no negative subscripts will be needed.

We have established in Eq. (2) the convention that ρ has the sign of h. A ρ with a component upward from the ray is negative and with a component downward is positive. A convention of this type is necessary in order that equations involving ρ be consistent. Note that a negative ρ is associated with negative curvature which seems appropriate.

In the computation of divergence loss, the quantities c_o at the source and g_i for each layer will be given along with layer depth. A preliminary computation of c at each layer boundary may be performed by using the relation

$$c_i = c_{i-1} + g_{i-1}\,(z_i - z_{i-1}). \tag{17}$$

All the h's may be computed from Eq. (1). The quantity h_o will be measured from the source, h_1 from boundary one, first below the source, etc. The mathematical procedure will then be to trace any reference ray from the source to consecutive layer boundaries, computing ϕ_i, ρ_i and x_i at each boundary in the order given.

Using Snell's law, the ϕ_i's are readily obtainable from ϕ_o and the c_i's already computed:

$$\frac{\cos \phi_i}{c_i} = \frac{\cos \phi_o}{c_o}. \tag{18}$$

The ρ_i are then obtainable by the use of Eq. (2).

The quantity $x_{i-1,i}$ is the increment in horizontal range between the reference depths i-1 and i. Referring to Fig. 10, $x_{i-1,i}$ is seen to be, noting that ρ is negative in the figure,

$$x_{i-1,i} = \rho_{i-1}(\sin \phi_i - \sin \phi_{i-1}). \tag{19}$$

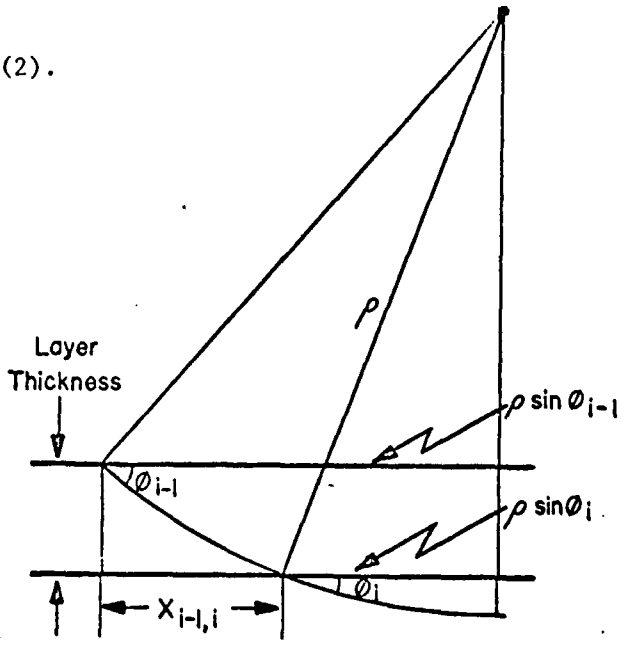

Horizontal Range Increment

Fig. 10

In using Eq. (19), the term in parentheses has the quantity subscripted for the first depth reached appearing with a negative sign. This sign, first-reached depth negative, must be retained for upward rays resulting in the higher subscripted quantity appearing with the negative sign. This change in sign is just offset by a change in sign of each ϕ, and thus of sin ϕ, on the way up. Consequently,

$$x_{i,i-1} = x_{i-1,i}. \tag{20}$$

The whole horizontal range through n layers is given by

$$x_n = \sum_{i=1}^{n} x_{i-1,i} \tag{21}$$

using the single subscript for the <u>whole</u> horizontal range to boundary n along the ray.

We next treat mathematically a neighboring ray which, at the source, is at an angle $\delta\phi_o$ with the reference ray ($\phi_o + \delta\phi_o$ with the positive x axis). At each layer boundary we compute a $\delta\phi_i$ and a $\delta x_{i-1,i}$. For the whole horizontal distance between the reference ray and the neighboring ray, we sum these $\delta x_{i-1,i}$ and obtain δx_n as for x_n in Eq. (21).

The calculation of $\delta\phi_i$ is a bit tricky. It would seem quite easy to start with Snell's law and differentiate obtaining

$$\frac{\sin \phi_i \delta\phi_i}{c_i} = \frac{\sin \phi_o \delta\phi_o}{c_o}.$$

Then solving for $\delta\phi_i$ and replacing the ratio of the c's by the ratio of the corresponding cosines, we would obtain

$$\delta\phi_i = \frac{\tan \phi_o \delta\phi_o}{\tan \phi_i}.$$

The equations fail for either $\phi_o = 0$ or $\phi_i = 0$. For this reason we choose not to number them. But now let us start with Snell's law for the neighboring ray

$$\frac{\cos(\phi_i + \delta\phi_i)}{c_i} = \frac{\cos(\phi_o + \delta\phi_o)}{c_o} \tag{22}$$

and expand each numerator in a Taylor's series in $\delta\phi_i$ retaining three terms and obtaining

$$\frac{\cos \phi_i - \sin \phi_i \delta\phi_i - \cos \phi_i (\delta\phi_i^2/2)}{c_i} =$$

$$\frac{\cos \phi_o - \sin \phi_o \delta\phi_o - \cos \phi_o (\delta\phi_o^2/2)}{c_o} \tag{23}$$

Next we replace the ratio of the c's by the ratio of the cosines and divide by the cosines. After subtracting unity from each side and changing signs, we obtain

$$\tan \phi_i \delta\phi_i + \frac{\delta\phi_i^2}{2} = \tan \phi_o \delta\phi_o + \frac{\delta\phi_o^2}{2}. \tag{24}$$

If $\frac{\delta\phi_o^2}{2}$ and $\frac{\delta\phi_i^2}{2}$ were negligible, we would obtain the previous result. But $\frac{\delta\phi_i^2}{2}$ is not negligible when $\tan \phi_i = 0$ making the first order term zero. Similar reasoning applies to $\frac{\delta\phi_o^2}{2}$. To get accuracy we must use all terms in Eq. (24) and consequently,

$$\delta\phi_i = - \tan \phi_i + \sqrt{\tan^2 \phi_i + 2 \tan \phi_o \delta\phi_o + \delta\phi_o^2}. \qquad (25)$$

In a computer program it is no great chore to use Eq. (25) consistently to assure its use for cases in which it is needed.

The computation of $\delta x_{i-1,i}$ offers no problem. We have an expression for $x_{i-1,i}$ given by Eq. (19). In Eq. (19) we replace ρ_{i-1} by $\frac{h_{i-1}}{\cos \phi_{i-1}}$ since h, unlike ρ, is independent of ϕ, and use Snell's law to obtain

$$x_{i-1,i} = h_{i-1} \left(\frac{c_i \tan \phi_i}{c_{i-1}}\right) - \tan \phi_{i-1} . \qquad (26)$$

Differentiating, we obtain the following expression:

$$\delta x_{i-1,i} = h_{i-1}\left(\frac{c_i}{c_{i-1}} \sec^2 \phi_i \delta\phi_i - \sec^2 \phi_{i-1} \delta\phi_{i-1}\right). \qquad (27)$$

Shifting back to ρ instead of h,

$$\delta x_{i-1,i} = \rho_{i-1}(\sec \phi_i \delta\phi_i - \sec \phi_{i-1} \delta\phi_{i-1}). \qquad (28)$$

In using Eq. (28), the term in parentheses has the quantity subscripted for the first depth reached appearing with a negative sign. The sign, first-reached depth negative, must be retained for upward

rays resulting in the higher subscripted quantity appearing with the negative sign. This change in sign is just offset by a change in sign of each $\delta\phi$ on the way up and thus,

$$\delta x_{i,i-1} = \delta x_{i-1,i} \tag{29}$$

and finally

$$\delta x_n = \sum_{i=1}^{n} \delta x_{i-1,i}. \tag{30}$$

Having δx_n at the position where divergence loss is to be computed, in most cases convert to $\delta s_{n\ curv}$ by the following relationship:*

$$\delta s_{n\ curv} = \delta x_n \sin \phi_n. \tag{31}$$

When ϕ_n is very small, Eq. (31) becomes inaccurate for finite $\delta\phi$ which has to be used in practice. When the neighboring ray is the steeper and ϕ_n is approximately equal to zero, we can side-step by using the relationship

$$\delta s_{n\ curv} = \delta x_n \sin (\phi_n + \delta\phi_n). \tag{32}$$

---

*Since we deal with a δs only in the vertical, we may drop the subscript 2 to indicate vertical and use the subscript to agree with that for δx.

If we desire still greater accuracy for small angles, we may extend or retract either ray along the arc of a circle by an amount $d\phi$ (not $\delta\phi$ in dealing with a single ray)given by the expression

$$d\phi_n = \frac{\delta x_n}{\rho_{n-1}}. \tag{33}$$

Except near the source, this will bring the extended or retracted ray into phase coincidence with the other ray. Then, since both rays are nearly horizontal

$$\delta s_n = \delta y_n = \rho_{n-1} \cos (\phi_n + d\phi_n) - \cos \phi_n . \tag{34}$$

If a ray, when extended, would actually be reflected at depth subscripted n, we may imagine the medium extended for this computation with the result that the sign of δy will be wrong. This is of no consequence.

For comparison of divergence loss with that for rectilinear propagation, we may compare areas of the wave fronts reached in the two cases for the same length of path. It is more enlightening, however, to take the equivalent step of forming ratios of each of the dimensions contributing to area in order to segregate their individual contributions to divergence loss.

We had for divergence in a horizontal plane

$$\frac{s_{1\ \mathrm{curv}}}{s_{1\ \mathrm{rect}}} = \frac{\cos \theta}{\cos \phi_o}. \tag{7}$$

Then 10 log of this ratio gives excess loss over the curvilinear path in decibels attributable to spreading in the horizontal.

In the complementary dimension in a vertical plane, we have $\delta s_{n\ curv}$, given by Eq. (32) or in Eq. (33) and Eq. (34), and $\delta s_{n\ rect}$, given by

$$\delta s_{\ rect} = r\ \delta\phi_o, \tag{35}$$

in which r is path length. The ratio may be formed, and may be converted to the decibel loss attributable to spreading in a vertical plane relative to the loss in rectilinear propagation. Then total loss from vertical spreading in db is

$$\text{Loss} = 10 \log r + 10 \log \frac{\delta s_{\ curv}}{\delta s_{\ rect}}. \tag{36}$$

Many of the equations here may be combined to express δs_2 in terms of ocean characteristics, ϕ_o and $\delta\phi_o$. The value of δs_2, so expressed, is quite complicated if we observe the niceties of Eq. (25) and Eq. (34). In fact it tends to lose the obvious physical interpretation of the simpler equations given here. In addition, the eliminated steps may contain information of considerable interest.

Summary of Computation for Divergence Loss in Vertical Plane

We can now summarize concisely, in practicable sequence, the eight steps necessary to obtain excess spreading loss, in decibels over that obtained in straight-line propagation. These steps follow:

1. Calculations are to be made for a model ocean for which the sound speed profile will be specified. From the profile, we

shall compute h_0, h_1, ... , from the following formula

$$h_i = - \frac{c_i}{g_i}. \qquad (1)$$

These h's are the vertical distances to the hypothetical planes of zero sound speed from reference depths such as layer boundaries.

2. Reference rays of different initial inclinations, that is ϕ_0's, will be considered. For each ϕ_0 compute by Snell's law the corresponding ϕ_1, ϕ_2, ... at layer boundaries and at the depth at which divergence loss is to be computed. Use tables and list sines, cosines, and tangents of all ϕ's used.

3. For each ϕ_i compute the ρ_i for each layer from the formula

$$\rho_i = \frac{h_i}{\cos \phi_i}. \qquad (2)$$

4. For each layer compute increment in x from the following formula

$$x_{i-1,i} = \rho_{i-1}(\sin \phi_i - \sin \phi_{i-1}). \qquad (19)$$

Sum these increments to get x_i (Eq. (21)).

5. Assume a $\delta\phi_0$* between each reference ray and an associated neighboring ray. Compute for each pair of rays, $\delta\phi_1$, $\delta\phi_2$, ... , from the following formula

$$\delta\phi_i = - \tan \phi_i + \sqrt{\tan^2 \phi_i + 2 \tan \phi_0 \delta\phi_0 + \delta\phi_0^2}. \qquad (25)$$

For upward directed rays designate the $\delta\phi$ by $\delta\phi_i^{up}$.

---

* In an example we shall choose $\delta\phi_1$ instead. Any layer boundary may be chosen. In Eq. (25), ϕ_0 may be replaced by any ϕ_i with $\delta\phi_0$ replaced by $\delta\phi_i$.

6. Compute δx_i at the depth where the propagation loss is to be derived from the formula

$$\delta x_i = \rho_o(\sec \phi_1 \delta\phi_1 - \sec \phi_o \delta\phi_o) + \rho_1(\sec \phi_2 \delta\phi_2 - \sec \phi_1 \delta\phi_1) + \ldots \qquad \text{(28) and (30) combined}$$

For multiple layers there may be several terms like those in parentheses, that is, the difference of two products of sec ϕ_i and $\delta\phi_i$. δx_v is the special designation for the difference in x coordinate between the vertices of the reference and neighboring ray. This is like the equation for δx_i except that the last $\delta\phi$, that is, the one with the highest subscript is taken as zero, since there is no difference in angle between two vertices each of zero angle.

7.A. When ϕ_i at the depth where the last computation is to be made is greater than or equal to 5^o, compute δs_i by the following formula

$$\delta s_i = \delta x_i \sin \phi_i. \qquad (31)$$

B. When ϕ_i is less than 5^o, compute $\delta s_i \simeq \delta y_i$ by applying the next two equations successively,

$$d\phi_i = \frac{\delta x_i}{\rho_{i-1}},$$

$$\delta s_i \simeq \delta y_i \simeq \rho_{i-1} \cos(\phi_i + d\phi_i) - \cos \phi_i .$$

This gives the spacing δs_i at the point where the neighboring ray reaches the depth at which the computation is to be made.

8. Compute $r_i \delta\phi_o$, the spread which would take place in straight-line propagations to the same range, and excess loss in decibels given by

$$\text{Excess Loss} = -10 \log \frac{r_i \delta\phi_o}{\delta s_i}.$$

DIVERGENCE LOSS APPLICATIONS

Multiple Layer Applications

A specific model of the ocean is chosen for some of the examples to follow. This is shown in Fig. 11. We have taken three layers with layer boundaries at 50 yards, and 1400 yards depth, and with the bottom at 6000 yards. Sound speed at the source (here taken as the surface) is c_o = 1650 yds/sec. Sound-speed gradients are g_o = .03000/sec, g_1 = -.042000/sec, g_2 = .016000/sec. The value of g_o chosen represents a very strong duct to emphasize duct effects. The five significant figures are assumed in order to obtain 2 or 3 in the final results. This necessity reflects the sensitivity of results to small changes in ocean characteristics.

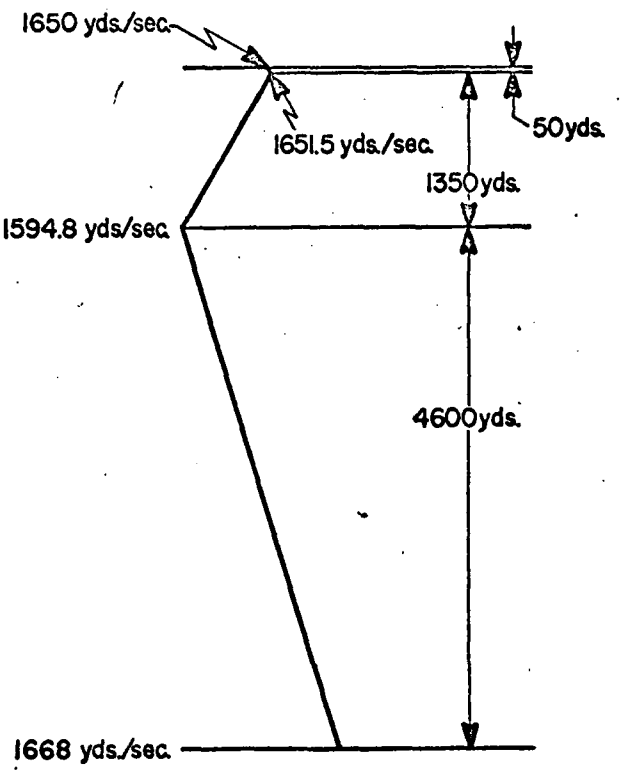

Model Ocean for Multiple Layer Applications

Fig. 11

Based on this model ocean, computations are carried out of divergence loss over various paths in Appendix A. The preceding paragraph is repeated there as Step One of the computations. Steps Two to Eight follow in the Appendix with results obtained at each step.

The model ocean is assumed for the purpose of illustrating multi-layer problems. All the rays considered are steep enough to escape from a surface bounded duct at angles from 0^{o} to 20^{o}. The small angles bring out major deviations in divergence loss from that for spherical divergence.

The three depths at which computation has been carried all the way through to a ray spread and a computation of divergence loss are 20 yards below the surface duct on the downward path, bottom, and surface after the downward excursion. At the surface, there will be rays which follow a bottom-bounce path (9^{o} to 20^{o}), and rays which follow a convergence zone path bending back to the surface from considerable depth but without reaching the bottom. The results will be taken up and discussed in the order just listed.

Loss to Ranges Twenty Yards Below Surface Duct

Fig. 12 is a graph of loss vs range at 20 yards below the surface duct in excess of spherical divergence loss. An excess of even a few db may be quite serious since this is doubled for round trip in echo ranging and since the echo excess over reverberation may not be very high to start with. It is therefore dubious whether those direct rays which reach to ranges beyond 2000 yards for the example case are really useful. At the steeper angles the loss becomes nearly equal to that of spherical divergence.

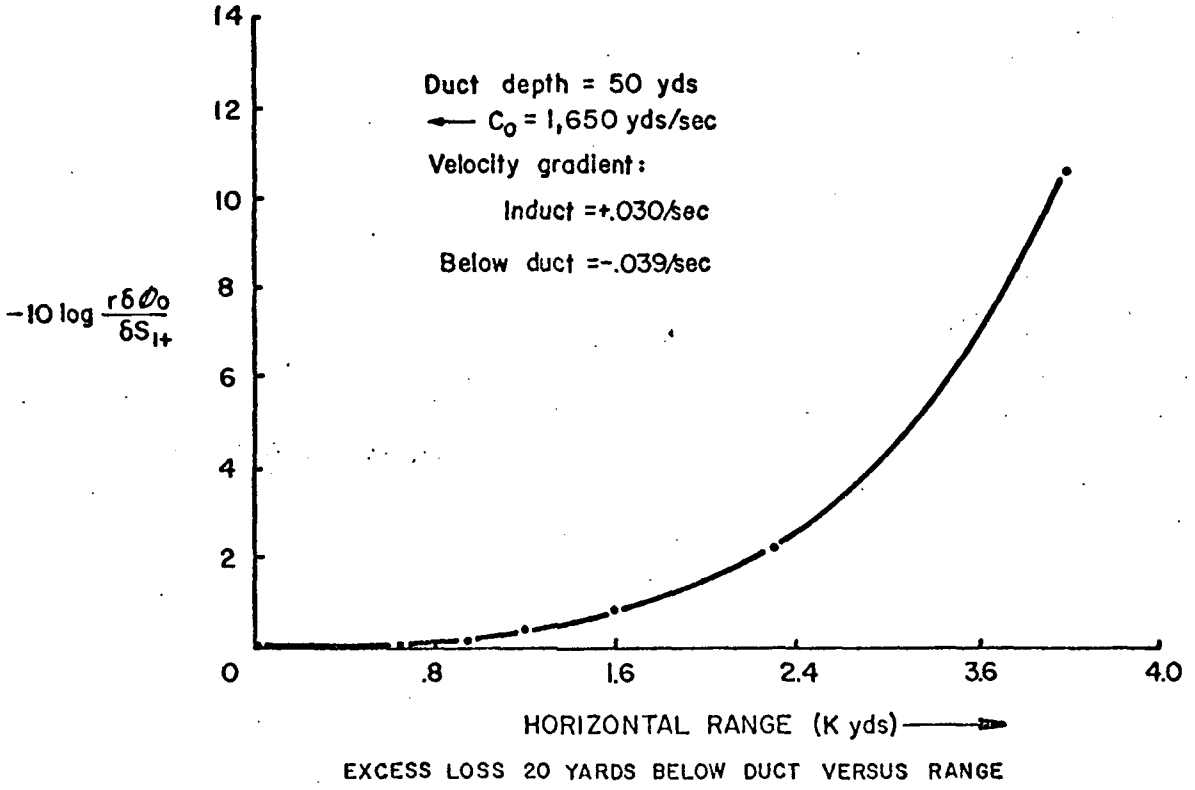

EXCESS LOSS 20 YARDS BELOW DUCT VERSUS RANGE

Fig. 12

In Step Six of the Appendix a δx_{1+} is computed for $\phi_1 = 0^o$ of about one-quarter mile. This is in spite of the fact that $\delta\phi_0$ is only about one minute for this ray and its neighbor. In rectilinear propagation, two rays starting out at the same angle with the reference ray arriving at the same end point would have a horizontal separation more like 50 yards. This point is cited in order to bring out the fact that this separation in the horizontal is very greatly enhanced when the rays approach very close to the horizontal.

It may be of interest to note that at small values of ϕ_1 Eq. (31), that is $\delta s = \delta x \sin \phi$, is at least approximately correct and consequently the fact that δx gets very large for small ϕ_1 is partially compensated for by the fact that the sin of ϕ_{1+} gets very small. As a matter of fact, if a calculation had been preformed before emergence from the duct but near the boundary where the rays make a small angle with the boundary, the decreased magnitude of sin ϕ would have overcompensated for the large δx. This sort of behavior will be observed in the next section at the other velocity maximum at the bottom of the ocean.

Divergence Loss to the Bottom

The computations show that only the rays for which ϕ_1 is greater than 8^o reach the bottom. Any pronounced effect on loss at the bottom caused by refraction is expected to occur at ϕ_1 slightly greater than 8^o. With steep angles the extent in space from surface to bottom is not great enough to produce large effects. The excess loss to the bottom is plotted against range in Fig. 13. The negative loss shown is a gain. All of the rays considered here gain something over spherical divergence with the most pronounced gain coming at small angles of incidence on the bottom. This would be even further accentuated at a value of ϕ_3 less than $3^o49'$, say 1^o. The reason for this crowding together at small grazing angles is that as the rays approach the horizontal δs approaches δy which is small because of the slow variation of cos ϕ_3. In Snell's law for small angles a change of a few degrees results in a very little change in the cosine, therefore, very little change in the sound speed and in the depth.

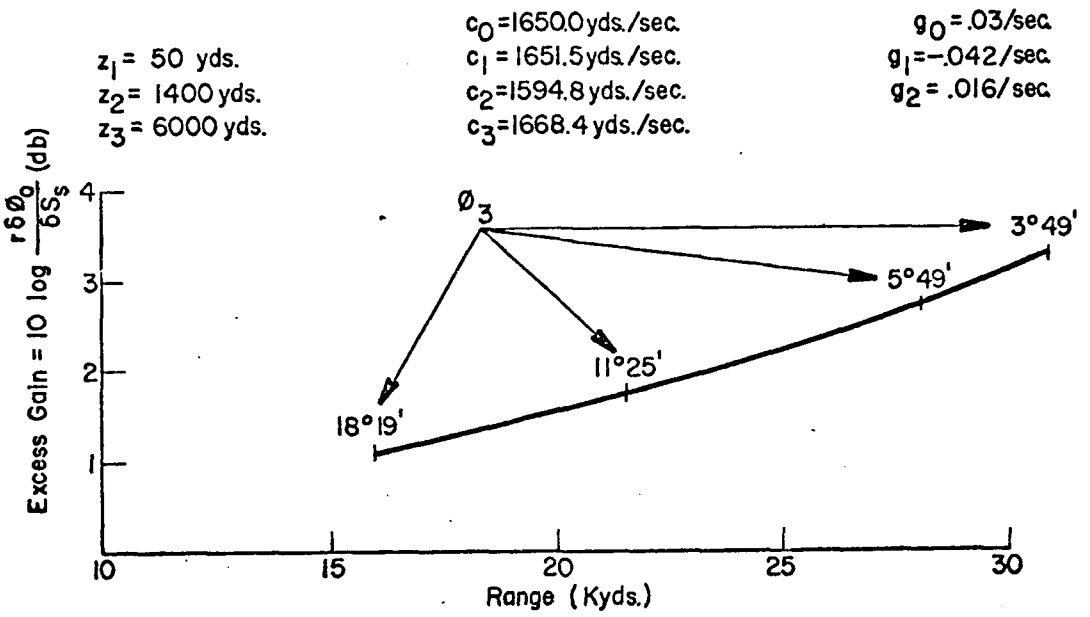

Excess Gain to the Ocean Bottom

Fig. 13

If we compute the range which would be reached if the rays starting at $\phi_o = 9^o19'$ were to continue in a straight line to the bottom, we would find that it substantially exceeds the horizontal range obtained by the same ϕ_o over the actual path. Thus the ocean crowds the rays together and thus it would be expected that on the average there would be a gain at the bottom. Furthermore, there is a gain in a horizontal plane given by 10 log $\frac{\cos\theta}{\cos\phi_o}$, which turns out to be only a fraction of a decibel.

Comparing ϕ_3 with ϕ_1 it will be obvious that the grazing angle at the bottom is substantially decreased especially for small angles at the bottom. This decrease will produce a decreased scattering loss at reflection. In the opposite direction, however, is the added divergence loss by refraction which we described with reference to Fig. 10.

Divergence Loss Surface to Surface via Bottom

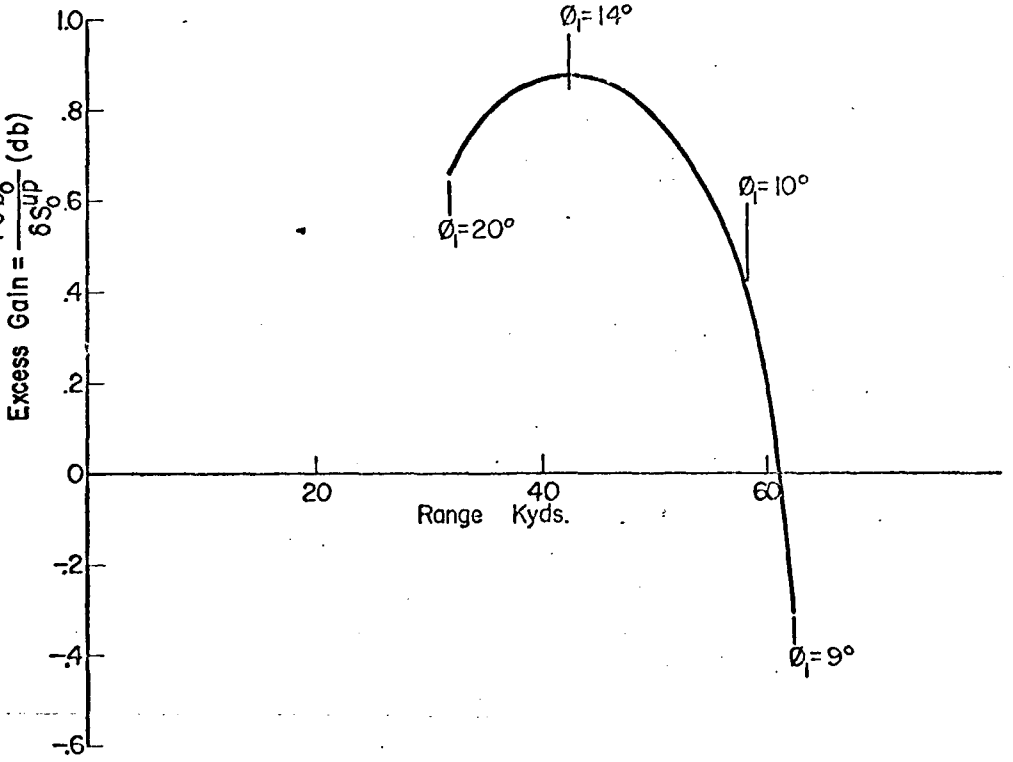

Excess Gain Over Spherical Divergence Loss Surface to Surface via Bottom Bounce. Model Ocean as for Loss to Bottom (3 Layers)

Fig. 14

The results are plotted in Fig. 14. We note that there is an excess loss experienced by the path followed by the r .y for which $\phi_1 = 9^o$, the smallest angle for which the calculation is carried out. This is the ray for which maximum gain was experienced on the downward trip. Apparently, the reflection loss experienced at the bottom more than offset this gain, and even greater loss would be expected for angles at the bottom from 0^o to $3^o49'$. The fact that on the average there is an excess gain over the bottom bounce path in this case is not surprising if one computes the range which

would be reached by straight-line propagation if the angle $9^{o}19'$ were maintained to the bottom and $-9^{o}19'$ from there to the surface in straight-line propagation. This range comes out 73148 yards which is substantially greater than the actual range x appearing in the column for horizontal range. In other words, the rays have been squeezed together to reach the lesser range. Therefore, there must be an average divergence gain via the bottom for this case.

Divergence Loss to the Convergence Zone

In our model ocean, all the rays which emerge from the first layer boundary at angles of 0^{o} to 8^{o} become horizontal at depths short of the bottom. Assuming the same sound-speed profile for the upward excursion, they all return to the surface at or near the convergence zone. The angles at which they reach the surface are the same as the angles at which they started except for a change of sign which takes place at the vertex or turning point. For this case $x_o^{up} = 2x_v$ and $\delta x_o^{up} = 2\delta x_v$. Keep in mind that x_v and δx_v are respectively the horizontal distance to the vertex and difference in horizontal distances to vertices of a pair of rays.

Referring to Table 3 of the Appendix, we note that x_v decreases from the ray for which $\phi_1 = 0^{o}$ to a minimum at the ray for which $\phi_1 = 5^{o}$, and then increases. This variation is doubled for the round trip. Without looking any further it is evident that the rays must crowd together in going through a minimum as the rate of change with angle goes through 0. In other words, there must be a high convergence zone gain at about 5^{o}.

The conclusion is substantiated in Table 5 for δx_v. This spacing of the rays becomes a minimum for $\phi_1 = 5^o$ and then increases.

The computation of δs is shown in Table 8. There is a δs for each value of ϕ_1. However, since the range at first recedes and then increases as ϕ_1 is increased, there is an overlap of energy. Hence, in order to express loss as a function of range, it is necessary to add two intensities together. The intensity is inversely proportional to the spacing of the rays and therefore, the reciprocals of the δs's must be added and the reciprocal of the sum taken to get an effective δs. This work has been carried out to obtain the graph of excess loss vs range appearing in Fig. 15.

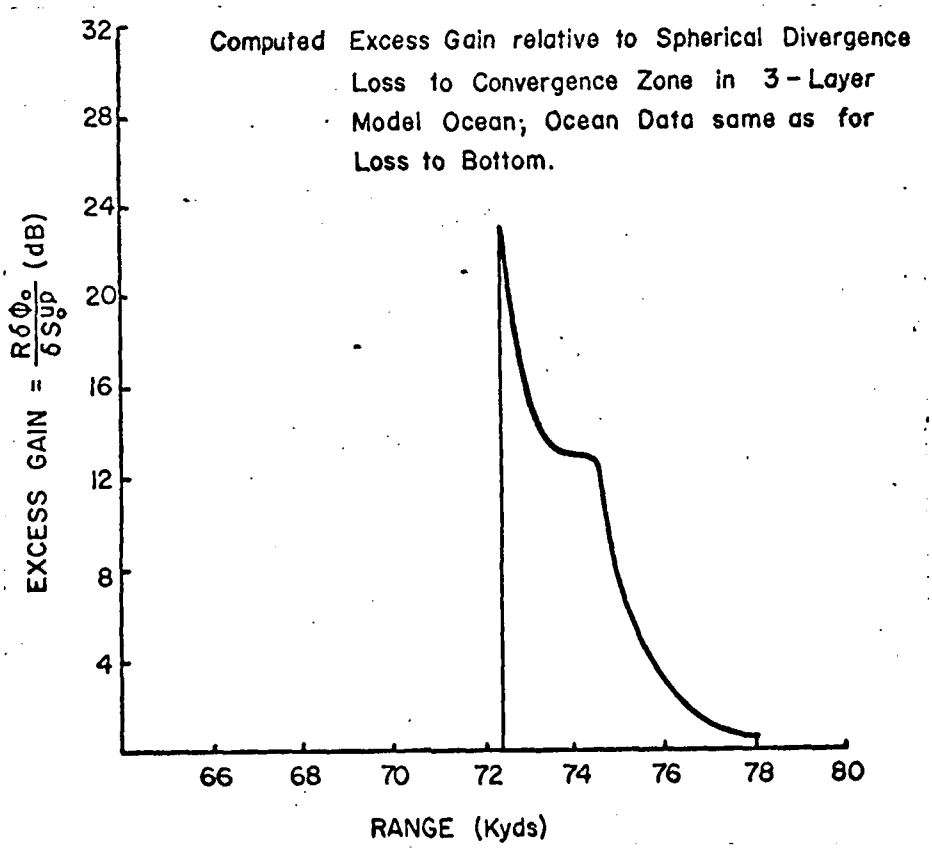

Fig. 15

In the figure, the high peak value due to convergence is observable at a range of 72480 yards. The height of this peak checks well with observation. The abrupt falling off at 74000 yards is due to the fact that the bottom has intercepted part of the energy that would have arrived there from steeper rays. This is a bottom cutoff.

The range calculated here is somewhat greater than that observed in the mid-Atlantic. This may be attributed to two factors, the stretching out that occurs for the small angle rays in the surface duct, and a value of g_2 which may be too low.

Any marked concentration of energy near the 0^o ray is prevented by the marked spreading of rays in the upper layer both on the upward and downward journeys. For this reason, we have computed convergence zone loss for a two layer case for which the upper layer has c_o = 1650 yds./sec., g_o = -.039/sec., z_1 = 1400 yds., and g_1 = .018/sec. For this case the curve of loss vs range is that of Fig. 16. Now it will be seen that there is a double peak with the rays near 0^o bunching up to form the peak at the longer range. The peak at minimum range remains. It will also be observed that here, where the gradient in the lower layer was taken somewhat higher, the range of the convergence zone is much shorter than in the preceding example. Lack of a surface duct also contributes to the shorter range.

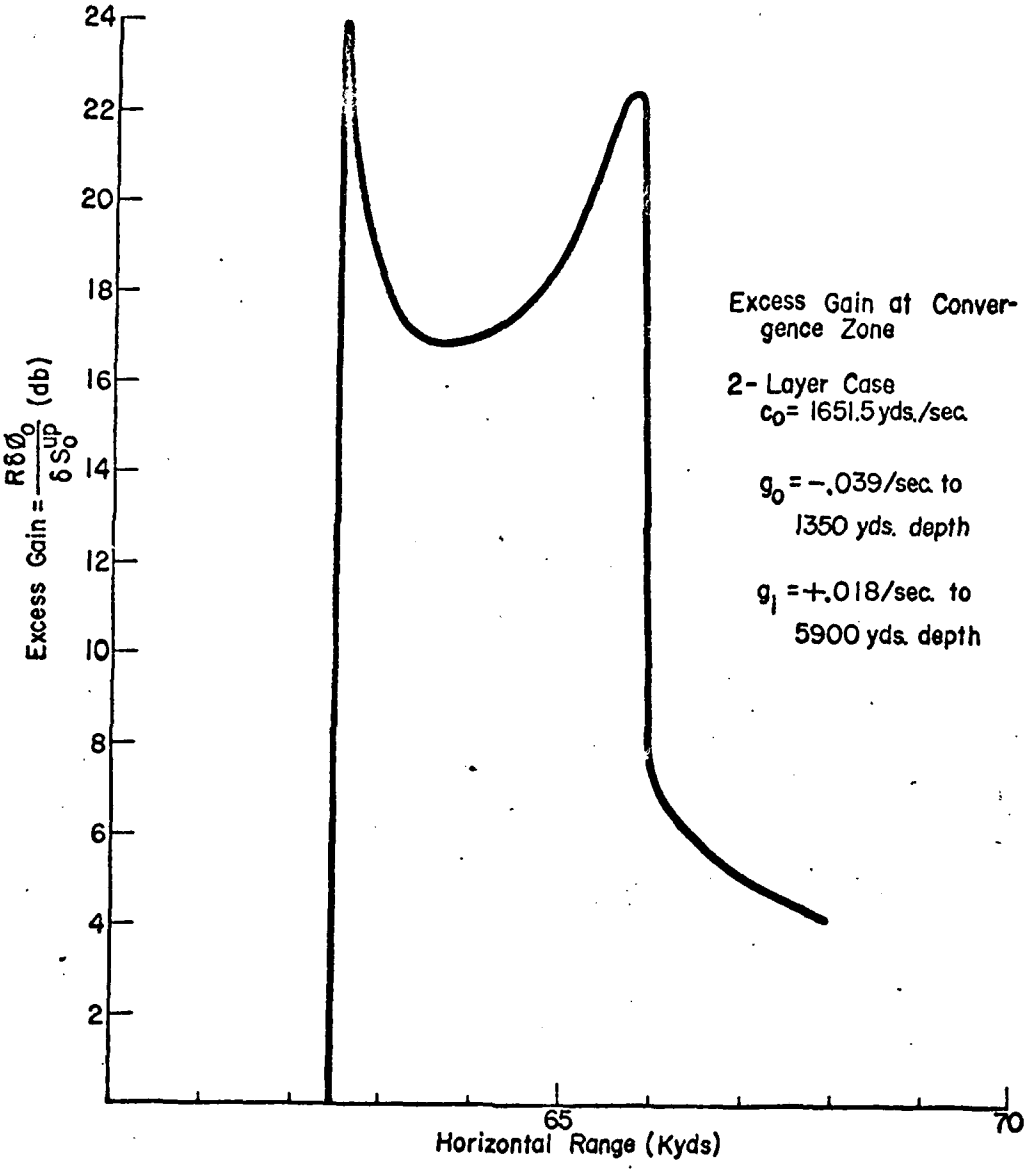
24
22
20
18
16
14
12
10
8
6
4
2
Excess Gain = $\frac{R\delta\phi_0}{6S_0^{up}}$ (db)
65
70
Horizontal Range (Kyds)
Excess Gain at Convergence Zone
2- Layer Case
c_0= 1651.5 yds./sec.
g_0 = -.039/sec. to 1350 yds. depth
g_1 = +.018/sec. to 5900 yds. depth

Fig. 16

Loss by Divergence in the Horizontal Plane

All the preceding computations for model oceans were excess loss resulting from the type of spreading that took place in vertical planes. There is additional small loss due to spreading in the horizontal given by 10 log $\frac{\cos \theta}{\cos \phi_o}$ with θ computed either to the point of incidence on the bottom or to the vertex of a ray which does not reach the bottom. For the model ocean which we have discussed in detail here, this loss comes out slightly negative meaning that there is a slight gain at the bottom and at the convergence zone. For some cases the loss may exceed 1 db. There is no problem in computing it.

For bottom bounce, the angle θ should be that made with the horizontal by a straight line to the point of incidence of the actual ray on the bottom. For convergence zone it should be the angle made with the horizontal by a straight line to the vertex or turning point of the actual ray. In both of these cases the excess loss in the horizontal is the same to the bounce or vertex as over the "round-trip" back to the surface.

Surface Duct Propagation

An important acoustic path to near-surface targets is the surface duct. This arises whenever a sound speed maximum at some depth exceeds any sound speed (maximum or otherwise) at lesser depth. The case of a linear gradient will illustrate the salient features. Here rays starting out at small horizontal angles travel through arcs of circles from surface to surface where they bounce and go through a repetition of the cycle. They are thereby trapped in what constitutes a surface-bounded duct.

We shall consider a constant, positive sound-speed gradient in which all rays are arcs of circles with radii of curvature given by Eq. (2).

Our first concern in this discussion is the question of what range of angles ϕ_o provides rays that stay in the duct. We shall resort to some approximations that are good because ϕ_o is small. We start by writing for the vertical distance from the source,

$$y = -\rho(\cos\phi - \cos\phi_o). \tag{37}$$

Letting $y = d$, the duct thickness, $\phi = 0$ and $\phi_o = \theta$ for the ray that vertexes at the bottom of the duct, we obtain

$$d = -\rho(1 - \cos\theta) \simeq -\frac{\rho\theta^2}{2}. \tag{38}$$

Solving the last equation for θ, we obtain $\theta \simeq \sqrt{2\,d/\rho}$. The range of angles at the surface of rays contained within the duct is 0 to θ. As an example, if $d = 50$ yards and $\rho = -90{,}000$ yards, then from Eq. (38) we have $\theta = 1/30$ radian or about 2^o.

The bundle of rays contained within the duct starts out experiencing spherical divergence and then bends around so that beyond the range where the limit ray reaches the bottom of the duct there is experienced, on the average, cylindrical divergence, all rays then contained within the duct being trapped and thereby restrained from further average spreading in the vertical. How can we express divergence loss acquired in the region of transition from spherical to cylindrical divergence? If the rays were to proceed in straight lines, each to its vertex depth, and then were to abruptly turn parallel to the surface, we would have the same rays contained as by the actual refraction.

The average divergence loss would then be spherical out to the range where all rays had turned and cylindrical thereafter. We shall compare this range where all rays would have turned with that at which the limit ray first vertexes.

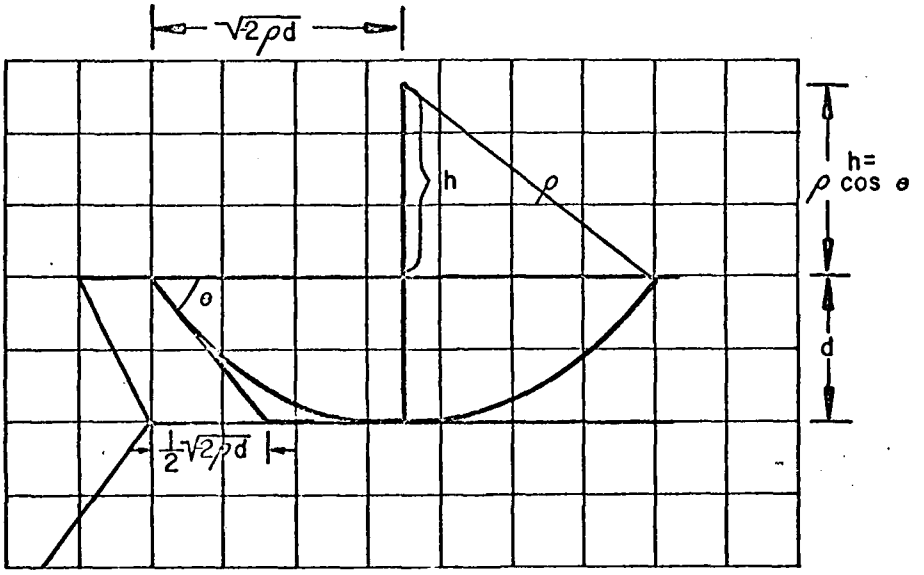

Equivalent Spherical and Cylindrical Divergence Losses

Fig. 17

In referring to Fig. 17, we note that the range x_v to the vertex of the trapped ray that penetrates deepest is given by

$$x_v = -\rho \sin\theta \simeq -\rho\theta = \sqrt{-2\rho d} \qquad (39)$$

with the last form following from Eq. (38). If the ray at this angle θ had traveled in a straight line to the bottom of the duct, the distance x_1

traversed would have been

$$x_1 = d \cot \theta \simeq -\frac{\rho\theta^2}{2} \cdot \frac{1}{\theta} = -\frac{\rho\theta}{2} = \frac{x_v}{2}. \qquad (40)$$

From this equation we conclude that the divergence loss is equivalent to spherical loss out to one-half the distance x_v given by Eq. (39) and is cylindrical thereafter. This statement applies to loss averaged in depth and at range beyond x_v. Mathematically, we have (x_o and r in yards)

$$\text{Divergence Loss} = 20 \log \frac{x_v}{2} + 10 \log \frac{r}{x_v/2}$$

$$= 10 \log \frac{x_v}{2} + 10 \log r. \qquad (41)$$

As an application of the foregoing results, let us take a case of constant temperature down to a depth of 50 yards, surmounting a pronounced negative gradient that limits the duct depth to 50 yards. The value of h, the vertical distance to the centers of curvature, will be taken as 90,000 yards corresponding to a sound speed at the surface of 1,620 yds./sec. and a gradient of .018/sec. From Eq. (38) we have $\theta = \sqrt{\frac{2d}{-\rho}} = \frac{1 \text{ radian}}{30} \simeq 2^o$. Then, from Eq. (39) and Eq. (40) we obtain x_v = 3000 yards and x = 1500 yards. At any range greater than 3000 yards, the following expression of divergence loss holds:

$$\text{Divergence Loss} = 10 \log 1500 + 10 \log r.$$

At 5000 yards, for example, this would give 68.8 db compared to spherical divergence loss all the way of 74 db.

We have hinted at a lack of uniformity within the duct from the surface to the bottom of the duct and would now like to examine this a little bit further. Since the surface is a pressure-release surface, the pressure variation there will be 0, and the normal component of particle velocity will double. If we were to plot pressure level versus depth, we would expect the pressure to rise rather rapidly from 0 at the surface to a maximum and then to fall off toward the bottom of the duct, in regions reached by only a few of the rays. (All the rays spend time near the surface.) This expectation agrees with actual observation in the field.

If this general picture were looked at in a little more detail, it would be found that there may be a number of maxima and minima of pressure from the surface to the bottom of the duct. The variation arises from propagation over multiple paths. For example, at short range there is a direct path and the surface-reflected path. Depending upon the two path lengths, the contributions of energy reaching a given point over the two paths will have a phase relationship that may be anything. At some ranges and depths there will be constructive interference; at other ranges and depths there will be destructive interference.

An interesting phenomenon within the duct is the existence of a caustic. This is a surface on all points of which neighboring rays are crossing each other. This caustic occurs after any ray has experienced one surface bounce. It will now be shown that the crossing of adjacent rays takes place at 4/3 of the space cycle from the source at the surface to the next incidence on the surface.for the case of one bounce only. There are other crossings further out.

We had the expression for ray depth in terms of angle ϕ with the horizontal as

$$y = -\rho(\cos\phi - \cos\phi_o). \tag{37}$$

The x distance out to some point beyond the first surface reflection is given by

$$\begin{aligned} x &= -\rho(3\sin\phi_o - \sin\phi) \\ &= \frac{-h}{\cos\phi_o}(3\sin\phi_o - \sin\phi). \end{aligned} \tag{42}$$

The first term in parentheses in Eq. (42) gives the distance out to the second vertex. The second term backs off toward the position of surface bounce. Substituting the value of $\sin\phi$ in terms of $\cos\phi_o$, we obtain

$$x = \frac{-h}{\cos\phi_o}\left[3\sin\phi_o - \sqrt{\left(1 - \frac{c^2}{c_o^2}\cos^2\phi_o\right)}\right]. \tag{43}$$

This expression for x contains no variables except ϕ_o provided that y is held constant so that c is constant. We may therefore differentiate it with respect to ϕ_o to determine the conditions under which the derivative is stationary, indicating crossing or osculations of rays. We obtain

$$\frac{dx}{d\phi_o} = -3h\sec^2\phi_o + \frac{h\sec^2\phi_o\tan\phi_o}{\sqrt{\left(\sec^2\phi_o - \frac{c^2}{c_o^2}\right)}} = 0. \tag{44}$$

Dividing by h $\sec^2 \phi_o$ and manipulating, we obtain

$$\sin \phi = \frac{\sin \phi_o}{3} \tag{45}$$

or approximately

$$\phi = \frac{\phi_o}{3}. \tag{46}$$

We substitute this value of ϕ in Eq. (37) and Eq. (42) to obtain parametric equations for x and y at the caustic, as follows:

$$y_1 = \frac{-h}{\cos \phi_o} \left(\cos \frac{\phi_o}{3} - \cos \phi_o \right) \simeq - \frac{4}{9} h \phi_o^2, \tag{47}$$

and

$$x_1 = \frac{-h}{\cos \phi_o} \left(3 \sin \phi_o - \sin \frac{\phi_o}{3} \right) \simeq - \frac{8}{3} h \phi_o \tag{48}$$

both good for small angles. Eliminating ϕ_o between Eq. (47) and Eq. (48), we obtain the equation relating x_1 to y_1 along the caustic as follows:

$$x_1^2 = -16 h y_1, \tag{49}$$

which is a parabola, as tabulated below for h =-87 kyds., a realistic value.

x(kyds.)	0	1.68	2.36	3.36	4.72	6.72	8.38
y(yds.)	0	2.00	4.00	8.00	16.00	32.00	50.00

Reliable Acoustic Path

We shall use our model ocean as the medium for the computation of the reliable-acoustic-path rays. The source depth required in order that an initially horizontal ray vertex at layer boundary one is that for which the sound speed is c_1. The vertical space interval below layer boundary two is $y_{2,3}$. The sound speed there is

$$c_3 = c_1 = c_2 + g_2 y_{2,3}$$

from which

$$y_{2,3} = \frac{1651.5 - 1594.8}{.016} \text{ yds}$$

$$= 3544 \text{ yds.}$$

This leads to $y_3 = 4944$ yds as source depth. Since all of the ray angles at the source are the same as at the first layer boundary, except for sign, we have a ready made set of angles for which most of the computations have been completed. Upward rays at the source will have ϕ_1 negative; downward rays will have ϕ_1 positive. The ρ_1 for any ϕ_3 will be that already determined for the same ϕ_1. The ρ_0 and ρ_2 will be the same as accompanied the corresponding ρ_1 before. The $\delta\phi_3^{up}$ will be taken arbitrarily as -.005. Then $\delta\phi_1^{up}$ will be -.005 and $\delta\phi_0^{up}$ will be that determined before for the corresponding ϕ_1 except for sign.

The change here is of course the depth y_3. This will lead to new $x_{3,2}$ and $\delta x_{3,2}$ but $x_{2,1}$, $x_{1,0}$, $\delta x_{2,1}$ and $\delta x_{1,0}$ are already computed for any given ϕ_1 now equal to ϕ_3 except for sign. We record in Table 1 the salient data.

ϕ_3	x_o^{up}	$\delta x_{3,2}$	$\delta x_{2,1}$	$\delta x_{1,o}$	δx_o^{up}	δs_o^{up}	$r\delta\phi_3$	Excess Gain
$+8^o$	+51701	-780.3	+103.7	+11.8	-664.7	+96.7	+259.6	+4.3
$+6^o$	+47124	-721.5	+122.7	+19.8	-579.0	+65.4	+236.9	+5.6
$+4^o$	+43486	-657.9	+144.5	+38.9	-474.5	+40.9	+218.8	+7.3
$+2^o$	+40706	-590.5	+168.8	+94.4	-327.3	+19.1	+205.0	+10.3
$+1^o$	+39779	-551.0	+183.2	+172.8	-194.7	+9.3	+200.4	+13.3
0^o	+39365	-511.1	-194.7	-259.2	-965.1	+49.7	+198.4	+6.0
-1^o	+36177	-481.6	-183.5	-172.8	-837.8	+44.9	+182.5	+6.0
-2^o	+33497	-443.0	-168.8	-94.4	-706.2	+43.5	+169.2	+6.0
-4^o	+29050	-379.3	-144.5	-38.9	-562.7	+49.0	+147.3	+4.8
-6^o	+25427	-322.2	-122.7	-19.8	-464.7	+52.5	+129.4	+4.0
-8^o	+22689	-272.3	-103.7	-11.8	-387.8	+56.4	+116.0	+3.1
-10^o	+19919	-230.4	-87.8	-8.0	-326.0	+58.3	+102.5	+2.5
-14^o	+15987	-166.5	-63.4	-4.0	-233.9	+57.4	+83.5	+1.6
-20^o	+12009	-107.5	-41.0	-2.1	-150.6	+51.9	+64.8	+1.0

Reliable Acoustic Path
Source Depth 4944 Yds.

Table 1

For the initially downward rays, ϕ_3 positive, x_o^{up} consists of a horizontal distance traversed in going down to the turning point and returning to source depth plus a horizontal distance exactly the same as for the ray for which ϕ_3 was negative and of the same magnitude. In traversing the distance to the turning point and back up to source depth, the neighboring ray travels a shorter horizontal distance than the reference ray so that δx for this segment of the path is negative, just as it is for every segment of an upward directed ray with a negative $\delta\phi_3$. Here the similarity ends because $\delta\phi_3$ at the source was negative but after the excursion to the turning point and back to source depth, it has become positive. Hence, from this level on up to the surface all $\delta x_{i,j}$ are positive and the pair of rays come closer and closer together. In the

table $\delta x_{2,1}$ and $\delta x_{1,0}$ will be seen to be positive for positive ϕ_3. As a result, δx_0^{up} experiences a large jump in going from initially downward rays through $\phi_3 = 0$ to initially upward rays. For the case of $\phi_3 = 0$, the value is relatively high as with the upward rays because ϕ_3 was given a negative value making the neighboring ray an upward ray. If $\delta\phi_3$ had been given a positive value, δx_0^{up} would have been even smaller for $\phi_3 = 0$ than for $\phi_3 = +1$. In other words, there is an abrupt break in the curve at $\phi_3 = 0$. The small value of δx_0^{up} at 1^o reflects in the value of δs_0^{up} and represents a high gain as shown in the table. Gain versus angle ϕ_3 is plotted in Fig. 18 and gain versus horizontal range is plotted in Fig. 19.

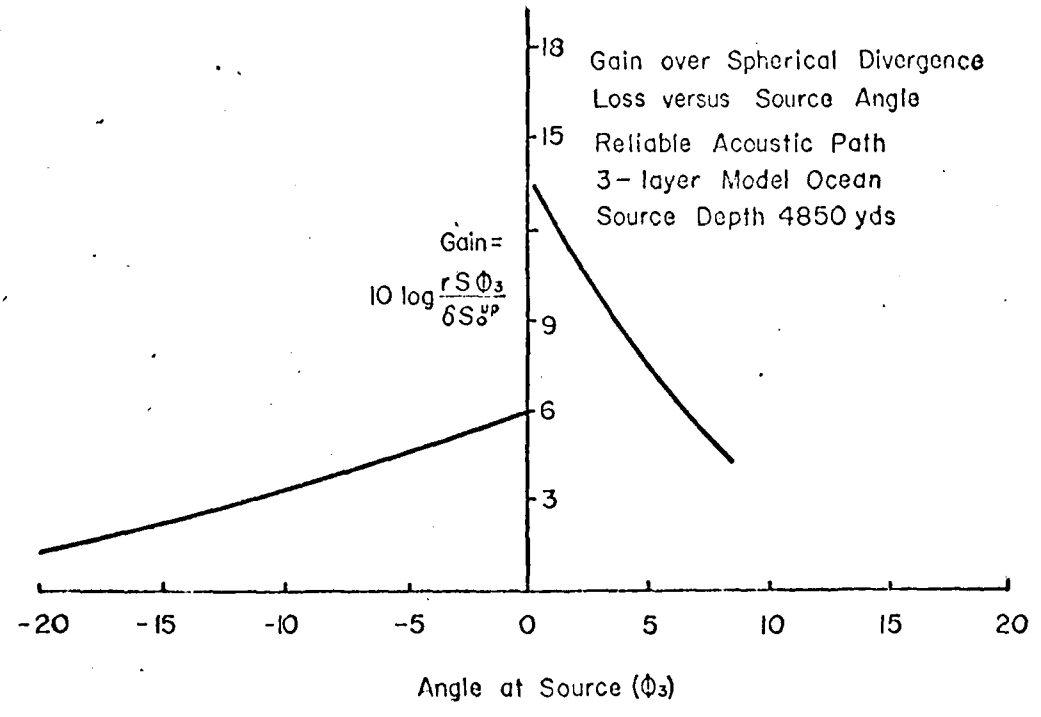

Fig. 18

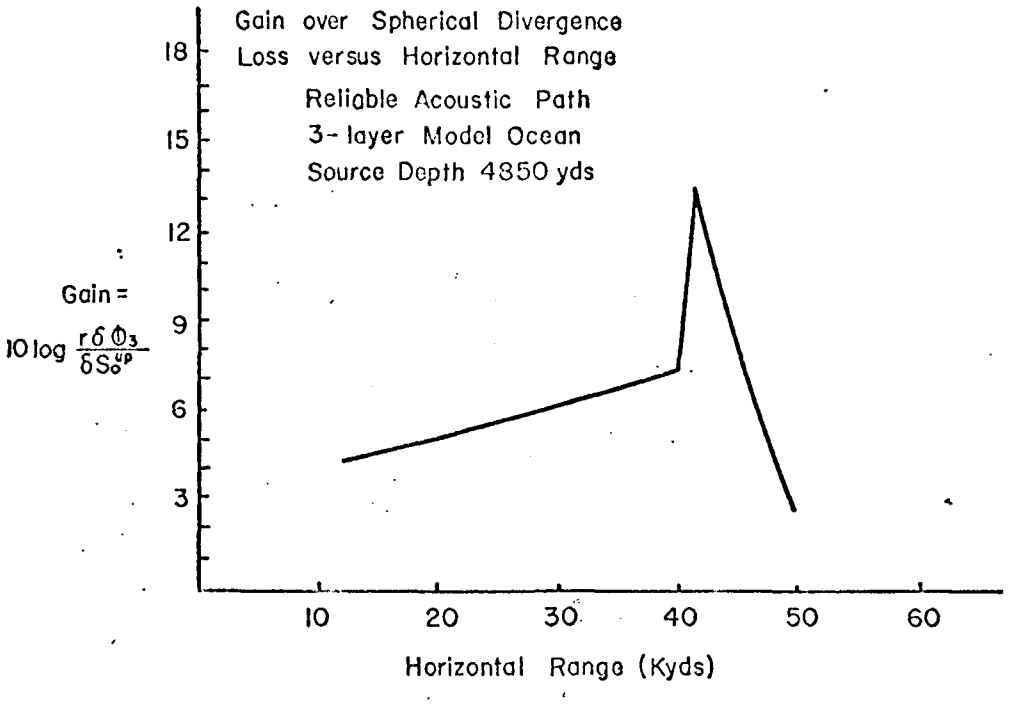

Fig. 19

This break in the curve has not been recognized in experimental data. This is probably attributable to the presence of large fluctuations over multiple paths, one of which enjoys a surface bounce before reception at the end point. With very short pulses and the hydrophone at sufficient depth the break should be detected, somewhat smoothed by diffraction.

The importance of the reliable acoustic path has already been discussed in the general descriptions at the beginning of this report. Now, the actual computations show that for this specific case very long ranges are reached, and of course, the insonification of the surface is continuous from directly over the source out to these ranges.

In the above table, the simple formula, Eq. (31) was used for angles ϕ_o^{up} of absolute value greater than 4^o, but the more accurate Eq. (32) together with Eq. (33) was employed for the smaller angles.

Excess gain in the horizontal is small and may be either positive or negative at different ranges. At the longer ranges there is a slight excess loss.

ATTENUATION

The term attenuation applies to any propagation loss that is expressible in terms of decibels per kiloyard. It includes primarily absorption, which is conversion to heat of a certain percentage of the remaining energy in each kiloyard of travel. It also includes loss by volume scattering, and in the special case of sound propagating in a surface-bounded duct it includes loss by surface scatter and diffraction out of the duct. Attenuation by any of these mechanisms is a function of frequency and ocean characteristics.

Absorption

Absorption in sea water has been measured in the laboratory with results partially shown in Fig. 20. It will be noted from the shape of the curves that absorption increases approximately as the square of the frequency. Different curves are given for different temperatures. It is thus apparent that there is a temperature dependence with less absorption at higher temperature. There are other dependencies that the curves do not show.

There is a dependency on magnesium sulphate content, which is credited with the jog in the absorption curve at high frequency, resulting in higher

absorption at low frequency than in water free from this salt. This mechanism is a relaxation phenomenon.

The dependence of absorption on pressure is not fully understood. However, losses over long acoustic paths near the axis of the deep-sound channel in the Atlantic (depth of about 1400 yards), reported by Thorp, indicate much higher attenuation of low frequencies at the relatively high pressure. Explosive charges were used as sources and comparisons at several long ranges permitted the assumption of cylindrical divergence loss in the space intervals between measurements. When the divergence loss was subtracted from the total, the higher-loss curve of Fig. 21 was obtained. Here attenuation is plotted against frequency. The curve appears

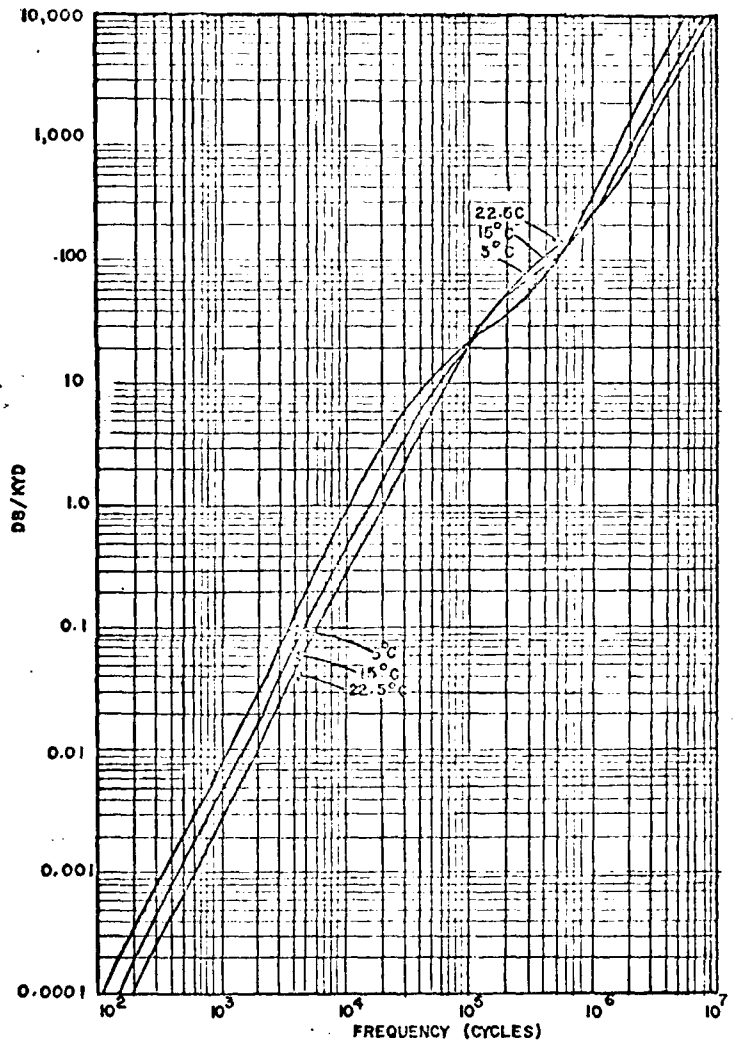

Absorption in Sea Water

Fig. 20

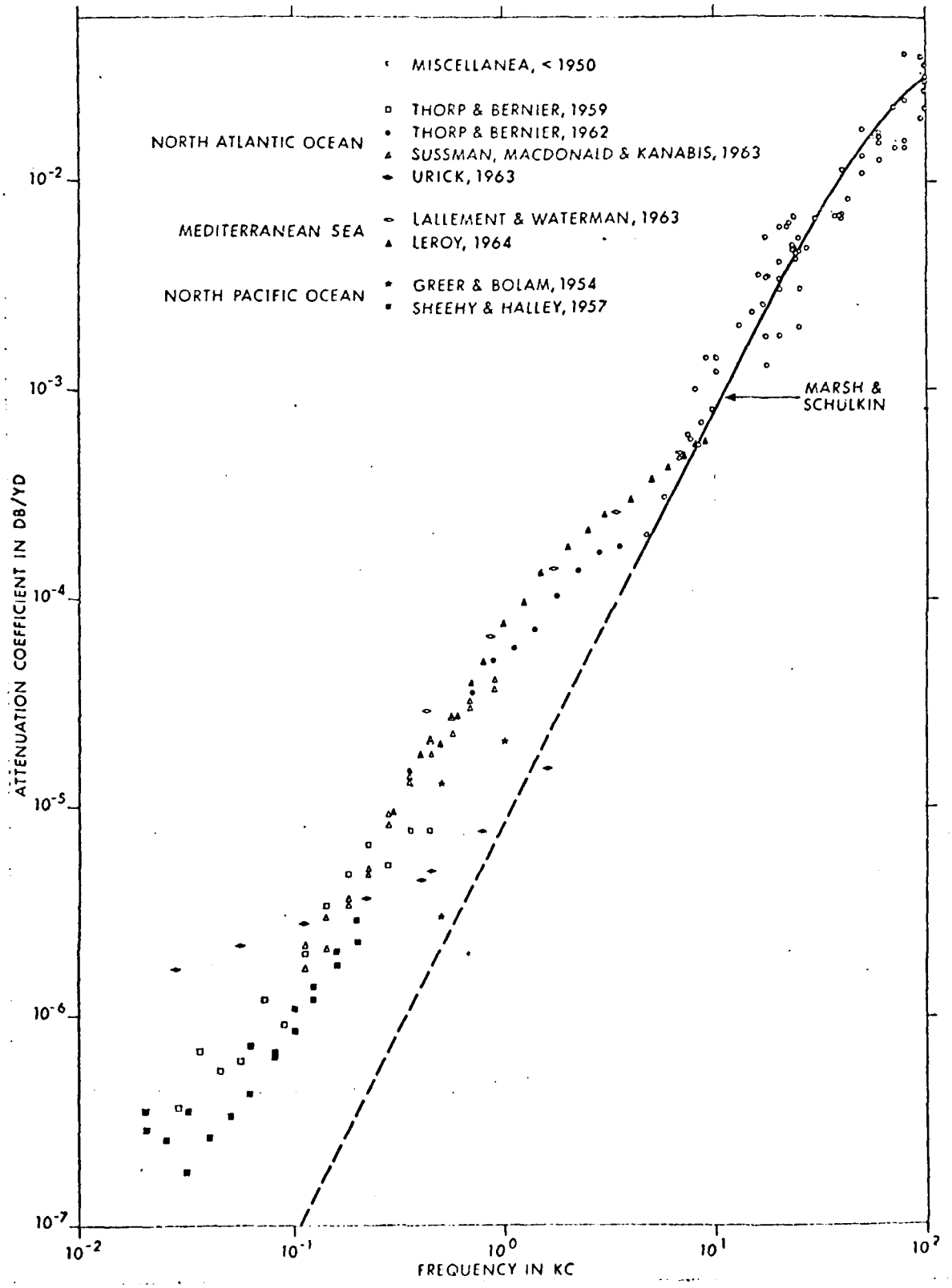

Absorption in Sea Water in Deep Sound Channel

Fig. 21

to fair into the low-pressure, lower-loss curve above 5 kc. The shape suggests a relaxation phenomenon so far observed only at high pressure. There is a trend toward the use of the Thorp loss curve for the whole path to the convergence zone and for the whole bottom-bounce path in deep water. This trend, adopted here, will affect the computation of bottom-reflection loss to be discussed later.

In practice, measurements in the ocean nearly always show propagation loss to exceed that calculated from divergence plus that from absorption using the laboratory-produced curves. In the case of low-frequency sound at high pressure, the Thorp curve includes the added attenuation. Part of this excess may be added absorption caused by the presence of bubbles.

We are fairly sure of absorption by bubbles in the case of propagation in surface-bounded ducts. As a matter of fact, some laboratory measurements have required repeated degassing of samples before the standard or accepted curves of Fig. 19 were obtained. Schulkin[5] has obtained a formula for attenuation by bubbles in db per limit-ray cycle that matches a curve compounded of AMOS data and NRL data. The curve is presented in Fig. 21. The formula is

$$\alpha_s = 1.64\ (fh)^{1/2}, \tag{50}$$

in which α_s is attenuation by bubbles in db per limit-ray cycle, f is frequency in kHz, and h is mean wave height in feet.

Schulkin's formula may be converted to db/kyd by dividing by limit-ray cycle and multiplying by 1000. The limit-ray cycle is $2\sqrt{2\rho d}$, in which ρ is radius of curvature in yards and d is duct thickness in yards. (The value is

$\rho \simeq 90{,}000$ yards in a mixed layer). This gives

$$\alpha_L^1 = \frac{582}{\sqrt{\rho d}} (fh)^{1/2} = \frac{1400}{\sqrt{\rho d}} (.3f^{1/2})(1.39h^{1/2}). \qquad (51)$$

The last form is presented in order to compare with Saxton's empirical formula,

$$\alpha_L = \frac{1400}{\sqrt{\rho d}} (\log f)(1.4^n), \qquad (52)$$

in which n is sea state. The quantity $.3f^{1/2}$ in α_L^1 agrees with log f at 10 kc where Eq. (52) is believed particularly reliable. The remaining factor of α_L^1, i.e., $1.39h^{1/2}$, has a generally similar shape to 1.4^n, but comes out appreciably lower valued at sea states above 4. The author accepts Shulkin's formula, Eq. (50). Its excellent fit with data is shown in Fig. 22 which is reproduced from Shulkin's report.

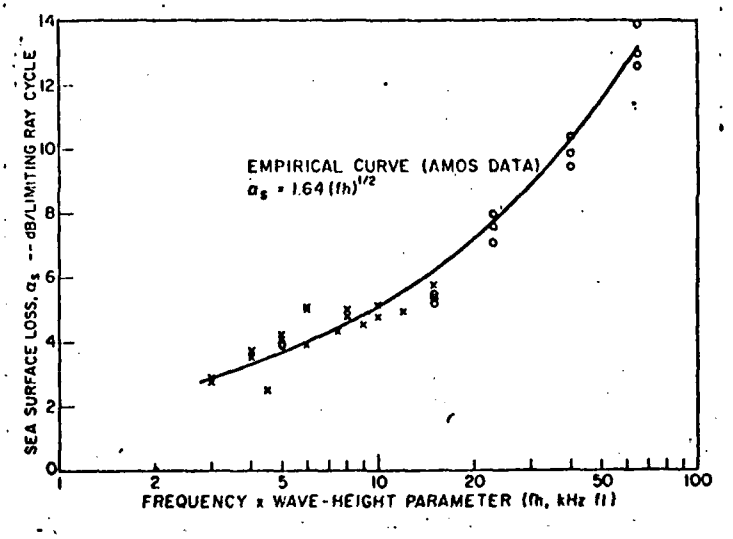

Fig. 22

Sea surface loss (decibels/limiting ray cycle) versus frequency x wave-height parameter (kilohertz feet) for surface sound channels. The solid curve represents an empirical fit to the AMOS data for 2.2-25 kHz (Ref.3). The crosses are for data obtained from Baker, Pieper, and Searfoss (Ref.4), and the circles are for data reduced from Saxton, Baker, and Shear (Ref.5). For comparison, the dashed theoretical curve is presented for sea surface scattering from Marsh, Schulkin, and Kneale (Refs. 18 and 19).

References in caption for Fig. 22 are those of Schulkin[5].

Scattering Loss in Surface-duct Propagation

Scattering loss in the duct is in db/kyd and is therefore a part of attenuation. Measurements of sound levels below the surface duct in what is commonly called the shadow zone show that there is sound energy there considerably in excess of the diffracted energy predicted by normal-mode theory that has been applied to the ideal case of a perfectly flat surface. This deficiency in the theory has been corrected in a paper by Bucker[7] that was published in January, 1969, issue of the U. S. Navy Journal of Underwater Acoustics. An explanation is not given in this text. The leakage may be several times as great as predicted by normal-mode theory for a smooth surface. This result must be attributed to scatter from the rough surface or from bubbles.

The totality of mechanisms of attenuation in the duct are absorption augmented by bubbles, scattering from the surface (and bubbles), and loss by diffraction. All of these combined give an attenuation coefficient that the author has designated $\alpha_o + \alpha_L$, where α_o is the absorption coefficient only (as measured in the laboratory) and α_L is the coefficient for all other contributors. The coefficient α_L has been discussed under "Absorption," the previous subheading, but now we claim a portion of α_L, let us say half, as loss by scatter.

Scattering out of the duct may be quite important. Let us consider some of the mechanisms involved in scatter. The one that we shall treat here is the result of sound energy incident on the surface impinging on facets of the rough surface boundary, which presents various angles with the horizontal. If the facet size is large enough (say a facet has dimensions greater than one wave length), it will scatter an appreciable amount of energy in a beam.

We must mention in passing that scattering can be produced by bubbles associated with surface roughness, and there can also be absorption introduced by these bubbles. Measurements have not revealed which mechanism is predominant. Patches of warm or cold water have been observed near the lower boundary of the duct, but their scattering ability appears slight.

In surface scatter it is desired to determine the distribution of incident energy with respect to grazing angle.

Near the source, within the small angular limits of ducted energy, intensity may be considered independent of angle. If the source is very near the surface, rays initially directed horizontally will traverse only a slight distance to their first surface bounce. The limit ray (that vertexing at the bottom of the duct) may travel several thousand yards before its first surface bounce. The more bounces there are, the faster will energy shift out of a mode because of scatter. Thus, a larger and larger portion of the total energy will be represented by the deeper going rays until a condition is reached in which a small fraction of this energy in the deep-running rays scattering out largely replenishes the large fraction of the energy of the shallow rays scattering out, after which equilibrium will be achieved. We shall introduce mathematics to describe the equilibrium distribution obtained.

We shall now embark on a dissertation on angular distribution of power in the duct at equilibrium. It will be assumed that surface scattering per bounce (fractional loss per bounce) is independent of angle of incidence over the narrow range of angles ϕ_o of trapped rays. We shall let power per

unit angle (for any desired extent in the horizontal) be $P(\phi)$ within the limits of the vertical angle ϕ at the surface for trapped rays, namely 0 to θ. This same power stays in the same small θ indefinitely unless absorbed or scattered out. We ignore absorption in the following.

For any given ϕ_1, the number of surface incidences per kiloyard will be $\frac{1}{2\rho\phi_1}$ with ρ in kiloyards, ϕ_1 in radians. At each surface bounce $P(\phi_1)$ will be multiplied by some factor $\delta<1$, and after $\frac{1}{2\rho\phi_1}$ incidences this power will be $P(\phi_1)\delta^{\frac{1}{2\rho\phi_1}}$.

In addition to the original power $P(\phi_1)\Delta\phi_1$, in any $\Delta\phi_1$, which is continually decreasing, there is power scattering back into $\Delta\phi_1$ as the $\Delta\phi$ outside of $\Delta\phi_1$ lose it. Let us suppose that a fraction s of the total trapped power P_t is redistributed uniformly over the angles trapped in each kiloyard of travel so that a fraction $\frac{\Delta\phi_1}{\theta}$ of sP_t goes into the $\Delta\phi_1$ under consideration. Adding this, we have

$$\text{Power in } \Delta\phi_1 \text{ after 1 kyd} = \left[P(\phi_1)\delta^{1/2\rho\phi_1} + \frac{sP_t}{\theta}\right]\Delta\phi_1. \qquad (53)$$

Now when some distribution of power in ϕ is stable, which is the condition sought, then every part of this distribution must lose the same fraction of intensity per kiloyard. If α_L is loss per kiloyard in db, then in absolute value the remaining power in $\Delta\phi_1$ after one kiloyard is $10^{-.1\alpha_L} P(\phi_1)\,\Delta\phi_1$, which may be equated to the right side of Eq. (53). Then solving for $P(\phi_1)$, we obtain

$$P(\phi_1) = \frac{sP_t}{\theta\left(10^{-1\alpha_L} - \delta^{1/2\rho\phi_1}\right)}. \qquad (54)$$

If $P(\phi_1)$ in Eq. (54) were to be integrated over ϕ from 0 to θ, we should obtain total trapped power. Integration appears rather difficult, but it is a simple matter to sum the powers in n small equal increments of angular width $\Delta\phi$ with a computer program to approximate the result of integration. Then we have, putting $n\,\Delta\phi = \theta$, and designating the angle of the midray within an increment by a subscript i

$$P_t = \sum_{i=1}^{n} P(\phi_i)\Delta\phi = sP_t \frac{1}{n} \sum_{i=1}^{n} \left(\frac{1}{10^{-.1\alpha_L} - \delta^{1/2\rho\phi_i}} \right), \tag{55}$$

from which

$$s = \frac{n}{\sum_{i=1}^{n} \left(\frac{1}{10^{-.1\alpha_L} - \delta^{1/2\delta\phi_i}} \right)} \tag{56}$$

Substituting Eq. (56) into Eq. (54) with a generalized subscript j, we have

$$P(\phi_j)\Delta\phi/P_t = \frac{\left(\frac{1}{10^{-.1\alpha_L} - \delta^{1/2\rho\phi_j}} \right)}{\sum_{i=1}^{n} \left(\frac{1}{10^{-.1\alpha_L} - \delta^{1/2\rho\phi_i}} \right)} \tag{57}$$

In using these formulas, some value of α_L is accepted. This may be about half the value of the anomalous absorption coefficient α_s of Eq. (50) the remainder of α_s being ascribed to absorption by bubbles. Next, since δ is a proper fraction, $\delta^{1/2\rho\phi_i}$ is largest for maximum ϕ_i, that is, for θ. Its largest permissible value must leave $\left(10^{-.1\alpha_L} - \delta^{1/2\rho\phi_i}\right)$ positive. We have to choose some δ with the above limitation. Then the distribution can be computed. Typical curves are shown in Fig. 23. In these curves we have used $\bar{r} = P_t/n$ instead of

P_t of Eq. (57). With δ arbitrary the result is not completely satisfying, but it does relate the general shape of power distribution with respect to ϕ to a mechanism.

At present we do have measured values of α_L determined to account for otherwise unexplained loss in ducts. These values include excess absorption by bubbles, but some portion like half of the db may be applicable here. Perhaps this theory may lead to some experimental tie-in with the value of δ.

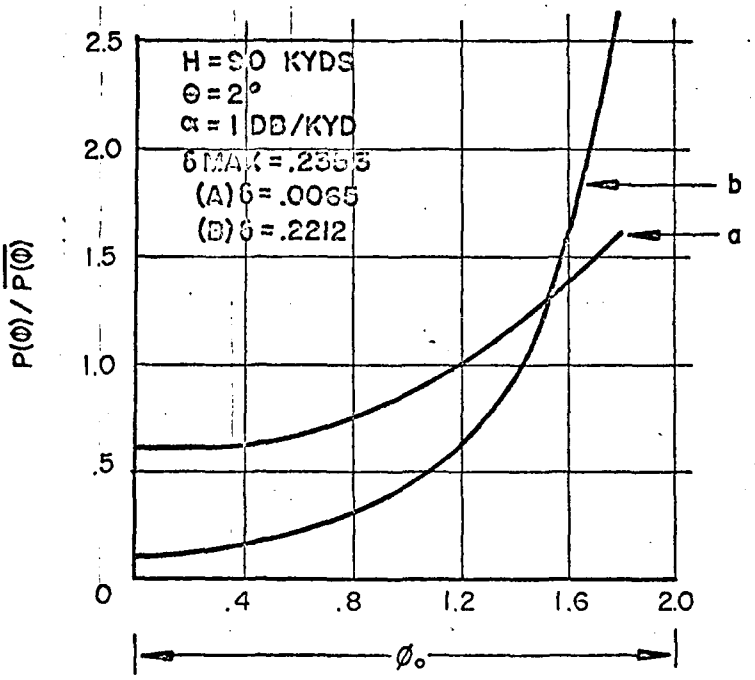

Distribution of Power with Respect to Grazing Angle ϕ_o in Surface Bounded Duct

Fig. 23

REFLECTION LOSSES

Reflection losses are of two kinds, those at bottom reflection and those at surface reflection. Loss resulting from repeated incidences in surface-duct propagation has been treated. Our next interest is in single bounce losses.

Our treatment will utilize a simple model that assumes specular reflection. It is known that reflection may be pure scattering at times, and some of the implications of scattering will now be discussed qualitatively since no quantitative theory is available. Then we shall come back to the usual simple model in order to use empirical formulas.

Scattering from the bottom is related to bottom topography, which modifies the image of the source transducer radiating the energy that produces the sound field. The inverse square law applies in the far field of a transducer (or is approximated when there is refraction). The far field is defined from the requirement that on the axis of the sound beam, the distances from a field point to all points on the transducer radiating face differ by no more than a small fraction of a wave length. (This definition applies strictly to a plane radiating face, but it is adequate for our discussion.) The distance from the transducer to the far field is relatively short, and all points on the bottom are in the far field. With specular reflection at the bottom, the field points after reflection see the image of the transducer and, on the axis of the reflected beam, are substantially equidistant from points on the face of this image. Therefore, the inverse square law holds for this case after reflection with distances reckoned from the source or its image. Reflection loss may occur from a portion of the power being drained off by penetration into the bottom or by passage through absorbing sediments and strata before reflection.

By Huygens' principle we could reconstruct the field after reflection by integrating the simultaneous contributions to any field point from all elements of the insonified bottom. Without actually attempting to go through this process, it is obvious that different elements of the bottom will contribute a variety of phases at the field point. Then, in order for the results to agree with the actual situation in which there is energy in the beam and substantially no energy outside the beam, these phases must balance in a delicate way.

If the bottom is rough, the image of the transducer is no longer clearly visible at points in the scatter field. However, Huygens' principle can still be applied and now obviously the integration over this rough bottom involves perturbed phases, giving a different result. The specular direction no longer has to be a preferred direction. Energy is scattered in every direction. This mechanism gives rise to a scatter field of the bottom considered as a new source. The scatter field now is from an area so large that field points of interest are in the near field, and this field is expected to be characterized by a multiplicity of very narrow lobes, possibly of only a few feet in width where they intersect the surface. Hurdle et al[8] have presented evidence of this field structure.

When this last mechanism exists, the term "reflection loss" is a misnomer. We are dealing with scattering rather than reflection. A loss in excess of divergence loss plus attenuation is to be expected, but this excess loss is an extremely complicated function of scatter angle and range.

At our present level of understanding of the scattering process, we do not know how to modify the simple reflection model in order to use scatter coefficients effectively. We shall therefore somewhat reluctantly accept the reflection model for the present. Let us say that measurements disclose a loss in excess of divergence loss and attenuation that will be called reflection loss.

What is measured is total one-way loss over the bottom-bounce path. The depth needs to be determinable from transit time in order that grazing angle to the horizontal may be computed for assumed specular reflection since it develops that the loss depends upon grazing angle. When divergence

loss and attenuation in db are subtracted from the total loss in db, we are left with the reflection loss. While it is not expedient to publish curves at this time, certain general statements about reflection loss may be made. At first glance the results are so highly variable as to seem almost random except when the bottom is known to be smooth and flat. For this case, the reflection loss in db is a few decibels and depends on grazing angle, being maximum at about 45°. The loss for this case could conceivably go to 0 at 0° grazing angle. As the bottom topography gets rougher, the reflection loss increases getting higher as roughness increases. The increased loss could be up 20 decibels or higher. With bottom roughness the curves cannot approach 0 at 0° angle since 0° angle cannot exist with all simultaneously reflecting portions of the bottom. When calculations in the low-frequency region assume Thorp attenuation, a fair average value over all deep-water terrains is 8 db per bounce. To get representative performance, we should carry out computations for cases of average, 5 db above average, and 5 db below average values. The association of each computation with specific areas is beyond the scope of this presentation but it may be mentioned that some work in this area has been carried out, notably by NUSL.

COMPUTATION OF TOTAL LOSS

Up to this point we have discussed the kinds of loss that may be encountered. We now proceed to put them together for each of the important acoustic paths to give total one-way loss.

We may write a formula for total loss H that includes losses, some of which are 0 for specific paths. We have

$$H = \text{divergence loss} + \text{attenuation} + \text{reflection loss}. \qquad (58)$$

Divergence loss includes corrections for refraction. Attenuation includes losses by absorption and scatter, and reflection loss is that at the bottom and that at the surface.

Direct Path to Short Ranges

This case is a simple one in which loss is comprised of spherical divergence loss, 20 log r, plus absorption. If the path is from shallow source to deep target at a ϕ_o of, let us say, 20^o or greater, the simple absorption α_o may be used. If the path is to stay near the surface, absorption by bubbles will be a factor, but for the direct path surface scattering will not be a factor. Therefore, in addition to spherical divergence there will be an absorption $\alpha_o R$ augmented by an additional absorption of only about $\frac{1}{2}\alpha_L \times R$. The R is range in kiloyards whereas r is range in yards.

Propagation loss over the paths followed by the rays that come close to the shadow zone below the surface duct will show an increased loss of a few db over spherical divergence loss. It would be unwise to anticipate good operation over these rays that emerge from the surface-bounded duct at angles of up to, let us say, 3^o.

Bottom-bounce Path

For this case divergence loss is very nearly spherical. A slight gain over spherical may be experienced in the rays incident on the bottom at very small grazing angles such as a few degrees. The gain in this case may be of the order of 2 or 3 db. Additionally, there is absorption for which the Thorp curve should be used and bottom reflection loss using three values of, let us say, 3 db, 8 db, and 13 db. Except for very precise work, the dependence of reflection loss on grazing angle may be ignored.

Convergence-zone Path

The divergence loss to the convergence zone may be considered to be spherical to about 1600 yards range and cylindrical thereafter. The Thorp curve should be used for attenuation. The range in mid-North Atlantic is about 70 kiloyards and in mid-North Pacific about 60 kiloyards.

Surface-bounded Duct

Beyond the range at which the limit ray vertexes, the divergence loss is spherical to half this distance plus cylindrical thereafter. At very short range, possibly out to one quarter of the distance to the vertex, spherical divergence loss may be used. If level is then plotted against range for very short range and for relatively longer ranges, the two curves may be faired together smoothly. The attenuation is $\alpha_o + \alpha_L$ in each kiloyard of range. A part of α_L is caused by the presence of bubbles, and another part is caused by scattering from the surface. Measurements of total loss do not distinguish well between these two mechanisms.

Reliable Acoustic Path

Divergence loss over paths from the deep source starting out nearly horizontally will in general be less than spherical by several db. If the rays strike the surface at angles greater than 10^o, the loss will be very nearly spherical. In addition, the Thorp absorption curve should be used.

Paths Involving Isolated Surface Bounces

The bottom-bounce path really includes paths from source to surface to bottom to target, from source to bottom to surface to target, and from source to surface to bottom to surface to target. These paths involve, in addition to a bottom reflection loss, also one or two surface reflection losses. This

situation is quite different from the surface reflection loss encountered in propagation in ducts. The loss per bounce obviously depends upon the sea state. It varies from a negligible amount in sea state 0 to about 8 db per bounce in sea state 6 at the frequencies employed.

Over the path to two or more convergence zones there is a surface bounce at each skip distance. Here again the loss may vary with sea state between the limits of 0 db and about 6 db, the upper value being reduced somewhat by the relatively small grazing angles for this path at the low frequencies which must be employed.

WAVE EQUATION

Introduction

When a vibrating motion is imparted to an elastic medium, this motion is propagated through the medium in the fashion described mathematically by the solution of a wave equation. For example, the simplest wave equation is

$$\frac{\partial^2 \psi}{\partial x^2} = \frac{1}{c} \frac{\partial^2 \psi}{\partial t^2} \tag{59}$$

for a plane wave in the x direction in a fluid medium. The variable t is time; c is sound speed, assumed constant for the present, and ψ is some state of the medium such as particle velocity, pressure increment, or a potential function from which the other two quantities may be derived. A solution of Eq. (59) is

$$\psi = A \cos\left[k(ct - x)\right] + B \cos\left[k(ct + x)\right] . \tag{60}$$

Some writers prefer the use of x - ct instead of ct - x. The physical association of increasing phase with increasing time (x constant) and decreasing phase with increasing distance from the source (t constant) is more appealing to us. In general, A and B are determinable from the boundary conditions in space and time. The significance of k and c becomes more obvious from the following discussion.

We let B = 0 as a special case. Then ψ is constant if ct - x is a constant, say $-x_o$, so that $x = ct + x_o$. In other words, ψ is constant if x increases linearly with time so that $\frac{dx}{dt} = c$. C is thus the speed with which the quantity represented by ψ is propagated in the positive x direction. A is the amplitude of ψ.

We now examine the space distribution with t fixed. We observe that the first cosine term in Eq. (60) lags by a complete cycle when its argument increases by 2π and this must occur in one wavelength for which $\Delta x = \lambda$. Thus since the wave number is defined as $\frac{2\pi}{\lambda}$, k is the wave number when $k\lambda = 2\pi$.

We now examine the time distribution at a fixed point in space. Let t be incremented by a period, T. This procedure must carry the argument through 2π radians and so $kcT = 2\pi$. The period T is then $T = \frac{2\pi}{kc} = \frac{\lambda}{c}$. T is also the reciprocal of frequency, thus $f = \frac{c}{\lambda}$. If ω is angular velocity, $\omega = 2\pi f = kc$. We may therefore write $\omega t - kx$ in place of $k(ct - x)$.

The second term on the right of Eq. (60) describes a wave of the same wave number as in the first term, but propagated in a negative x direction. Either part of the solution may be dropped by placing its amplitude, A or B, equal to 0.

Summarizing what has gone before, a simple form, Eq. (59), of the wave equation has a simple solution of the form Eq. (60) which constitutes a mathematical description of two plane waves propagated with a speed c in the x direction (one wave in the positive sense and the other in the negative sense). Sound speed c is a characteristic of the medium. The constant k is the wave number and the solution holds for any real k. The following relations hold:

wave length, λ, equals the fraction $\frac{2\pi}{k}$,

period, T, equals the fraction $\frac{2}{kc} = \frac{\lambda}{c}$,

frequency, f, equals $\frac{1}{T} = \frac{c}{\lambda} = \frac{kc}{2\pi}$, and

angular velocity, ω, equals $2\pi f = kc$.

Having brought these relationships out, we shall hereafter prefer using ω for kc so that the argument of the cosine term is $(\omega t - kx)$, or $(\omega t + kx)$.

Derivation of the Wave Equation

The derivation is for a fluid medium. We use a Cartesian coordinate system. We deal with forces in excess of static forces. Given a small parallelepiped of dimensions dx, dy, dz, we desire to apply the equation of motion. The force in the x direction is p(dy)(dz) on the yz face at x and $(p + \frac{\partial p}{\partial x}dx)(dy)(dz)$ on the yz face at x + dx, in which p is pressure in excess of static pressure. Since pressure acts inward on the volume, the latter force is in a negative direction, and the sum of the two forces in the positive x direction is $-\frac{\partial p}{\partial x}dx(dy)(dz)$. By Newton's second law this force equals the mass p(dx)(dy)(dz) times the acceleration $\frac{d^2\xi}{dt^2} \simeq \frac{\partial^2 \xi}{\partial t^2}$ where ξ is displacement in the x direction. Thus, dividing both sides of the equation by dx(dy)(dz), we have

$$-\frac{\partial p}{\partial x} = \rho \frac{\partial^2 \xi}{\partial t^2}. \qquad (61)$$

Differentiating Eq. (61) with respect to x*, we obtain

$$-\frac{\partial^2 p}{\partial x^2} = \rho\frac{\partial^2}{\partial t^2}\left(\frac{\partial \xi}{\partial x}\right). \tag{62}$$

Similarly, we obtain for the y and z directions, with η and ζ representing respective displacements,

$$-\frac{\partial^2 p}{\partial y^2} = \rho\frac{\partial^2}{\partial t^2}\left(\frac{\partial \eta}{\partial y}\right), \tag{63}$$

$$-\frac{\partial^2 p}{\partial z^2} = \rho\frac{\partial^2}{\partial t^2}\left(\frac{\partial \zeta}{\partial z}\right). \tag{64}$$

Adding Eqs. (62), (63), and (64) and using ∇^2 for the Laplacian operator $\frac{\partial^2}{\partial x^2} + \frac{\partial^2}{\partial y^2} + \frac{\partial^2}{\partial z^2}$, we obtain

$$-\nabla^2 p = \rho\frac{\partial^2}{\partial t^2}\left(\frac{\partial \xi}{\partial x} + \frac{\partial \eta}{\partial y} + \frac{\partial \zeta}{\partial z}\right). \tag{65}$$

The part in parenthesis in Eq. (65) may be written $\nabla \cdot d$, where d is total displacement with components ξ, η and ζ. The term $\nabla \cdot d$ is the dilation Δ, that is, change in volume per unit volume. We now have

$$-\nabla^2 p = \rho\frac{\partial^2 \Delta}{\partial t^2} = \rho\frac{\partial^2}{\partial t^2}(\nabla \cdot d). \tag{66}$$

Now let us make use of Hooke's law, which states that stress is proportional to strain. The stress is -p and the strain is Δ for the hydrostatic case. Therefore, we have

$$-p = \mu\Delta = \mu\nabla \cdot d \tag{67}$$

---

* ρ is treated as a constant, a procedure which is generally an adequate approximation.

in which μ is the bulk modulus of elasticity. Substituting Eq. (67) into Eq. (66), we obtain

$$\nabla^2 p = \frac{\rho}{\mu} \frac{\partial^2 p}{\partial t^2} = \frac{1}{c^2} \frac{\partial^2 p}{\partial t^2}. \tag{68}$$

This is the wave equation for excess pressure.

We choose to use velocities henceforth rather than displacements. These will be designated as follows

$$u = \dot{\xi}, \; v = \dot{\eta}, \; w = \dot{\zeta}. \tag{69}$$

We now define a velocity potential* by the equations

$$u = -\frac{\partial \psi}{\partial x}, \; v = -\frac{\partial \psi}{\partial y}, \; w = -\frac{\partial \psi}{\partial z}. \tag{70}$$

or

$$\dot{d} = -\nabla \psi. \tag{71}$$

Rearranging order of differentiation in Eq. (66) and substituting for $\dot{d}$ from Eq. (71), we obtain

$$\nabla^2 (p - \rho \frac{\partial \psi}{\partial t}) = 0 \tag{72}$$

from which

$$p = \rho \frac{\partial \psi}{\partial t}. \tag{73}$$

*Officer[9] defines also a displacement potential for alternate use. Tolstoy and Clay[10] use displacement potential altogether.

So we see that both p and $\dot{d}$ are derivable from ψ.

We now proceed to express the wave equation in terms of ψ. Substituting Eq. (73) into the wave equation for p, Eq. (68), we obtain

$$\nabla^2(\rho\frac{\partial\psi}{\partial t}) = \frac{1}{c^2}\frac{\partial^2}{\partial t^2}(\rho\frac{\partial\psi}{\partial t}) \tag{74}$$

or

$$\rho\frac{\partial}{\partial t}(\nabla^2\psi - \frac{1}{c^2}\frac{\partial^2\psi}{\partial t^2}) = 0. \tag{75}$$

In all cases with which we are concerned ψ will have the form

$$\psi(u, v, w, t) = \phi(u, v, w)e^{iwt}. \tag{76}$$

When the partial derivative with respect to time is taken in Eq. (75), $\frac{d}{dt}$ is replaced by $i\omega$ and we may divide by $i\omega\rho$ to obtain:

$$\nabla^2\psi = \frac{1}{c^2}\frac{\partial^2\psi}{\partial t^2}. \tag{77}$$

This is the wave equation for the velocity potential. It is formally the same as that for pressure. A solution of Eq. (77) for plane waves in the x direction and for constant c has already been given in Eq. (60).

WAVE GUIDES

Wave guides are ducts with perfectly reflecting boundaries. We consider a plane wave propagated in the x direction between reflecting boundaries at $z = 0$ and $z = L$. We start with the assumption that these boundaries are perfectly rigid so that no change of phase and no loss take place at reflection. The wave equation in Cartesian coordinates is simplest and appropriate for this case. This equation was given as Eq. (77). However, Eq. (77) is now

simplified somewhat by the fact that there is no variation in the y direction. The equation is therefore

$$\frac{\partial^2\psi}{\partial x^2} + \frac{\partial^2\psi}{\partial z^2} = \frac{1}{c^2}\frac{\partial^2\psi}{\partial t^2}. \tag{78}$$

A common method of solving partial differential equations is by separation of variables. We therefore wish to equate ψ to the product of two or more functions of different variables. We anticipate that as far as the x direction and the time t are concerned, the functional form will be $e^{i(\omega t - \alpha x)}$. We therefore shall try as the velocity potential

$$\psi = e^{i(\omega t - \alpha x)}\,\phi(z). \tag{79}$$

Substituting this in Eq. (78) leads to the following equation, which is an ordinary differential equation.

$$\frac{d^2\phi}{dz^2} + \gamma^2\phi = 0, \tag{80}$$

in which

$$\gamma^2 = \frac{\omega^2}{c^2} - \alpha^2. \tag{81}$$

We encountered $K = \frac{\omega}{c}$ in Eq. (60) and identified it as the wave number along the ray. The terms α and γ are now seen to be x and y components of K.

The solution to Eq. (80) is

$$\phi = a\cos\gamma z + b\sin\gamma z. \tag{82}$$

and Eq. (82) substituted in Eq. (79) yields

$$\psi = e^{i(\omega t - \alpha x)}\left[a\cos\gamma z + b\sin\gamma z\right]. \tag{83}$$

Here we have three undetermined constants, a, b, and γ. We can find two of them by matching boundary conditions. At hard boundaries which are postulated at z = 0 and L, $\frac{\partial \psi}{\partial z} = 0$, that is to say, there can be no particle velocity in the z direction at the boundaries. Taking the derivative of ψ, with respect to z, in the z direction, we obtain for particle velocity

$$w = e^{i(\omega t - \alpha x)} \gamma(a \sin \gamma z - b \cos \gamma z) . \tag{84}$$

Putting z = 0, we find that the first term in parentheses vanishes. The second term must also vanish, which requires that b = 0. Now we are left with only the sine term. In it, putting z = L, we must require that $\gamma L = (n - 1)\pi$ in order that this term vanish at z = L. We thus have

$$\gamma_n = \frac{(n - 1)\pi}{L} \tag{85}$$

and

$$\phi = a_n \cos \gamma_n z. \tag{82a}$$

In Eq. (85), we have introduced the subscript n to designate the particular value of γ for a particular n. Any positive integral value of n will satisfy the boundary condition. Therefore, *the solution can be written with any* integral n up to n_c (to be discussed presently) or, more generally, as the summation of terms as n takes on all integral values from 1 to n_c. Negative n's give redundant terms and so are left out.

We have seen that α and γ are components of the wave number K in the x and z direction respectively. Therefore, for each γ_n, there is an α_n given by

$$\alpha_n^2 = K^2 - \gamma_n^2, \tag{86}$$

or

$$\alpha_n^2 = \frac{w^2}{c^2} - \frac{(n-1)^2\pi^2}{L^2} \tag{87}$$

Examining Eq. (87), we note that real values of α_n occur only if

$$n < 1 + \frac{wL}{c} = 1 + \frac{2ft}{c}.$$

The largest value of n admissable for a given frequency, n_c, limits the number of modes at that frequency. Also, for a given n, there is a low frequency cutoff, f_c, such that

$$f_{cn} \geq \frac{(n-1)c}{2L} .$$

We are now ready to write the final equations for ψ, u, w, and p as follows:

$$\psi = \Sigma\, a_n \cos \gamma_n z \cos \left[(\omega t - \alpha_n x) - \beta_n\right], \tag{88}$$

$$u = -\frac{\partial \psi}{\partial x} = \sum_{n=1}^{n_c} a_n \alpha_n \cos \frac{n\pi z}{L} \sin \left[(\omega t - \alpha_n x) - \beta_n\right], \tag{89}$$

$$w = -\frac{\partial \psi}{\partial z} = +\sum_{n=1}^{\infty} a_n \gamma_n \sin \gamma_n z \cos \left[(\omega t - \alpha_n x) - \beta_n\right], \tag{90}$$

$$p = \rho \frac{\partial \psi}{\partial t} = \rho\omega \Sigma\, a_n \cos \gamma_n z \sin \left[(\omega t - \alpha_n x) - \beta_n\right]. \tag{91}$$

In each of the last four formulas we have constants a_n and β_n which would be determinable from initial space and time conditions. We note that w vanishes at the boundaries while $|w|$ is maximum at the boundaries, as is $|p|$. At this point we may look upon w(z) as simply a density function of particle velocity

in the z direction. Each n contributes a normal mode of ψ which is characteristic of standing wave patterns.

Let us note that p and u are everwhere in phase, a condition required for the transmission of power. Another way of looking at this solution, which has some interesting ramifications, is led into by noting in Eq. (88) that the product of the cosines is the cosine of the sum plus the cosine of the difference, all over 2. The cosine of the difference has the following argument:

$$\text{Arg. } \Delta = \omega t - (\alpha_n x + \gamma_n z) - \beta_n. \tag{92}$$

This represents a wave traveling in the xz plane with a component in the positive x direction with wave number α_n and one in the positive z direction with the wave number γ_n. The sum term experiences a change of sign of $\gamma_n z$ and is representative of a wave traveling in the positive x direction and the negative z direction with wave numbers α_n and γ_n. It follows that the downward wave (positive z direction) makes an angle θ_n with the x axis given by

$$\theta_n = \sin^{-1} \frac{\gamma_n}{K} = \sin^{-1} \frac{(n - 1)\pi}{KL} \tag{93}$$

while the upward wave for the same n has the sign of θ_n minus. These two waves together form a standing wave pattern, or mode, in the vertical. Figure 24 illustrates the geometry involved.

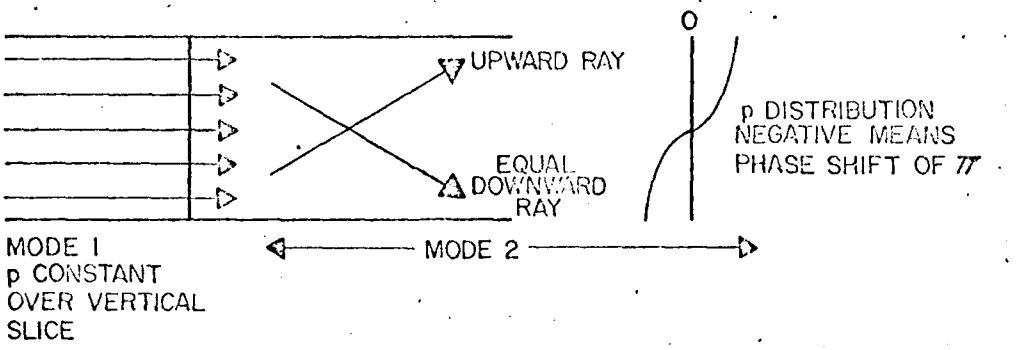

TRAVELLING WAVES EQUIVALENT TO MODE

Fig. 24

It would have been equally easy to have taken soft boundaries in which pressure disappears at the boundaries. For this case the only term which would remain in ψ of Eq. (83) would be the sine term. The term γ_n would have been the same as in Eq. (85) Or we could have taken one boundary hard and the other soft, and in this case we should have ended up with

$$\gamma_n = \frac{(n - 1/2)\pi}{L}$$

These derivations are good exercises for the student.

Phase and Group Velocity

We note that as the wave progresses in the x and z directions with a speed c, the point of intersection of the wave with the surface (or with any plane z = const.) travels with a speed $\frac{c}{\cos \theta_n}$ where θ_n is the angle between the surface and the wave front. This speed is the phase velocity V, as can be seen by reference to Fig. 25. In the figure while the constant phase

surface advances from C to D, the phase of this surface progresses along the lower boundary from A to D. Thus its velocity along the boundary is its velocity along the ray multiplied by AD/CD or by $\frac{1}{\cos \theta}$. We have then

$$V_n = \frac{c}{\cos \theta_n} = \frac{ck}{\alpha_n} = \frac{\omega}{\alpha_n}. \tag{94}$$

As n increases, α_n decreases and V increases. Therefore, the higher the mode number, the higher the phase velocity.

Group velocity is the velocity with which energy is propagated. For a plane wave in free space this is just the sound velocity c in the direction of propagation. In layered media with total reflection at the boundaries there is a simple expression for group velocity for a single frequency in a single mode, namely c cos ϕ. For more modes or a sum of frequencies we have to sum the individual energy densities each multiplied by its own group velocity and divide by total energy density to get group velocity.

Physical Interpretation of Modes

Before proceeding to more complicated cases, we should like to discuss the physics involved in the wave guide rather than the mathematics. To this end we shall proceed to present two points of view.

The first point of view can be presented with the aid of Fig. 25. In this figure, 1 and 2 are boundaries both assumed to be hard, perfect reflectors. L is the wave guide thickness. AB is a constant phase surface of which the section in the plane of the paper is a straight line. CDEFG is a ray path from one point on the wave front to another point on the same wave front. θ is the grazing angle which this ray makes with the horizontal [illegible]. The illustration loses its meaning for θ less than $\pi/4$.

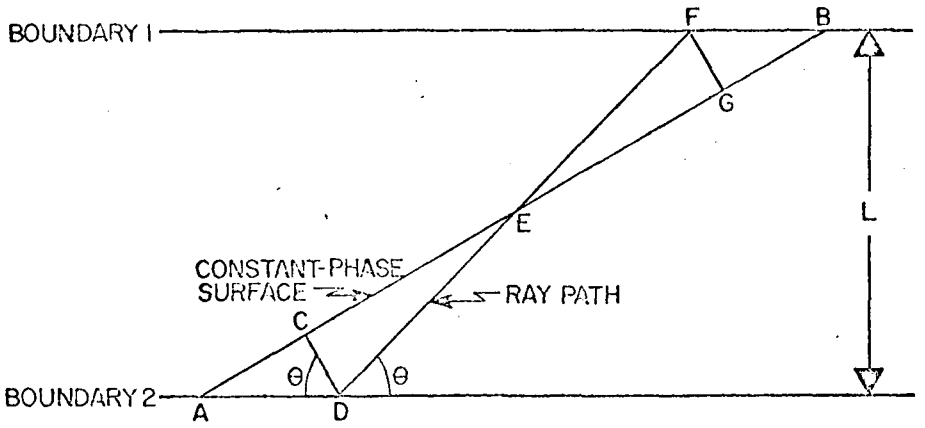

Fig. 25

The condition for this wave to have permitted wave number components is that the phase now existing at point G, taken as ϕ, recur only after some whole number of periods. The transit time from C to E to F to G is given by

$$t = \frac{\text{Path length}}{c} = \frac{2L \sin \theta_n}{f\lambda}. \tag{95}$$

This is derived by noting that

$$\overline{CD} = - \overline{DE} \cos 2\theta, \tag{96}$$

$\cos 2\theta$ being negative for $\theta > 45^\circ$. Similarly,

$$\overline{FG} = - \overline{EF} \cos 2\theta. \tag{97}$$

Adding these together along with $\overline{DF}$, we obtain

$$\overline{CDFG} = \overline{DF}(1 - \cos 2\theta) = 2\,\overline{DF}\,\sin^2\theta \tag{98}$$

from which Eq. (95) follows, since $L = \overline{DF}\,\sin\theta$.

At time t the phase at G will be $\phi + \varepsilon_1 + \varepsilon_2$ in which ε_1 and ε_2 are phase shifts at boundaries 1 and 2. This is not the same phase we started with and need not represent a whole number of periods. However, at an earlier time, earlier by $\frac{\varepsilon_1 + \varepsilon_2}{2\pi f}$, the phase ϕ would have recurred. Therefore,

$$t - \frac{\varepsilon_1 + \varepsilon_2}{2\pi f} = (n - 1)T = \frac{n - 1}{f} \tag{99}$$

T being period, f being frequency, and n being an integer.

Substituting t from Eq. (95) into Eq.(99) and multiplying by $2\pi f$, we obtain

$$\frac{2\pi}{\lambda}(2L \sin\theta_n) + \varepsilon_{10} + \varepsilon_{12} = 2(n - 1)\pi. \tag{100}$$

Substituting γ_n for $\frac{2\pi \sin\theta_n}{\lambda}$, we convert Eq. (100) to

$$2\gamma_n L + \varepsilon_{10} + \varepsilon_{12} = 2(n - 1)\pi. \tag{101}$$

We may solve this for γ_n for the special case when $\varepsilon_1 = \varepsilon_2 = 0$, obtaining

$$\gamma_n = \frac{(n - 1)\pi}{L} \tag{102}$$

which checks Eq. (85) derived by application of boundary conditions. The ε's which have been put equal to zero here would also enter Eq. (85) if the reflection coefficients used there had involved a phase shift.

Let us write also an expression which we previously had,

$$\frac{\omega}{c} = \frac{\gamma_n}{\sin \theta_n}, \tag{103}$$

in which for the moment we consider ω fixed. This tells us that for every γ_n there is a θ_n given by

$$\sin \theta_n = \frac{\gamma_n}{\omega}. \tag{104}$$

If, on the other hand, we choose a fixed θ, this equation may be written

$$\omega_n = \frac{\gamma_n}{\sin \theta}$$

or

$$f_n = \frac{\gamma_n}{2\pi \sin \theta}, \tag{105}$$

and we thus have a frequency set for the given θ.

A second point of view is now presented in order to emphasize the mechanism involved. Given a point source within the wave guide, the response at field points may be considered to be that of the source, its images (treating both boundaries as mirrors), and successive images of images. The

effect is that of an array of point sources which have a far-field beam pattern consisting of very sharp lobes at any given frequency, corresponding to the mode directions θ_n at that frequency.

Take the case of a point source halfway between hard boundaries with successive images spaced integral multiples of L from the source. Rays from each source at an angle θ with a horizontal will be in phase and normal to a constant phase surface only if the differences in path lengths from the different sources to the surface are each an integral number of wave lengths. This requires

$$L \sin \theta = (n - 1)\lambda, \quad n = 1, 2, 3, \ldots \tag{106}$$

or

$$\gamma_n = \frac{2(n - 1)\pi}{L} \tag{107}$$

Equation (107) differs from Eq. (85) by a factor of 2. The reason for this is that a source at the middle of the wave guide cannot excite modes which have a pressure null at the middle of the wave guide. Therefore, only alternate modes are excited and the steps in γ are twice as large for the permitted modes. In general, particle velocity in the z direction is zero when pressure is maximum. This means that at the depths for which $p_o = 0$ the motions of upward and downward rays cancel. For our case, even when particle velocity in the z direction is not zero, it is 90^o out of phase with pressure so that no net average power is propagated in the z direction. Pressure and particle velocity in the x direction are maximum together and in phase with each other.

Still another form of the last equation is

$$f_n = \frac{c}{\lambda} = \frac{(n - 1)c}{L \sin \theta}. \qquad (108)$$

Since f_n can never be less than $\frac{(n - 1)c}{L}$, the n^{th} mode has this frequency, f_c, as a low-frequency cut off. So we see that n is not in general permitted to go to infinity unless the frequency also approaches infinity.

It may be informative to inquire into the excitation of the different modes when the source is off center. If the source is a distance $D < L/2$ from either boundary, the system of images will consist of pairs of elements, each pair having a separation 2D, with pair centers separated by 2L. Putting $D = L/2$, we obtain the previous case: all separations L. But now, the far-field response pattern in general has the form

$$R = \cos\frac{2\pi d \sin \theta}{\lambda}\left[\frac{1}{2} + \sum_{i=1}^{\infty} \cos\left(\frac{4\pi i L}{\lambda}\sin \theta\right)\right]. \qquad (109)$$

See Fig. 26. The part in brackets will give terms all in phase when

$$\frac{4\pi L \sin \theta}{\lambda} = 2(n - 1)\pi,$$

$$k = \frac{(n - 1)\pi}{L \sin \theta_n}, \text{ or}$$

$$\gamma_n = \frac{(n - 1)\pi}{L}. \qquad (110)$$

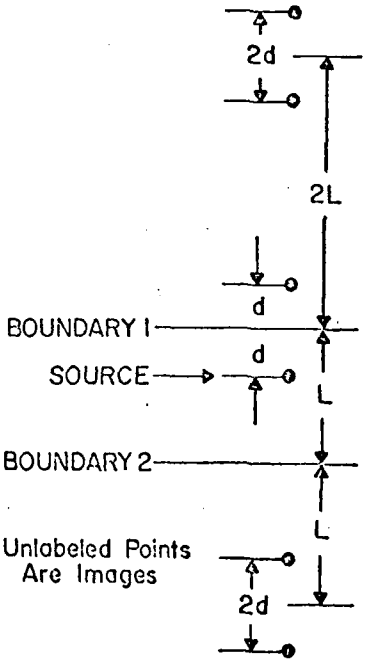

PATTERN OF EQUIVALENT ARRAY OF SOURCES

Fig. 26

Equation (110) is identical with Eq. (85). The factor $\cos\frac{2\pi d \sin\theta}{\lambda}$ may be regarded as a weighting factor which emphasizes those modes for which $\frac{2\pi d \sin\theta}{\lambda}$ is nearest some multiple of 2π or -2π. As a special case when $d = L/2$, this requires $\frac{\pi L \sin\theta}{\lambda} = (n-1)\pi$ which takes us back to Eq. (106) for the same special case.

WAVE GUIDE IN CYLINDRICAL COORDINATES

This section is an expression of wave guide theory in cylindrical coordinates with sound propagating radially outward from a line source (or a sum of point sources in line) which is perpendicular to the boundaries. This case is preliminary to the study of layered media.

Let the boundaries be the planes $z = 0$ and $z = L$. Let the source be along the Z axis. Let sound speed c be constant. The wave equation in cylindrical coordinates is (see Appendix B)

$$\frac{\partial^2\psi}{\partial r^2} + \frac{1}{r}\frac{\partial\psi}{\partial r} + \frac{\partial^2\psi}{\partial z^2} = \frac{1}{c}\frac{\partial^2\psi}{\partial t^2}. \tag{111}$$

Let us assume

$$\psi = R(r)\ Z(z)e^{i\omega t}. \tag{112}$$

Substituting this in the wave equation and dividing by ϕ, we obtain

$$\frac{\frac{d^2R}{dr^2} + \frac{1}{r}\frac{dR}{dr}}{R} + \frac{\frac{d^2Z}{dz^2}}{Z} + \frac{w^2}{c^2} = 0, \tag{113}$$

or

$$\frac{\frac{d^2R}{dr^2} + \frac{1}{r}\frac{dR}{dr}}{R} = -\frac{\frac{d^2Z}{dz^2} + \frac{w^2}{c^2}Z}{Z} \tag{114}$$

The reason for grouping $\frac{w^2}{c^2}$ with Z is that c may sometimes be a function of z.

Equation (114) can hold for all r and z only if each side of the equation is constant. Introducing a separation constant $-\alpha^2$, we have

$$\frac{d^2R}{dr^2} + \frac{1}{r}\frac{dR}{dr} + \alpha^2 R = 0 \tag{115}$$

and

$$\frac{d^2Z}{dz^2} + \left(\frac{w^2}{c^2} - \alpha^2\right) Z = 0. \tag{116}$$

The solution of Eq. (115) is

$$R = H_o^{1,2}(\alpha R). \tag{117}$$

See Appendix B. H_o^2 is the outgoing wave* and the one in which our interest centers. Its asymptotic expansion, good for $(\alpha r) > 1$, is

$$H_o^2(\alpha R) = \sqrt{\frac{2}{\pi\alpha r}}\ e^{-i(\alpha r - \pi/4)}. \tag{118}$$

Equation (118) may be combined with $e^{i\omega t}$ to yield a traveling wave,

$$Re^{i\omega t} = \frac{a}{\sqrt{r}}\, e^{i(\omega t - \alpha r + \pi/4)}. \tag{119}$$

The exponential may be written as a cosine with a phase angle β determinable from initial conditions at a specified position.

* Because we chose plus sign in the exponent of the factor $e^{i\omega t}$.

Equation (116) for Z is identical with that of the last previous section, Eq. (80), and the various standing-wave solutions are obtained by identical procedures. For two "hard" bounding planes, the whole general solution of Eq. (111) is

$$\psi = \frac{1}{\sqrt{r}} \sum_{n=1}^{n_c} a_n \cos \frac{n\pi z}{L} \cos\ (\omega t - \alpha_n r) - \beta_n \ . \qquad (120)$$

Equations for particle velocity u in the radial direction and w in the z direction and for p are

$$u = - \frac{\partial \psi}{\partial r} = \frac{1}{2r^{3/2}} \sum_{n=1}^{n_c} a_n \cos \frac{n\pi z}{L} \cos(\omega t - \alpha_n r - \beta_n),$$

$$- \frac{1}{r^{1/2}} \sum_{n=1}^{n_c} a_n \alpha_n \cos \frac{n\pi z}{L} \sin(\omega t - \alpha_n r - \beta_n), \qquad (121)$$

$$w = - \frac{\partial \psi}{\partial z} = \frac{1}{r^{1/2}} \sum_{n=1}^{n_c} \frac{a_n n\pi}{L} \sin \frac{n\pi z}{L} \cos(\omega t - \alpha_n r - \beta_n), \qquad (122)$$

$$p = p \frac{\partial \psi}{\partial t} = - \frac{pw}{r^{1/2}} \sum_{n=1}^{n_c} a_n \cos \frac{n\pi z}{L} \sin(\omega t - \alpha_n r - \beta_n). \qquad (123)$$

Only the second term in u is in phase with p and contributes power. The first term is a reactance term which may appreciably increase the motion at short range. At a transducer face, for a given maximum motion, pressure and power will be lower because of the reactance term, for a given particle velocity.

In the last four equations, the n^{th} term of the summations describes the n^{th} mode. N_c is the highest mode present for a given ω. It will be appreciated that for the present case, as for the plane wave, α_n is related to the wave number $\frac{\omega}{c}$ along the ray by

$$\alpha_n^2 = \left(\frac{\omega}{c}\right)^2 - \left(\frac{n\pi}{L}\right)^2. \tag{124}$$

This is to say, the wave numbers in the r and z directions may be looked upon as the legs of a right triangle of which the wave number along the ray is the hypotenuse. Furthermore, the phase velocity of the n^{th} mode is

$$V_n = \frac{\omega}{\alpha_n}. \tag{125}$$

Thus, V_n gets greater as the mode number gets higher, as with the plane wave, and for the same reason.

Almost parenthetically because of its remoteness from ocean acoustics, we call attention to the solution for standing waves in the radial direction, that is, for transmission of sound through a long tube with axis vertical. For this case,

$$\psi = \sum A_n J_o(\alpha_n r)\, e^{i(\omega t - \gamma_n z)} \tag{126}$$

satisfies the wave equation with α_n determinable from

$$\frac{\partial J_o}{\partial r} = 0 \tag{127}$$

at r_o = radius of the tube. These maxima and minima may be located in tables,

and α_n thus determined. Then $\gamma_n^2 = \frac{\omega}{c}^2 - \alpha_n^2$. If the tube is of finite length, the added constraints will limit the solution to preferred frequencies as well as wave numbers.

REFLECTION COEFFICIENT

We consider a half space of constant density ρ_1 and constant sound speed c_1 surmounting one or more horizontally stratified layers of thickness h_2, h_3, ..., densities ρ_2,ρ_3 , ..., and sound speeds c_2, c_3, ..., with the upper of these boundaries, that with the half space, at $z = 0$. Let a plane wave be incident on the boundary at $z = 0$ from above with the vertical factor in the velocity patential represented by $Ae^{-i\gamma_1 z}$. This wave will in general be partially reflected and partially transmitted. The velocity potential of the reflected part will have its component designated by $AR_{12}e^{i\gamma_1 z}$. R_{12} may be complex indicating a phase shift as well as an amplitude change at reflection. The transmitted part will be designated by $Be^{-i\gamma_2 z}$. If the second medium is not a half space extending to infinity, there will be an upward ray in the second medium reflected from below designated by $Ce^{i\gamma_2 z}$.

Our immediate objective is to express R_{12}, B and C in terms of the wave numbers $\gamma_i = \frac{\omega}{C_i} \sin \phi_i$, A and R_{23}. R_{23} may then be determined in terms of wave numbers and R_{34} and this process may be continued until the succession of stratified layers is terminated in some designated way. We write the vertical factors of the potentials, then, as follows:

$$\phi_1 = A(e^{-i\gamma_1 z} + R_{12}e^{i\gamma_1 z}) \tag{128}$$

$$\phi_2 = Be^{-i\gamma_2 z} + Ce^{i\gamma_2 z}. \tag{129}$$

Let the second layer be of thickness h_2 and let there be a reflection coefficient R_{23} from the 2, 3 boundary at $z = h_2$. Then

$$(\phi_2)_{z=h_2} = Be^{-i\gamma_2 h_2} + Ce^{i\gamma_2 h_2}. \tag{130}$$

Now

$$R_{23} = \frac{Ce^{2i\gamma_2 h_2}}{B}$$

or

$$C = Be^{-2i\gamma_2 h_2} R_{23}. \tag{131}$$

Substituting Eq. (131) in Eq. (129), we obtain a new expression for ϕ_2, viz:

$$\phi_2 = B\left[e^{-i\gamma_2 z} + R_{23}e^{i\gamma_2 (z - 2h_2)}\right], \tag{132}$$

at $z = 0$

$$\rho_1 \phi_1 = \rho_2 \phi_2. \tag{133}$$

Consequently,

$$\rho_1 A(1 + R_{12}) = \rho_2 B(1 + R_{23}e^{-2i\gamma_2 h_2}) \tag{134}$$

also at $z = 0$,

$$\frac{\partial \phi_1}{\partial z}_o = \frac{\partial \phi_2}{\partial z}_o \tag{135}$$

Consequently, performing this operation

$$\gamma_1 A(1 - R_{12}) = \gamma_2 B(1 - R_{23}e^{-2i\gamma_2 h_2}). \tag{136}$$

From Eq. (134) and Eq. (136) we wish to determine B and R_{12}. We have

$$\rho_1 A R_{12} - \rho_2 (1 + R_{23} e^{-2i\gamma_2 h_2}) B = -\rho_1 A \tag{134a}$$

$$\gamma_1 A R_{12} + \gamma_2 (1 - R_{23} e^{-2i\gamma_2 h_2}) B = \gamma_1 A \tag{136a}$$

and

$$R = \frac{\begin{vmatrix} -\rho_1 & -\rho_2 (1 + R_{23} e^{-2i\gamma_2 h_2}) \\ \gamma_1 & \gamma_2 (1 - R_{23} e^{-2i\gamma_2 h_2}) \end{vmatrix}}{\begin{vmatrix} \rho_1 & -\rho_2 (1 + R_{23} e^{-2i\gamma_2 h_2}) \\ \gamma_1 & \gamma_2 (1 - R_{23} e^{-2i\gamma_2 h_2}) \end{vmatrix}}$$

from which we have factored out an A in both numerator and denominator. Expanding the determinants,

$$R_{12} = \frac{\rho_2 \gamma_1 (1 + R_{23} e^{-2i\gamma_2 h_2}) - \rho_1 \gamma_2 (1 - R_{23} e^{-2i\gamma_2 h_2})}{\rho_2 \gamma_1 (1 + R_{23} e^{-2i\gamma_2 h_2}) + \rho_1 \gamma_2 (1 - R_{23} e^{-2i\gamma_2 h_2})}. \tag{137}$$

Solving the Eqs. (134a) and (136a) for B, the numerator for the determinantal form of solution becomes

$$A \begin{vmatrix} \rho_1 & -\rho_1 \\ \gamma_1 & \gamma_1 \end{vmatrix}$$

and B becomes

$$B = \frac{2\rho_1 \gamma_1 A}{\rho_2 \gamma_1 (1 + R_{23} e^{-2i\gamma_2 h_2}) + \rho_1 \gamma_2 (1 - R_{23} e^{-2i\gamma_2 h_2})}. \tag{138}$$

We shall consider a few special cases of R_{23}.

a) $R_{23} = 0$. This means no reflection or second layer extending to ∞. Substituting in Eq. (137),

$$R_{12} = \frac{\rho_2\gamma_1 - \rho_1\gamma_2}{\rho_2\gamma_1 + \rho_1\gamma_2}. \tag{139}$$

If γ_2 is real, R_{12} is real, positive and < 1. If $\rho_2\gamma_1 = \rho_1\gamma_2$, there is no reflection (matched impedances). At normal incidence $\frac{\gamma_1}{\gamma_2} = \frac{c_2}{c_1}$, and

$$R_{12} = \frac{\rho_2 c_2 - \rho_1 c_1}{\rho_2 c_2 + \rho_1 c_1} = \frac{Z_2 - Z_1}{Z_2 + Z_1}, \tag{140}$$

where $Z = \rho c$ is characteristic impedance of the medium. If γ_2 is imaginary, $R_{12} = e^{-2i\tan^{-1}\frac{\rho_1|\gamma_2|}{\rho_2\gamma_1}}$ which has a magnitude 1 (total reflection) with a phase shift $-2\tan^{-1}\frac{\rho_1|\gamma_2|}{\rho_2\gamma_1}$. As γ_1 approaches zero by letting the grazing angle at incidence on the boundary approach zero, the phase shift approaches 180°.

b) $R_{23} = 1$. This is the case of the boundary of infinite impedance. Multiplying numerator and denominator of Eq. (121) by $e^{i\gamma_2 h_2}$, we obtain

$$R_{12} = \frac{\rho_2\gamma_1 \cos\gamma_2 h_2 - i\rho_1\gamma_2 \sin\gamma_2 h_2}{\rho_2\gamma_1 \cos\gamma_2 h_2 + i\rho_1\gamma_2 \sin\gamma_2 h_2}. \tag{141}$$

This has an absolute value of unity. There is total reflection with

a phase shift

$$\theta = -2\tan^{-1}\left(\frac{\rho_1\gamma_2}{\rho_2\gamma_1}\tan\gamma_2 h_2\right), \tag{142}$$

$\theta \to -180^\circ$ as $\gamma_1 \to 0$, that is, as grazing angle approaches 0.

c) $R_{23} = -1$, approximately for water to air is given by

$$R_{12} = -\frac{\rho_1\gamma_2\cos\gamma_2 h_2 - i\rho_2\gamma_1\sin\gamma_2 h_2}{\rho_1\gamma_2\cos\gamma_2 h_2 + i\rho_2\gamma_1\sin\gamma_2 h_2}. \tag{143}$$

Again $|R| = 1$, there is total reflection with a phase shift

$$\theta = 180^\circ - 2\tan^{-1}\left(\frac{\rho_2\gamma_1}{\rho_1\gamma_2}\tan\gamma_2 h_2\right), \tag{144}$$

$\theta \to 180^\circ$ as $\gamma_1 \to 0$, and also as $h_2 \to 0$. This last condition reverts to the simple case of reflection from a water to air interface with the air of infinite extent for which $\theta \simeq 180^\circ$.

WAVE GUIDE MODIFICATION

Suppose now that we look again at the wave guide and this time let the lower boundary at $z = L$ have a reflection coefficient $e^{i\theta}$ in which θ is given by Eq. (142) or (144). Now let us write the solution, Eq. (82) in the form

$$\phi = Ae^{-i\gamma z} + Be^{i\gamma z}. \tag{145}$$

Here our interpretation is of a downward wave designated by $Ae^{-i\gamma z}$ and an upward wave designated by $Be^{i\gamma z}$, the direction being apparent from the way in which these exponentials combine with $e^{i\omega t}$. This form lends itself well

to relating upward and downward rays at the boundaries to reflection coefficients.

At the upper boundary we require $\frac{\partial \phi}{\partial z} = 0$. This is satisfied if

$$A - B = 0. \tag{146}$$

At the lower boundary we now require

$$A\left[e^{-i\gamma L} + e^{i(\gamma L + \theta)}\right] = 0. \tag{147}$$

This is satisfied only if

$$i(\gamma_n L + \theta) = - i\left[\gamma_n L - (2n - 1)\pi\right], \tag{148}$$

or if

$$\gamma_n = \frac{(2n - 1)\pi - \theta}{2L}. \tag{149}$$

These are the eigenvalues for this case.

We can also write in the format of Eq. (88)

$$\psi = \Sigma\, a_n \cos\left(\gamma_n z + \frac{\theta_n}{2}\right) \cos\left[(\omega t - \alpha_n x) - \beta_n\right] \tag{150}$$

TWO-LAYER WAVE GUIDE

We now replace the half space by a layer of finite thickness h_1 assumed to be homogeneous liquid density ρ_1 and sound speed c_1 bounded at its upper surface by air so that $R_{10} \simeq -1$. The lower layer is assumed to be a homogeneous liquid of thickness h_2 density ρ_2 and sound speed c_2, bounded beneath by a relatively high impedance material so that $R_{23} \simeq 1$. The 1, 2 interface is at $z = 0$.

The z-coordinate factor of velocity potential is

$$\phi_1 = Ae^{-i\gamma_1 z} + Be^{+i\gamma_1 z} \tag{151}$$

in layer 1, and

$$\phi_2 = Ce^{-i\gamma_2 z} + De^{+i\gamma_2 z} \tag{152}$$

in layer 2, where γ_1 and γ_2 are vertical wave numbers in the respective media.

The boundary condition to be satisfied at the 1 to 0 interface is that p = 0, and therefore, $\phi_1 = 0$ when $z = -h_1$ Thus

$$Ae^{i\gamma_1 h_1} + Be^{-i\gamma_1 h_1} = 0, \tag{153}$$

$$B = - Ae^{+2i\gamma_1 h_1}. \tag{154}$$

The boundary condition at $z = h_2$ is

$$\left(\frac{\partial \phi_2}{\partial z}\right)_{h_2} = 0, \tag{155}$$

meaning no particle velocity in the vertical, therefore

$$- Ce^{-i\gamma_2 h_2} + De^{i\gamma_2 h_2} = 0, \tag{156}$$

$$D = Ce^{-2i\gamma_2 h_2}. \tag{157}$$

Substituting Eq. (154) and Eq. (157) into Eq. (151) and Eq. (152) respectively, we find

$$\phi_1 = A\left[e^{-i\gamma_1 z} - e^{i\gamma_1 (z + 2h_1)}\right], \tag{158}$$

$$\phi_2 = C\left[e^{-i\gamma_2 z} + e^{i\gamma_2 (z - 2h_2)}\right]. \tag{159}$$

A is arbitrary. We now need to determine C in terms of A. There are two conditions at the 1, 2 interface which need to be satisfied as follows

$$\rho_1(\phi_1)_o = \rho_2(\phi_2)_o, \tag{160}$$

$$\text{and } \left(\frac{\partial\phi_1}{\partial z}\right)_o = \left(\frac{\partial\phi_2}{\partial z}\right)_o. \tag{161}$$

Putting $z = 0$ in Eq. (158) and Eq. (159) and substituting into Eq. (160) yields

$$\rho_1(1 - e^{2i\gamma_1 h_1})A - \rho_2(1 + e^{-2i\gamma_2 h_2})C = 0. \tag{162}$$

Taking the partial derivatives of Eq. (158) and Eq. (159), putting $z = 0$ and equating to each other, one obtains

$$\gamma_1(1 + e^{2i\gamma_1 h_1})A - \gamma_2(1 - e^{-2i\gamma_2 h_2})C = 0. \tag{163}$$

In order that the simultaneous equations, (162) and (163) in A and C both be satisfied, the determinant of the coefficients must vanish. Solving the determinants leads to

$$\frac{\rho_1}{\gamma_1}\tan\gamma_1 h_1 = \frac{\rho_2}{\gamma_2 \tan\gamma_2 h_2}. \tag{164}$$

The dissymetry results from the difference between upper and lower boundaries of the dual medium. Eq. (164) in combination with Snell's law from which

$$\gamma_2 = \sqrt{\gamma_1^2 - \omega^2\left(\frac{1}{c_2^2} - \frac{1}{c_1^2}\right)}, \tag{165}$$

determines the permitted values of γ_1 and γ_2.

For any permitted pair of values of γ_1 and γ_2, Eq. (162) may be solved for C in terms of the arbitrary A.

$$C = \frac{\rho_1 (1 - e^{2i\gamma_1 ih})A}{\rho_2 (1 + e^{-2i\gamma_2 ih})}. \tag{166}$$

Since the relationship between γ_1 and γ_2, Eq. (164), depends on angular velocity ω, different sets of permitted values are obtained at different frequencies.

If the student wishes to work out a case, it is suggested that he put $\rho_1 = \rho_2$, compute and tabulate γ_2 for various values of γ_1 and then, against each γ_1, plot the right and left sides of Eq. (164) and find intersections.

Reference 11 carries calculations much further and develops solutions to the general multilayer problem. Some of the symbols used there are different than ours and their use of angles of incidence and reflection for reference instead of grazing angles interchanges sines and cosines.

NORMAL MODE THEORY

The ultimate in precision of solutions of the wave equation has been sought in Normal Mode Theory. We would be remiss not to discuss the general approach, and to indicate limitations. Right at the start let us assert that ray theory is adequate for at least 90% of the cases we shall encounter and necessary in many cases where the complexity of normal mode solutions is beyond our current capability or patience. In this connection we quote from Ref. 12. "Even when the boundary conditions can be formulated exactly, and initial conditions are simple, the exact solution of the

problem cannot be presented." Vast strides have been made in the use of this approach since the quoted words were written; nevertheless, we still require approximations to actual conditions before we can solve the wave equation exactly and we still assume plane surface and bottom boundaries because other assumptions are too complex for mathematical manipulation to solutions.

More recent comment on this situation is given in Ref. 13 which is directed to a comparison of methods as its title indicates. In the last paragraph of this paper, Tolstoy states, "It appears, therefore, that natural causes and experimental error limit the use of exact solutions to about the same ranges as numerical error will limit the use of W.K.B. and traditional ray methods."

In view of the limitations of normal mode solutions, why should we spend time on them? First of all, they give us an insight into mechanisms beyond that apparent from ray theory. They describe diffraction. They describe behavior at caustics. They predict a phase shift of $\pi/2$ at a turning point or vertex. The tedium of solution is greatly reduced by reliance on computer programs. There is a great deal of literature on this method and no one can pose as an expert in the field without a knowledge of the approach.

Before taking up the general approach to the normal mode method, let us clear up a few odds and ends.

We first assumed a solution in Cartesian coordinates for the plane wave in a wave guide (Eq. (79)). The factor in the x (horizontal) direction in our solution could have been written $Ae^{-i\alpha x} + Be^{+i\alpha x}$ in which we could

interpret the first term as an outgoing wave and the second term as an incoming wave. This is common practice. However, we omitted $Be^{i\alpha x}$ on the assumption that there is no incoming wave and combined the other term with $e^{i\omega t}$. We see that when we combine this with a factor $e^{i\omega t}$, we obtain $Ae^{i(\omega t - \alpha x)} + Be^{i(\omega t + \alpha x)}$. The quantities $\omega t - \alpha x$ and $\omega t + \alpha x$ are phases as functions of time and x dimension from which expressions for sound speed and wave length are derivable. Another form of solution in the x direction is $a \cos \alpha x + b \sin \alpha x$. This does not readily combine with $e^{i\omega t}$ to express a travelling wave. Hence, the first form is preferred when we have travelling waves.

In the simple wave guide in Cartesian coordinates, we had a situation in the z (vertical) direction where $a \cos \gamma z + b \sin \gamma z$ was the chosen solution. We could have used the exponential form and will do so in some cases. This would have combined with $e^{i(\omega t - \alpha x)}$ to give a wave with a downward component $e^{i(\omega t - \alpha x - \gamma z)}$ and a wave with an upward component $e^{i(\omega t - \alpha x + \gamma z)}$ which together constitute a standing wave best expressed in spherical functions to bring out the standing wave characteristic. Whenever we have confinement between two or more boundaries, we have a standing wave situation.

When a solution comes out in Bessel functions, we have a similar choice to make. A Hankel function has a real and an imaginary part which can be combined with $e^{i\omega t}$ to give a phase. We indicated in Eq. (118) an approximation for H_o^2 at moderate or long range which was exponential in form. If the approximation were not made, the combination $H_o^2 e^{i\omega t}$ would still have a phase for each combination of x and t. So the Hankel function

is to be regarded as corresponding to an exponential with imaginary exponent combined with a variable amplitude. Tables give amplitude and phase as functions of the argument.[14] To be still more specific suppose α is 1 ft^{-1} and x is 10 ft. Then αx is 10 radians or 573^{o}. Tables of the Hankel function H_o^2 (Ref.) give for an argument of 10, a phase lag of $\simeq 440^{o}$ as compared with a lead of $\simeq 61^{o}$ for $\alpha x = 1$, a difference of about 501^{o}. A shift of 9 radians in circular functions would be 515^{o}. But also, with the Hankel function the amplutude has fallen off from .897 to .253, a ratio of 3.54 in proceeding from 1 ft. range to 10 ft. range. This is close to $\frac{1}{\sqrt{x}}$ as in the approximation. From x = 8 to x = 16, the ratio is almost exactly $\frac{1}{\sqrt{x}}$.

In the x direction (or r direction in cylindrical coordinates) we usually have travelling waves and use Hankel functions.

How about standing wave patterns with Bessel functions? Corresponding to the circular functions we have Bessel functions of the first kind. We shall encounter these in considering sound speed c variable in depth whenever we wish to emphasize the standing wave pattern in the vertical dimension. However, using an upward and a downward wave in combination represented by Hankel functions may simplify matching boundry conditions.

The complete problem in normal modes consists of first a solution in whatever functions are required for the particular depth variation of c, and second the determination of various constants depending upon the satisfying of boundary conditions at every boundary as already carried out for the case of the two-layer waveguide. Satisfying boundary conditions for solutions other than circular functions or exponentials is generally tedious but straight-forward.

General Approach to the Problem of Stratified Media

It was stated early in this report that the sound speed profile may often advantageously be approximated by a succession of gradients of different values, each value for a particular layer. The best we can do in describing these profiles is to specify a succession of horizontally stratified layers and in each a sound speed as a function of depth for that layer, sometimes a linear function, sometimes more complicated.

In exact solutions of the wave equation we need to use analytic functions for which we know how to get solutions in not too complicated form. A number of authors (Ref. 15, Ref. 16, and Ref. 17) have used

$$c = \frac{c_o}{\sqrt{1 + \beta z}} \tag{167}$$

which can also be written

$$K = K_o\sqrt{1 + \beta z}. \tag{168}$$

in which K is the wave number along the ray at depth z and K_o is its value at a reference depth z = 0. Since the separated part of the wave equation for depth contains a factor $\gamma^2 = K^2 - \alpha^2$, this becomes

$$\gamma^2 = K_o^2(1 + \beta z) - \alpha^2 \tag{169}$$

which is fairly simple and can be handled.

Note that for the function c in Eq. (167), the gradient is

$$\frac{dc}{dz} = \frac{-c_o\beta}{2(1 + \beta z)^{3/2}} \tag{170}$$

which is very nearly constant for $\beta z << 1$. Of course, β may be positive yielding a negative gradient, or negative yielding a positive gradient. Solutions will be in Bessel functions.

Tolstoy and Clay (Ref. 10) obtain solutions also for the sound speed profile $\frac{1}{c^2} = \frac{1}{c_o^2} - a^2Z^2$.

A further requirement in boundary conditions is some manageable form of ultimate boundary. This may be any boundary for which the reflection coefficient is taken as 0, 1, or -1, corresponding respectively to constant sound speed to infinity, hard boundary of infinite impedance and soft boundary of zero impedance. More complicated cases have been treated.

When there is total reflection at the boundaries there will be standing wave patterns, the unknown constants are determinable from boundary conditions, and the solution for the depth factor of velocity potential will be a set of eigenfunctions, i.e. all boundary conditions can be satisfied only for a set of eigenvalues γ_i belonging to a set of eigenfunctions. When one ultimate boundary has zero reflection coefficient, sometimes called the radiation condition, γ is continuous unless the general solution for the whole velocity potential requires otherwise, a situation which will be brought out later.

In the case where sound speed is a function of depth, we encounter occasions when rays become horizontal and have therefore $\gamma = 0$. Suppose that the ray travels downward to this turning point with c increasing downward. At greater depths than for $\gamma = 0$, γ becomes imaginary and our solutions have imaginary wave numbers. If the depth function were of the form $e^{-i\gamma z}$, then clearly an imaginary γ would produce a real exponent meaning decay with depth. So it is with other functions. In the case

of a modified Hankel function, for example, γ may become imaginary and the function will decay. Nevertheless, the same function holds throughout the layer and matching of different functions is carried out only at layer boundaries. Let us not be misled by the fact that some of the functions with which we deal are commonly given new letter designations and are separately tabulated for imaginary arguments. This practice is just a convention for convenience. We can readily shift to a different table when the argument becomes negative (imaginary γ).

The depth functions with which we usually deal go to infinity at a turning point. This gives us a narrow region of indeterminancy. However, in spite of this, transferring from positive to negative arguments (γ going from real to imaginary) gives fitting values which are finite outside a narrow region.

We now proceed to outline a few special cases treated by normal mode theory. In every case we shall be dealing with horizontally stratified media. In every case the solution can be written as

$$\psi(r_1 z_1 t) = \phi(z)\ R(r)\ e^{i\omega t}. \qquad (171)$$

For plane waves $R(r) = e^{-i\alpha r}$ which combines with the time to give $e^{i(\omega t - \alpha r)}$. For cylindrical spreading $R(r) = H_o^2(\alpha r)$ which is expressible in polar coordinates as $|R|e^{-i\theta}$ so that it combines with the time factor to give $|R|e^{i(\omega t - \theta)}$. θ and $|R|$ are tabulated.[14] At moderate or long range this becomes $\frac{a}{\sqrt{\alpha r}}\ e^{i(\omega t - \alpha r + \pi/4)}$. In the following cases $R(r)e^{i\omega t}$ may be written at once. Only the depth function ϕ offers any complexity since sound speed may be a function of depth and since it is to the depth function that boundary conditions are applied.

Bilinear Gradient, Hard Bottom

Here we take up a case like that of the two-layer wave guide already treated except that the sound speed profile is a positive gradient next to the surface and a negative gradient below it bounded beneath by a hard bottom ($Z = \infty$). The boundary between the two liquid layers is taken as $z = 0$. Thicknesses are l_1 for the upper layer and l_2 for the lower so that the ultimate boundaries are air ($Z = 0$) at $z = -l_1$ and hard bottom ($Z = \infty$) at $z = + l_2$. The densities ρ_1 and ρ_2 are taken as constant and equal. The functional form of the sound speed is taken as

$$c = \frac{c_o}{\sqrt{1 + \beta z}} \tag{172}$$

with subscripts 1 and 2 for β denoting layer 1 and layer 2 and with c_o equal to the value of sound speed at the layer boundary.

We repeat the wave equation for velocity potential in cylindrical coordinates

$$\frac{\partial^2 \psi}{\partial r^2} + \frac{1}{r}\frac{\partial \psi}{\partial r} + \frac{\partial^2 \psi}{\partial z^2} = \frac{1}{c^2}\frac{\partial^2 \psi}{\partial t^2} \tag{173}$$

The solution is obtained in Appendix B for the case where c is given by Eq. (172). As a matter of fact, two different solutions for $\phi(z)$ of Eq. (171) are presented. We shall choose that expressed in modified Hankel functions. We have the following solutions.

In layer 1

$$\psi_{1n} = \left[a_n h_1(\eta_n) + b_n h_2(\eta_n)\right] \left|H_o^2(\alpha r)\right| e^{i(\omega t - \theta)}. \tag{174}$$

and in layer 2

$$\psi_{2n} = \left[c_n h_1(\eta_n) + d_n h_2(\eta_n)\right] \left|H_o^2(\alpha_n r)\right| e^{i(\omega t - \theta)}. \qquad (175)$$

In Eq. (174) and Eq. (175), ω is 2n times the frequency (any frequency we choose), θ is the modulus of $H_o^2(\alpha r)$ and η_n is given by

$$\eta_n = \frac{K_o^2(1 + \beta z) - \alpha_n^2}{(K_o^2\beta)^{2/3}} \qquad (176)$$

as defined in Eq. (1.225) of Appendix B. Beta takes on values β_1 in layer 1 and β_2 in layer 2. K_o is wave number along any ray at $z = 0$, $K_o^2(1 + \beta z)$ is K^2 as a function of z and $K^2 - \alpha^2$ is r^2, the square of the wave number in the vertical (z) dimension. We shall find how certain discrete values of α_n are arrived at with corresponding $\gamma_n(z)$. $\gamma_n(0)$ will identify permitted grazing angles at the 1,2 boundary through the relation

$$\gamma_o = K_o \sin\theta_o = \frac{\omega}{c_o} \sin\theta_o.$$

Since α_n and ω do not vary with depth z, the z factor ϕ_{2n} is the only difference between these ψ's at the same r and t. As in cases already covered, the problem remaining is to apply boundary conditions to express b_n, c_n and d_n in terms of a_n and to determine eigenvalues of γ_n which must exist because no energy escapes from either ultimate boundary. When this is done we shall have a set of ψ_n's in each layer which are interrelated for each η.

We now concentrate on the vertical factors

$$\phi_{1n} = a_n h_1(\eta_n) + b_n h_2(\eta_n), \qquad (177)$$

and

$$\phi_{2n} = c_n h_1(\eta_n) + d_n h_2(\eta_n). \tag{178}$$

In each of these last equations h_1 advances in phase and h_2 lags as βz increases. We now take β negative in the upper layer to give a positive sound speed gradient and we take β positive in the lower layer to give a negative sound speed gradient. Then h_1 may be interpreted as a wave travelling toward the 1, 2 boundary in either medium and h_2 as a wave travelling away from the 1, 2 boundary. Reversing the signs of both β's reverses the interpretation. The distinction here is unnecessary for the simple ultimate boundaries assumed for the present case since the ratio of reflected to incident waves is the same as its reciprocal at each ultimate boundary.

Just as with the 2-layer waveguide, we require $(\phi_{1n})_{z = -L_1} = 0$ for a pressure release surface. Then

$$b_n = - a_n \frac{\left[h_1(\eta_n)\right]_{z = -L_1}}{\left[h_2(\eta_n)\right]_{z = -L_1}}. \tag{179}$$

At the 2, 3 boundary, vertical particle velocity is zero so we put $\left(\frac{\partial \phi_2}{\partial z}\right)_{z = L_2} = 0$. This gives

$$d_n = - \frac{c_n \left[h_1^1(\eta_n)\right]_{z = L_2}}{\left[h_2^1(\eta_n)\right]_{z = L_2}}. \tag{180}$$

We now have our potentials expressible in terms of 2 constants a_n, c_n, of which the first may be regarded as arbitrary. We still have two conditions to satisfy at the 1, 2 boundary so that restrictions will be placed on permitted values of α and, for each permitted values α_n, c_n will be determinable in terms of a_n.

At the 1, 2 boundary, z = 0, pressure and vertical component of particle velocity must match in the two media. Thus,

$$\rho_1\left[a_n h_1(\eta_n) + b_n h_2(\eta_n)\right]_{z=0} = \rho_2\left[c_n h_1(\eta_n) + d_n h_2(\eta_n)\right]_{z=0} \quad (181)$$

$$\beta_1^{1/3}\left[a_n h_1^1(\eta_n) + b_n h_2^1(\eta_n)\right]_{z=0} = \beta_2^{1/3}\left[c_n h_1^1(\eta_n) + d_n h_2^1(\eta_n)\right]_{z=0} \quad (182)$$

In both Eq. (181) and Eq. (182), b and d have been solved for in terms of a and c respectively so that we have relationships here between c and a. In Eq. (182) the other factor $K_o^{2/3}$ resulting from differentiation with respect to z has been cancelled from the two sides of the equation.

Again as with the 2-layer waveguide, we may set up a determinant of the coefficients of a and c and equate it to zero. This will be satisfied for discrete values of $(\eta_n)_{z=0}$. For positive (η_n) the solution is oscillatory, for negative (η_n) hyperbolic. Any permitted value of η_n may be substituted into Eq. (181) to permit solving for c_n in terms of a_n and the solution is thereby completed. These computations should really be carried out on a computer.

If β_1 is negative and β_2 positive, η_n will be negative for some of its permitted values at z = 0. This corresponds to rays that make small angles with the surface and bottom and bend to become horizontal for $\eta_n = 0$ at some depths. Near the 1, 2 boundary where η is negative the solution is hyperbolic.

If β_1 is positive and β_2 negative, $(\eta_n)_{z=0}$ is always positive but some of its values for $z \neq 0$ will become negative near the ultimate boundaries corresponding to rays that oscillate about the 1, 2 boundary without reaching the ultimate boundaries, 1, 0 and 2, 3.

Mode Excitation

The general solution of Eq. (173) is a summation of modes, with each vertical factor containing an a_n so far arbitrary. The relative weights of these modes are related to the values of the coefficients of the modified Hankel functions. By adjusting the a_n's any desired function of z can be obtained. So if we know this function we can determine the a_n's. For a discussion of the method see Ref. 18, pp. 439-446. It develops that for a given source depth, every mode is excited in proportaion to the values of the modified Hankel functions for a given η has a null at source depth, the nth mode will not be excited and $a_n = 0$. (This happened in the case of our discussion of beam patterns in the section on "Physical Aspects".) In addition the pressure p at some field point is proportional to the depth function there so that the overall effect from source to receiver involves the square of the depth function.

Reference (9) pp. 61-66 describes the meaning of normal modes and illustrates this with the very simple case of a vibrating string leading up through excitation of modes. This discussion is worthy of attention if a still simpler case than treated here is sought for better understanding.

LEAKAGE FROM SURFACE DUCTS

Schulkin[19] has discussed the physical aspects of scattering from the surface bringing out the complications of the problem.

Schweitzer[20] has presented some nice graphs of depth functions in a surface duct. These show the n oscillations of the nth mode in the duct and the hyperbolic decay fitted on at the duct boundary. Schweitzer assumes that phase relations between the modes are destroyed by surface scatter and that consequently the modes add by power. This is probably appropriate for wave heights approaching a wavelength.

The Navy Underwater Research and Development Center has carried the computation of normal modes much further than anybody else for a variety of sound profiles. Reference is made to Pedersen and Gordon[21]. They have reported cases of excellent fit with experimental data at short ranges, taking phase relations of the modes into account. This agreement would be expected only at low frequency and low sea states.

Reference must be made to the theme issue of JUA on Scattering from the Surface Duct. We mention three papers as follows.

Bartberger and Ackler treat various two and three-layer cases which approximate ocean conditions in some cases with a surface duct, and which take typical ocean bottom conditions into account. Since their cases do not have a perfectly reflecting bottom, the depth functions by themselves are not restricted to permitted values. Hence, the most general solution instead of being a summation of potential functions ψ_n, has the form of an integral over the continuous wave numbers α, as follows

$$\psi(r,z,t) = e^{i\omega t}\int_0^\infty \phi(r,z)d\alpha. \qquad (183)$$

Since α is independent of depth for any given ray, its variation implies rays at different angles to the horizontal at any given depth. When Eq. (183) is integrated in a complex plane, the contributions to the integral come principally from the poles and therefore the integral may be replaced by the sum of the residues at these poles. This process yields a set of eigenvalues α_n which are complex corresponding to phase shift and attenuation per unit distance. The attenuation accounts for loss by propagation into the bottom.

Bucker[7] applies wave theory to a rough surface by ascribing a reflection coefficient of magnitude less than 1 to the surface. After getting solutions which would be applicable if the non-reflected energy were lost to the air, he then accounts for its presence below the surface duct as energy scattered into the shadow zone.

Murphy[22] presents a special mathematical procedure valid at turning points which eliminates the indeterminancy usually encountered there.

WKB METHOD

The WKB method, like ray acoustics, is an approximation method. As Tolstoy[13] has pointed out it may describe ocean sound propagation with no more error than is intrinsic in the data. In other words, if we must use widely fluctuating and incomplete data, and if even this must be approximated to give analytic depth functions susceptible to exact analysis, then the exact analysis does not yield results exactly describing actual conditions. Perhaps approximate methods would do as well.

We now derive the WKB approximation for stratified media, following the style of Ref. 10. We consider the vertical factor in the velocity potential. Its equation was obtained as

$$\frac{d^2\phi}{dz^2} + \gamma^2\phi = 0, \tag{184}$$

in which γ may be a function of z.

In the WKB method we let

$$\phi = \rho e^{is} \tag{185}$$

with s and ρ functions of z. Then

$$\frac{d\phi}{dz} = \left(\frac{d\rho}{dz} + i\rho\frac{ds}{dz}\, e^{is}\right), \tag{186}$$

$$\frac{d^2\phi}{dz^2} = e^{is}\left[\left(\frac{d^2\rho}{dz^2} + i\frac{d\rho}{dz}\frac{ds}{dz} + i\rho\frac{d^2s}{dz^2}\right) + i\frac{ds}{dz}\left(\frac{d\rho}{dz} + i\rho\frac{ds}{dz}\right)\right]. \tag{187}$$

Adding $\gamma^2\phi$ from Eq. (185) to $\frac{d^2\phi}{dz^2}$ from Eq. (187), dividing by e^{is}, and separating real and imaginary parts we obtain

$$\frac{d^2\rho}{dz^2} - \rho\left[\left(\frac{ds}{dz}\right)^2 - \gamma^2\right] = 0, \tag{188}$$

$$\rho\frac{d^2s}{dz} + 2\,\frac{d\rho}{dz}\frac{ds}{dz} = 0. \tag{189}$$

The last equation may be written

$$\rho\frac{d}{dz}\left(\frac{ds}{dz}\right) + 2\,\frac{ds}{dz}\left(\frac{d\rho}{dz}\right) = 0, \tag{190}$$

which has a solution

$$\rho = A\left(\frac{ds}{dz}\right)^{-1/2}, \tag{191}$$

A being a constant of integration.

The WKB approximation is made by assuming the first term of Eq. (188) negligible in comparison to the others. This requires that it be negligible with respect to say the third term so that

$$\left|\frac{d^2\rho}{dz^2}\right| << \left|\rho\gamma^2\right|,$$

or

$$\left|\frac{1}{\rho\gamma^2}\frac{d^2\rho}{dz^2}\right| << 1. \tag{192}$$

The inequality (188) must be satisfied for the WKB approximation to be good.

When the first term of Eq. (188) is neglected

$$\frac{ds}{dz} = \pm\gamma, \tag{193}$$

and therefore,

$$s = \pm\int_{z_o}^{z} \gamma dz + s_o. \tag{194}$$

Equation (193) substituted in Eq. (191) and this in turn substituted in Eq. (185) yields

$$\phi = A\gamma^{-1/2}\, e^{is}. \tag{195}$$

Equation (195) tells us that in this approximation ϕ has a magnitude proportional to $\gamma^{-1/2}$ and a phase s given by Eq. (194). It may be noted

that ϕ becomes infinite at a turning point where $\gamma = 0$. This is a region where Eq. (192) is not satisfied. The exact solution is well behaved at a turning point.

Tolstoy and Clay have shown that s_o in Eq. (194) is approximately $+\frac{\pi}{4}$ * for some special cases in which z is at a turning point. We have to use $-\frac{\pi}{4}$ to correspond to our choice of exponent $+ i\omega t$. Also we have to choose the sign in Eq. (194) which makes the definite integral negative whether we are integrating along a downward path or an upward path as long as we proceed in the direction of propagation.

We now make use of the fact that ϕ is a function of z only so that tracing the ray from a given z through a cycle to the same z headed in the same direction (up if we started up, down if we started down), the change in phase must be some integer times 2π. Thus for the surface duct with $\gamma_m = \sqrt{K_o^2(1 + \beta z) - \alpha_m^2}$, β negative, total phase shift is

$$- 2\int_o^{zt} \sqrt{K_o^2(1 + \beta z) - \alpha_m^2} - \frac{\pi}{2} - \pi = - 2m\pi. \qquad (196)$$

The last π on the left is the effect of a surface reflection to complete the cycle. The integration is readily carried out and we obtain the approximation to the eigenvalues α_m corresponding to different whole numbers m. Almost any kind of layered media in which rays go through a spatial cycle can be handled. We may have a duct with turning points above and below the axis or with boundaries at which phase shifts are function of grazing angle. In the latter case it may be easier to solve for angles at some reference level 1 for which

$$\frac{\alpha_m}{K} = \cos\theta.$$

* Wood[23] denies that this $\pi/4$ is present at the turning point for a constant sound-speed gradient.

It is interesting to integrate this space phase shift in the vertical over a round trip for the waveguide with γ constant. Here there is no $\frac{\pi}{4}$ for a turning point and

$$-2\int_0^L \gamma dz = -2\gamma L.$$

From this we subtract $\varepsilon_{10} + \varepsilon_{20}$, the phase leads at the boundaries, and equate the result to a whole number times 2π radians, $-2(n-1)\pi$, obtaining Eq. (101).

SUMMARY

Many useable acoustic paths characterized by a specified source position, a specified receiver or target position, and a path between, exist in the ocean. Losses over any path include divergence loss and attenuation. To a first approximation divergence loss is independent of frequency. Attenuation is highly frequency dependent. Over all paths there is an attenuation coefficient α_o characterizing pure absorption (conversion to heat). This includes loss by friction and loss by relaxation processes which involve storage of energy which is given up by hysteresis - that is by falling back too late to be fully retained in the sound wave. A dependency of α_o on acoustic path used has been observed (Thorp curve). Some paths exhibit other characteristic losses. An anomalous attenuation in the surface duct is attributed to absorption by bubbles and to leakage by scattering from a rough surface. Reflection loss over the bottom-bounce path is very significant. All these losses have been discussed and quantitative values have been assigned to them.

The tracing of ray paths over significantly different paths was approached by approximating sound-speed profiles in depth by layers each with its own linear segment. The ray path in each layer is then a segment of a circle of radius simply related to sound speed and sound-speed gradient. These circular segments of the paths have x and z components. Formulas for the spreading of two neighboring rays were developed and the spreading was simply related to divergence loss. Examples were computed in detail.

After the bread and butter approach of ray geometry had been covered, that is the "How," we approached the "Why" by more basic considerations. This involved new definitions, introduction to the wave equation and solutions of the wave equation for a series of cases of gradually increasing complexity, preparing the student for exposure to referenced literature which assumes quite a lot of background knowledge. The solutions employed are derived in Appendix B.

Derivation of reflection coefficients added to the potential scope of our solutions.

It has been brought out here that the normal-mode solutions are of greater academic than practical importance. This is not to deny the existence of experimental data which tends to confirm the validity of features of normal-mode solutions easily overlooked in ray theory.

The WKB method of approximation for stratified media was described and shown to yield approximate eigenvalues for paths cycling in the z-direction.

REFERENCES

1. S. Kuwahara, "Velocity of Sound in Sea Water and Calculation of Velocity for Use in Sonic Soundings," Hydrographic Review, 16, 123(1939).

2. V. A. Del Grosso, "The Velocity of Sound in Sea Water at Zero Depth," NRL Report 4002, 1952. Also see Letter to Editor, JASA, March 1970.

3. W. D. Wilson, "Speed of Sound in Sea Water as a Function of Temperature, Pressure, and Salinity," JASA 32, 641(1960). Also Letter to Editor, JASA 32, 13 (1960).

4. K. V. Mackenzie, "Formulas for the Computation of Sound Speed in Sea Water," JASA 32, 100(1960).

5. H. W. Marsh, M. Schulkin and S. G. Kneale, "Scattering of Underwater Sound by the Sea Surface," JASA 33, 334(1961).

6. H. L. Saxton, "Propagation of Sound in Surface-bounded Ducts," A Summary of Underwater Acoustic Data, Part VII (1956) - Conf. paper.

7. H. F. Bucker, "Wave Theory Solution for Sound Propagation in a Surface Duct with a Rough Surface," USN J. Underwater Acoustics 19, 13(1969).

8. G. Hurdle, R. H. Ferris, K. D. Flowers, "Effect of Transducer Velocity on the Structure of Signals Scattered from the Ocean Bottom," JASA 36, 1936(Oct. 1964). Also B. G. Hurdle, "Fine Structure of Acoustic Fields Scattered from the Ocean Bottom," Letter to Editor, JASA 40, 255(1966).

9. C. B. Officer, "Introduction to the Theory of Sound Transmission," McGraw Hill (1958).

10. Ivan Tolstoy and C. S. Clay, "Ocean Acoustics," McGraw Hill (1966).

11. L. M. Brekhovskikh, "Waves in Layered Media," translated by D. Lieberman and R. T. Beyer, Academic Press (1960).

12. P. G. Bergmann and A. Yaspan, Part I, "Physics of Sound in the Sea," Summary Technical Report, Div. 6, NDRC.

13. Ivan Tolstoy, "Comparison of Normal Mode and Ray Theoretic Treatments of Acoustic Propagation in the Ocean," A presentation at the Symposium on Quasi-Optics, Polytechnic Institute of Brooklyn, (June 8-10, 1964).

14. G. N. Watson, "A Treatise on the Theory of Bessel Functions," Cambridge Univ. Press (1966).

15. W. H. Furoy, "Theory of Characteristic Functions in Problems of Anomalous Propagation," Mass. Institute Technological Lab. Report, 680(1945).

16. H. G. Booker, "The Mode Theory of Tropospheric Refraction and its Relation to Waveguides and Diffraction," Physical Society and Royal Meteorological Society, (1946).

17. H. W. Marsh, "Theory of the Anomalous Propagation of Acoustic Waves in the Ocean," U. S. Navy Underwater Sound Lab. Report, 111, (1950). Conf. Report.

18. E. A. Guillemin, "The Mathematics of Circuit Analysis," M.I.T. Press (1949).

19. M. Schulkin, "Surface-coupled Losses in Surface Sound Channels," Letter to Editor, JASA 44, 1152 (1968). See also USNJ Underwater Acoustics, 19, Jan. 1969.

20. B. S. Schweitzer, "An Approximate Method for Determining the Distribution of Intensity in the Mixed Layer Sound Channel," USNJ Underwater Acoustics, 2, 66 (1952).

21. M. A. Pedersen and D. F. Gordon, "Normal Mode Theory Applied to Short-range Propagation in an Underwater Acoustic Surface Duct," JASA 37, 105(1965).

22. C. L. Bertberger and L. L. Ackley, "Normal Mode Solutions for Two- and Three-layer Velocity Profiles," USNJ Underwater Acoustics 19, 67(1969). Conf. Report.

23. E. L. Murphy, "Where is the Split Shadow?," USNJ Underwater Acoustics 19, 1(1969).

24. D. H. Wood, "No Phase Change in a Constant Gradient Medium," Letter to Editor, JASA 44, 1154(1968).

APPENDIX A

Computation of Losses in Specified Model Ocean

Ocean Specification and Derived Parameters (Step 1)

A specific model of the ocean is chosen for some of the examples to follow. This is shown in Fig. 11. We have taken three layers with layer boundaries at 50 yards, and 1400 yards depth, and with the bottom at 6000 yards. Sound speed at the source (here taken as the surface) is c_0 = 1650 yds./sec. Sound-speed gradients are g_0 = .030000/sec., g_1 = -.042000/sec., g_2 = .016000/sec. The value of g_0 chosen represents a very strong duct to emphasize duct effects. The five significant figures are assumed in order to obtain 2 or 3 in the final results. This necessity reflects the sensitivity of results to small changes in ocean characteristics.

In this model ocean, divergence loss as a function of range is desired at

a.) 20 yards below the duct (z_{1+})
b.) the bottom (z_3)
c.) the surface after a bottom bounce (z_0^{up})
d.) the surface at the convergence zone (z_0^{up})

Multiplication of the g's by depth increment in yards gives Δc in yds./sec. We compute

$$c_1 = 1650 + 50(.030000) \text{ yds./sec.}$$
$$= 1651.5 \text{ yds./sec}$$
$$c_{1+} = 1651.5 - 20(.042000) \text{ yds./sec}$$
$$= 1650.66 \text{ yds./sec.}$$

$$c_2 = 1651.5 - 1350(.042000) \text{ yds./sec.}$$

$$= 1594.8 \text{ yds./sec.}$$

$$c_3 = 1594.8 + .016000(4600) \text{ yds./sec.}$$

$$= 1668.4 \text{ yds./sec.}$$

Now the h's may be computed from Eq. (1) of the main text, giving

h_0 = -55000 yds. (upward from surface)

h = +39321 yds. (downward from first layer boundary)

h_2 = -99675 yds. (upward from second layer boundary)

These h's are measured from the top of the layer boundary designated by the subscript and each applies to the layer below the designated boundary.

Ray Paths to be considered (Step 2)

The rays of interest cross the first boundary at angles of 0°, 1°, 2°, 3°, 4°, 5°, 6°, 8°, 9°, 10°, 14°, and 20°. For each ϕ_1, the cosine may be looked up and then Snell's law may be applied to get the cosines of ϕ_0, ϕ_{1+}, ϕ_2, and ϕ_3. Then from these cosine values the angles, the sines, and the tangents can be found in the tables. The following is a suggested format. In it, the quantity first derived from the angle ϕ_1 is underlined twice. The quantities next derived from Snell's law are underlined once.

Subscript	0	1	1+	2
ϕ	$2^\circ 27'$	0°	$1^\circ 50'$	$15^\circ 3'$
cos ϕ	.99909	1	.99949	.96567
sin ϕ	.04275	0	.03199	.25966
tan ϕ	.04279	0	.03201	.26888

Table 1

Similar tables can be compiled for all angles considered. For $\phi_1 \leq 8^o$ the rays will not reach the bottom. For $\phi_1 \geq 9^o$ there will be also a ϕ_3 at the bottom.

Radii of Curvature (Step 3)

The radii of curvature are computed from the formula

$$\rho_i = \frac{h_i}{\cos \phi_i}.$$

Table 2 lists the radii of curvature in the three layers for a selected set of angles.

ϕ_1	ρ_0	ρ_1	ρ_2
0^o	-55050	+39321	-103218
1^o	-55058	+39327	-103232
2^o	-55084	+39345	-103281
4^o	-55185	+39417	-103472
5^o	-55261	+39471	-103613
8^o	-55591	+39707	-104231
14^o	-56735	+40525	-106378
20^o	-58584	+41845	-109843

Table 2

These radii of curvature apply to either upward or downward paths without change in sign.

Horizontal Range (Step 4)

We wish to obtain x_{1+}, x_3 from the rays that reach the bottom, and x_v from the rays which vertex short of the bottom. Our tabulation will not include the increments in each layer, although the formulae are set up as a sum of such increments. These formulae are

$$x_{1+} = \rho_0 (\sin \phi_1 - \sin \phi_0) + \rho_1 (\sin \phi_{1+} - \sin \phi_1)$$

$$x_3 = \rho_0 (\sin \phi_1 - \sin \phi_0) + \rho_1 (\sin \phi_2 - \sin \phi_1) + \rho_2 (\sin \phi_3 - \sin \phi_2).$$

When the rays vertex, ϕ_3 is replaced by ϕ_v which is zero. Thus, the term sin ϕ_3 will drop out.

The following table lists the accumulated x values at important depths or boundaries.

ϕ_1	x_{1+}	x_v	x_3
0	3611.27	39365	
1	2311.88	37527	
2	1612.22	37102	
4	946.50	36268	
5	772.02	36242	
6	646.93	36277	
8	489.83	36910	
9	430.12		30478
10	402.07		27498
14	272.57		20659
20	201.44		15057

Table 3

The horizontal distance traversed in the round trip from source to bottom and back to the surface again for the same ocean parameters on both legs is twice that to the bottom alone. Likewise, all vertexing rays return to the surface at twice the horizontal range at which they vertex.

Computation of $\delta\phi_i$ (Step 5)

The $\delta\phi_i$ are computed from Eq. (25) starting with all $\delta\phi_1 = .005$. The equation becomes

$$\delta\phi_i = - \tan \phi_i + \sqrt{\tan^2 \phi_i + .01 \tan \phi_1 + .000025}.$$

A few values of these $\delta\phi$'s are given below.

ϕ_1	$\delta\phi_0$	$\delta\phi_{1+}$	$\delta\phi_2$	$\delta\phi_3$
0	.000291	.000388	.00004648	
2	.003284	.003792	.000689	
8	.004785	.004881	.002330	
9	.004832	.004909	.002544	.011130
10	.004855	.004919	.002738	.008429
20	.004960	.004978	.003940	.005490

Table 4

In the foregoing table, $\delta\phi_1$ was .005 in each case.

Computation of δx_i (Step 6)

In this step we compute the $\delta x_{i-1,i}$ and the δx_n by the following equations

$$\delta x_{i-1,i} = \rho_{i-1}(\sec \phi_i \delta\phi_i - \sec \phi_{i-1} \delta\phi_{i-1}) \qquad (28)$$

and

$$\delta x_n = \sum_{i=1}^{n} \delta x_{i-1,i}.$$

The first of these equations gets the subscripts reversed for upward paths. Thus, the two terms within the parentheses get interchanged and this just compensates for the change in sign of $\delta\phi_i$ and $\delta\phi_{i-1}$. Consequently,

$$\delta x_{i-1,i} = \delta x_{i,i-1}.$$

except when $\delta x_{i,i-1}$ includes a turn around.

Again we shall tabulate a few values. Columns 2, 3, 4, and 5 are the results of computations by the first of the above formulae, while columns 6 and 7 are the results of summing by the second formula.

ϕ_1	$\delta x_{o,1}$	$\delta x_{1,1+}$	$\delta x_{1,2}$	$\delta x_{2,3}$ or δx^*_{2v}	δx_{1+}	δx_3 or δx^*_v
0	-259.22	-181.34	-194.71	+4.9670*	-440.56	-448.96*
2	-94.42	-47.48	-168.76	+73.74*	-141.90	-189.44*
4	-38.89	-16.86	-144.50	+139.31*	-55.75	-44.07*
5	-26.84	-11.71	-133.28	+170.18*	-38.55	+10.06*
8	-11.83	-4.67	-103.74	+253.96*	-16.50	+138.39*
9	-9.23	-3.89	-95.35	-886.97	-13.12	-991.55
10	-7.98	-3.18	-87.76	-586.26	-11.16	-682.00
20	-2.05	-.84	-40.96	-158.31	-2.89	-201.32

Table 5

Computation of δs_i (Steps 7 and 8)

Steps 7 and 8 of the summary will be performed separately for each of four cases as follows:

1. Loss to points 20 yards below duct,
2. Loss to bottom,
3. Loss to surface via bottom bounce, and
4. Loss to convergence zone.

Region below Surface Duct

The remaining steps are the computations δs_i from equations below then the computation of $r_i \, \delta\phi_o$ for the straight-line path, and finally computation of the ratio of spreading over the curvilinear path to that over the straight-line path as a measure of excess divergence loss due to the geometry in a vertical plane. The last quantity will be expressed in decibels.

The following equations will be applicable.

$$\delta s_i = \delta x_i \sin \phi_i,$$

for $\phi_1 > 4^o$. For $\phi_1 < 4^o$:

$$\delta s_{1+} = \delta y_{1+} = \rho_1 \cos(\phi_{1+} + d\phi_{1+}) - \cos \phi_1 ,$$

$$d\phi_{1+} = \frac{\delta x_{1+}}{\rho_1},$$

$$\text{Excess Loss} = -10 \log \frac{r_{1+} \delta\phi_o}{\delta s_{1+}}.$$

ϕ_1	δx_{1+}	sin ϕ_{1+}	δs_{1+}	$r_1 \delta \phi_o$	Excess Loss (db)
0	-440.60		11.40	1.04	10.4
1	-277.90		9.05	4.30	3.2
2	-141.90		6.30	5.30	.8
4	-55.75	.07672	4.28	4.07	.2
8	-16.50	.14263	2.35	2.37	0
14	-5.60	.24390	1.37	1.38	0

Table 6

Results are discussed in the body of the report. Equations used are the same for other cases except for subscripts.

Divergence Loss at the Bottom

We have observed that only the rays for which ϕ_1 is greater than 8^o reach the bottom. Any pronounced effect on loss at the bottom caused by reflection is expected to occur at ϕ_1 slightly greater than 8^o. With steep angles the extent in space from surface to bottom is not great enough to produce large effects.

Our procedure will be to complete computations and tabulate results for this case. We shall include ϕ_3 in the table because scattering loss at reflection, in the text, is a function of ϕ_3. We shall also include horizontal range. Slant range to the bottom in yards for this case is given by

$$r = \sqrt{x^2 + 6000^2}.$$

Results are given in Table 7 which follows.

ϕ_1	ϕ_3	δx_3	δs_3	$r_3 \delta\phi_o$	Excess Loss (db)	Horizontal Range (x)
9^o	$3^o49'$	-991.55	71.06	150.1	-3.25	30478
10^o	$5^o49'$	-682.00	73.37	136.6	-2.74	27498
14^o	$11^o25'$	-352.23	69.15	106.1	-1.90	20659
20^o	$18^o19'$	-201.32	60.41	80.4	-1.04	15057

Table 7

Divergence Loss Surface-to-Surface via Bottom

We may refer to "surface-to-surface via the bottom" as "round trip" which it really is as far as the vertical is concerned. The relation $x_o^{up} = 2x_3$ holds. Likewise, $\delta x_o^{up} = 2\delta x_3$. The angles at the surface are $\phi_o^{up} = -\phi_o$. δs_o^{up} will not be $2\delta s_3$ because the δx_o^{up} gets multiplied by $\sin \phi_o^{up}$ rather than by $\sin \phi_3$, to give δs_o^{up}. The gain observed at the bottom will not necessarily be evidenced in the round trip.

For rectilinear propagation the range r_o^{up} is $2r_3$, that is, the corresponding rectilinear path experiences a bottom bounce.

In the following table ϕ_o^{up} and δx_o^{up} are derived from ϕ_o and δx_3 respectively.

ϕ_1	ϕ_o^{up}	$\sin \phi_o^{up}$	δx_o^{up}	δs_o^{up}	$r_o^{up} \delta\phi_o$	Excess Loss (db)	H-Range (x)
9^o	$-9^o19'$	-.16189	-1983.1	321.0	300.2	+.3	60956
10^o	$-10^o18'$	-.17880	-1364.0	243.9	273.2	-.5	54996
14^o	$-14^o12'$	-.24531	-704.5	172.8	212.2	-.9	41318
20^o	$-20^o9'$	-.34448	-402.6	138.7	160.8	-.6	30114

Table 8

Results are discussed in the body of the report.

Divergence Gain to Convergence Zone

We note that $\delta\phi$ changes sign in going through a vertex and returning to a depth reached by both the reference and neighboring rays. Neighboring ray steeper downward means $\delta\phi$ positive. Neighboring ray steeper upward means $\delta\phi$ negative. This causes the rays to converge and perhaps to cross. A negative δx_o^{up} means the rays have crossed.

ϕ_1	ϕ_o^{up}	sin ϕ_o^{up}	δx_o^{up}	δs_o^{up}	$r_o^{up}\delta\phi_o$	Excess Gain (db)	H-Range (x)
0^o	$-2^o27'$	-.04275	-898	38.39	23.1	-2.2	78730
1^o	$-2^o38'$	-.04594	-643	29.55	141.0	+6.75	75054
2^o	$-3^o10'$	-.05524	-379	20.93	246.0	+10.7	74204
4^o	$-4^o42'$	-.08194	-88.1	7.22	315.0	+16.3	72536
5^o	$-5^o34'$	-.09700	+20.1	1.95	331.0	+22.3	72484
6^o	$-6^o29'$	-.11291	+1141	12.92	241.0	+14.3	72554
8^o	$-8^o22'$	-.14551	+277	40.27	358.0	+9.3	73820

Table 9

Results are discussed in the body of the report.

APPENDIX B* Bessel Functions

GAMMA FUNCTIONS

The Γ function is defined for positive real ν by:

$$\Gamma(\nu) = \int_0^\infty e^{-t}\, t^{\nu-1} dt. \tag{1.87}$$

When ν is an integer n, successive integrations by parts reduce Eq. (1.87) to

$$\Gamma(n) = (n - 1)! \tag{1.88}$$

and as with the factorial we have a recursion formula

$$\Gamma(n + 1) = n\Gamma(n). \tag{1.89}$$

Equation (1.89) holds for any n, real or complex, and may be used to give either ascending or descending arguments (e.g. solving for $\Gamma(-1/3)$ from $\Gamma(2/3)$).

The Eq. (1.87) may be integrated for $\nu = 1/2$ by the substitution $t = u^2$, yielding

$$\Gamma(1/2) = \sqrt{\pi}. \tag{1.90}$$

Then successive applications of Eq. (1.89) yield $\Gamma(3/2)$, $\Gamma(5/2)$, ... , as well as $\Gamma(-1/2)$, $\Gamma(-3/2)$, ...

We record also:

$$\Gamma(2/3) = 1.35412$$
$$\Gamma(1/3) = 2.67893. \tag{1.91}$$

* Extracted from another report by the present author.

BESSEL FUNCTIONS

Bessel Functions of the First Kind

In problems involving cylindrical coordinates (e.g. sound propagation in stratisfied media), we encounter Bessel functions. Most useful functions are solutions to differential equations. The Bessel functions may be taken up as solutions of Bessel's equation.

Bessel's equation is

$$\frac{d^2Z}{dz^2} + \frac{1}{z}\frac{dZ}{dz} + \left(1 - \frac{\nu^2}{z^2}\right) Z = 0 \qquad (1.92)$$

and a solution is $Z = J_\nu(z)$. By writing Z as a power series, substituting in Eq. (1.92) and equating coefficients of the different powers of z in the equation independently to 0, we find certain relationships among the coefficients of the power series for Z that are satisfied by the following formula when ν equals a positive integer n.

$$J_n(z) = \sum_{m=0}^{\infty} \frac{(-1)^m (z/2)^{(n + 2m)}}{m!\ (n + m)!}. \qquad (1.93)$$

The value $J_n(z)$ is called a Bessel function of the first kind of order n and argument z. The values of $J_o(x)$ and $J_1(x)$ are plotted in Fig.1.13.

For negative integral orders it can be shown that

$$J_{-n}(z) = (-1)^n J_n(z). \qquad (1.94)$$

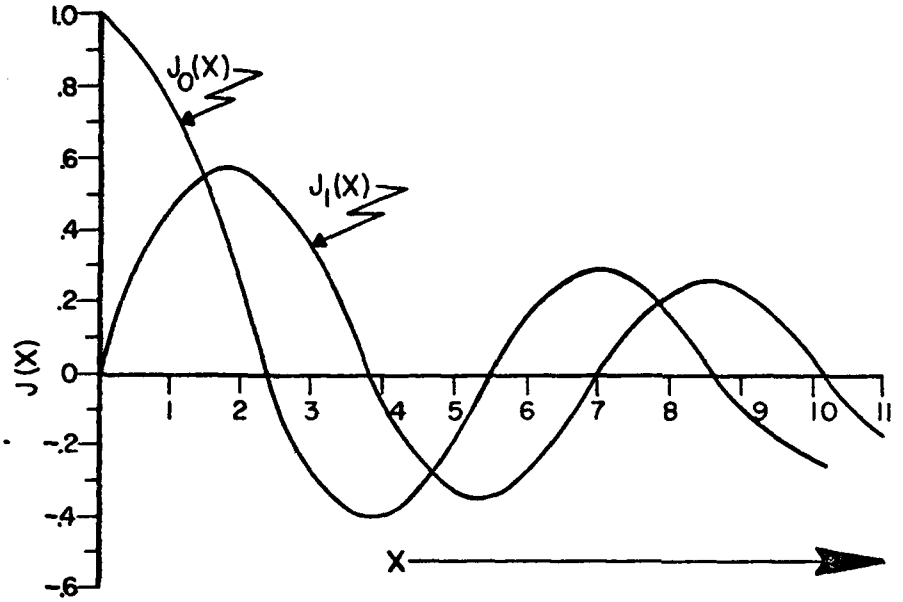

BESSEL FUNCTION OF FIRST KIND

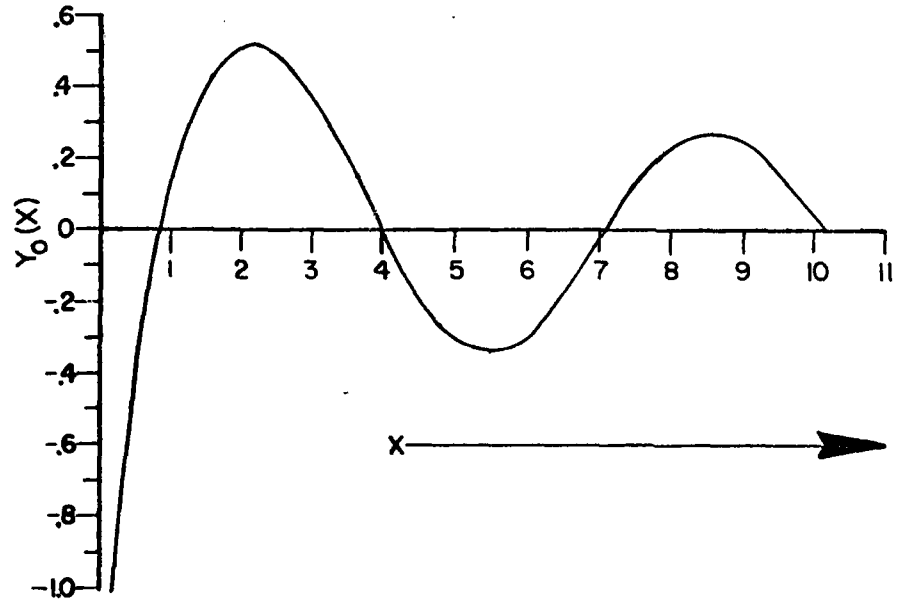

BESSEL FUNCTION OF SECOND KIND

FIGURE 1.13

Equation (1.93) may be expressed in terms of Γ functions as follows:

$$J_n(z) = \sum_{m=0}^{\infty} \frac{(-1)^m (z/2)^{(n + 2m)}}{\Gamma(m + 1)\Gamma(n + m + 1)}. \tag{1.95}$$

It develops that for any positive ν we may substitute this ν for n in Eq. (1.96) obtaining

$$J_\nu(z) = \sum_{m=0}^{\infty} \frac{(-1)^m (z/2)^{(\nu + 2m)}}{\Gamma(m + 1)\Gamma(\nu + m + 1)}. \tag{1.96}$$

Bessel Functions of the Second Kind

The solution $J_\nu(z)$ evolves from the straight forward procedure just indicated. The student may substitute the solution in the form given in Eq. (1.93) into Eq. (1.92) thereby verifying that Eq. (1.93) is a solution of Eq. (1.92). However, there must be a second independent solution of a second order differential equation. This will be given without derivation.

Because ν enters Eq. (1.92) as ν^2, substituting $-\nu$ for ν gives the identical equation. Therefore, $J_{-\nu}(z)$ is a solution of Eq. (1.92). When ν is an integer, $J_{-n}(z)$ and $J_n(z)$ are not independent as can be seen from Eq. (1.94). However, when ν is not an integer, it turns out that $J_{-\nu}(z)$ is linearly independent of $J_\nu(z)$, and a solution

$$Z = AJ_\nu(z) + BJ_{-\nu}(z) \tag{1.97}$$

constitutes a "fundamental system" of solutions.

It should also be apparent that the combination of $J_\nu(z)$ and a function of $Y_\nu(z)$ which is a linear combination of $J_\nu(z)$ and $J_{-\nu}(z)$ constitutes a fundamental system of solutions since

$$\begin{aligned} aJ_\nu(z) + bY_\nu(z) &= aJ_\nu(z) + b\left[cJ_\nu(z) + dJ_{-\nu}(z)\right] \\ &= (a + bc)\, J_\nu(z) + bdJ_{-\nu}(z) \\ &= AJ_\nu(z) + BJ_{-\nu}(z) \end{aligned}$$

A precise relationship between $Y_\nu(z)$ and the J's is commonly used, namely

$$Y_\nu(z) = \frac{J_\nu(z)\cos \nu\pi - J_{-\nu}(z)}{\sin \nu\pi} \qquad (1.98)$$

The Eq. (1.98) *defines a Bessel function of the second kind* and is called a Weber function. (Ref. 3)

When ν is an integer n, $Y_n(z)$ is indeterminate from Eq. (1.98). However, it may be defined as the limit of the right side of Eq. (1.98) as ν converges to n. It has been evaluated and is linearly independent of $J_n(z)$; therefore, we have the equation

$$Z = AJ_\nu(z) + BY_\nu(z) \qquad (1.99)$$

which holds for all real ν. $Y_0(X)$ is plotted in Fig. 1.13. $Y_0(0) = -\infty$.

By using kz in place of z in Eq. (1.92) and taking the special case of $\nu = 0$, we obtain

$$\frac{d^2Z}{dz^2} + \frac{1}{z}\frac{dZ}{dz} + k^2Z = 0 \qquad (1.100)$$

a form which may develop in the process of solving the wave equation in cylindrical coordinates with k^2 introduced in the separation of variables. Since we have substituted kz for z, a solution is $J_o(kz)$. A fundamental system of solutions is

$$Z = AJ_o(kz) + BY_o(kz). \tag{1.101}$$

It sometimes develops that only certain values of k permit satisfying boundary conditions. These permitted values of k are called eigenvalues, and the Z obtained for any eigenvalue is an eigenfunction belonging to its eigenvalue, which in turn belongs to it. Boundary conditions may also require that either A or B be zero.

Bessel Functions of the Third Kind

There are two functions of the third kind, usually called Hankel functions, and designated H_ν^1 and H_ν^2. These functions are given by

$$H_\nu^1(z) = J_\nu(z) + iY_\nu(z) \tag{1.102}$$

and

$$H_\nu^2(z) = J_\nu(z) - iY_\nu(z). \tag{1.103}$$

Either Hankel function is a solution of Eq. (1.92), and the two together comprise a fundamental system of solutions. In some solutions to the wave equations we shall use this fundamental system of solutions. Specifically, we shall encounter a solution

$$Z = EH_o^1(z) + FH_o^2(z) \tag{1.104}$$

where E and F are constants. The function $H_o^{1}(z)$ will be interpreted as an incoming* wave and H_o^{2} as an outgoing* wave so that the two together may comprise standing waves and in addition traveling waves (when $E \neq F$).

Since J and Y are real, the Hankel functions are complex and conjugate to each other. The interpretation of a complex solution is an amplitude $|H_o^{1}|$ or $|H_o^{2}|$, and a phase lead $\tan^{-1}(\pm Y/J)$, the plus sign for H_o^{1}, and minus sign for H_o^{2}. The amplitude and phase are tabulated in Ref. 9.

We should note that this complex form is analogous to our use of $e^{\pm ikz}$ to stand for harmonic space functions. As a matter of fact, the limiting forms of J_o, Y_o, and H_o as the argument increases without limit are cosines, sines, and exponentials as follows:

$$\lim_{z\to\infty} J_o(z) = (2/\pi z)^{1/2} \cos\left(z - \frac{\pi}{4}\right), \tag{1.105}$$

$$\lim_{z\to\infty} Y_o(z) = (2/\pi z)^{1/2} \sin\left(z - \frac{\pi}{4}\right), \tag{1.106}$$

and

$$\lim_{z\to\infty} H_o^{1,2}(z) = (2/\pi z)^{1/2}\, e^{\pm i}\left(z - \frac{\pi}{4}\right). \tag{1.107}$$

The phase for each of these functions approaches $(z - \frac{\pi}{4})$ at large z. The major difference from the harmonic functions is the factor $z^{-1/2}$, which will be associated in our applications with divergence loss characteristic of cylindrical spreading.

---

* The respective roles of H_o^{1} and H_o^{2} are often reversed arbitrarily to match an arbitrary choice of the negative sign in $e^{+i\omega t}$ in the solutions of the wave equation which will follow. We shall use $e^{+i\omega t}$ and this convention determines the specified interpretations of H_o^{1} and H_o^{2}.

Modified Bessel Functions*

In physical problems we sometimes encounter negative and complex wave numbers. As an example, if we have the complex wave number

$$k = k_o + ik_1 \tag{1.108}$$

it follows that

$$e^{ikx} = e^{ik_o x}\, e^{-k_1 x}. \tag{1.109}$$

The last factor is an exponential damping factor. A factor $e^{-k_1 z}$ in the Hankel functions of zero order with large arguments would emerge from Eq. (1.107) if z were replaced by kz, k given by Eq. (1.108).

Imaginary wave numbers will often occur in problems of stratified media. These may appear in the arguments of a Bessel function in such a way as to render the argument imaginary. Bessel functions of the three kinds are all given special designations for imaginary arguments and are all called "modified" Bessel functions. We have the relationships

$$I_\nu(z) = J_\nu(iz) \tag{1.110}$$

$$K_\nu(z) = Y_\nu(iz) \tag{1.111}$$

$$L_\nu^{1,2}(z) = H_\nu^{1,2}(iz). \tag{1.112}$$

It should be noted that imaginary arguments lead to modified functions which are real. Furthermore, the variable z here is not necessarily depth.

* The meaning of this terminology should not be confused with the meaning of "Modified Hankel functions" to be introduced later on Page 62.

The modified Bessel functions which we shall need have some function of depth as argument.

Up to this point we have shown various forms of solutions to Bessel's equation and have stated that if z is replaced by kz, k^2 being introduced as a separation constant of undetermined value, it may develop that k can take on only certain permitted values (eigenvalues) and still permit satisfying boundary conditions. Even so, there is a solution (eigenfunction) for each eigenvalue, and a linear combination of eigenfunctions is a solution. Thus, Eq. (1.104) as an example might more generally take the form

$$Z = \sum_{i=1}^{\infty} E_i H_o^{1}(k_i z) + F_i H_o^{2}(k_i z). \tag{1.113}$$

If there are no restrictions on k, the summation is replaced by an integration over k.

Solutions of Equation for Depth Function

The following equation occurs in the study of sound propagation in stratified media

$$\frac{d^2\phi}{dz^2} + \left[k_o^{2}(1 + \beta z) - \alpha^2 \right]\phi = 0. \tag{1.114}$$

There are at least two approaches to its solution. The first approach which we shall describe reduces Eq. (1.114) to a Bessel's equation of order (1/3).

Eq. (1.114) is of the form

$$\frac{d^2\phi}{dz^2} + (Bz + C)\phi = 0. \tag{1.115}$$

We let

$$Bz + C = \left(\frac{3}{2}B\xi\right)^{2/3} \tag{1.116}$$

and

$$\phi(z) = (Bz + C)^{1/2}V(\xi) = \left(\frac{3}{2}B\xi\right)^{1/3}V(\xi). \tag{1.117}$$

Then

$$\xi = \frac{2}{3B}(Bz + C)^{3/2}, \tag{1.118}$$

and

$$\frac{d\xi}{dz} = (Bz + C)^{1/2} = \left(\frac{3}{2}B\xi\right)^{1/3}. \tag{1.119}$$

We then find

$$\frac{d\phi}{dz} = \frac{d}{d\xi}\left[\left(\frac{3}{2}B\xi\right)^{1/3}V(\xi)\right]\frac{d\xi}{dz}$$

and

$$\frac{d^2\phi}{dz^2} = \frac{d}{d\xi}\left\{\frac{d}{d\xi}\left[\left(\frac{3}{2}B\xi\right)^{1/3}V(\xi)\right]\frac{d\xi}{dz}\right\}\frac{d\xi}{dz}. \tag{1.120}$$

Substituting Eq. (1.116), Eq. (1.117, and Eq. (1.120) worked out, into Eq. (1.115), we obtain

$$\frac{d^2V}{d\xi^2} + \frac{1}{\xi}\frac{dV}{d\xi} + \left(1 - \frac{1}{9z^2}\right)V = 0 \tag{1.121}$$

which is the desired form.

Expressing V as Hankel functions we have *

$$V = AH^{1}_{\frac{1}{3}}(\xi) + BH^{2}_{\frac{1}{3}}(\xi). \tag{1.122}$$

Finally, the full expression for ϕ in terms of Hankel functions involving z is

$$\phi = A\gamma H^{1}_{\frac{1}{3}}\left(\frac{2\gamma^3}{3K_o^2\beta}\right) + B\gamma H^{2}_{\frac{1}{3}}\left(\frac{2\gamma^3}{3K_o\beta}\right) \tag{1.123}$$

in which

$$\gamma = \left[k_o^2(1 + \beta z) - \alpha^2\right]^{\frac{1}{2}}. \tag{1.124}$$

The second procedure is to make the substitution

$$\eta = \frac{K_o^2(1 + \beta z) - \alpha^2}{(K_o^2\beta)^{2/3}}. \tag{1.125}$$

Substitution of Eq. (1.125) in Eq. (1.114) yields the Stokes equation

$$\frac{d^2\phi}{d\eta^2} + \eta\phi = 0. \tag{1.126}$$

Solutions to this equation may be found readily by expressing ϕ in a power series of ascending powers, substituting in Eq. (1.126), collecting coefficients of like powers and equating the collected coefficients of each power to zero. The coefficients $a_{(3n)}$, n = 1, 2, 3, ..., are all expressible in terms of a_o. This gives one series solution of the following form

$$f(\eta) = a_o\left(1 - \frac{1}{3!}\eta^3 + \frac{1\cdot 4}{6!}\eta^6 - \frac{1\cdot 4\cdot 7}{9!}\eta^9 + \ldots\right). \tag{1.127}$$

* See reference 6

The coefficients a_{3n+1}, $n = 1,2,3,\ldots$, are all expressible in terms of a_1, giving a second solution

$$g(\eta) = a_1\left(\eta - \frac{2}{4!}\eta^4 + \frac{2\,5}{7!}\eta^7 - \frac{2\,5\,8}{10!}\eta^{10} + \ldots\right) \tag{1.128}$$

Note that in both $f(\eta)$ and $g(\eta)$ the signs alternate but with negative argument all signs are alike in either function. All other coefficients, a_2, a_5 are zero.

The Airy functions, which have been tabulated, are related to f and g as follows:

$$\mathrm{Ai}(-\eta) = \frac{3^{-\frac{2}{3}}}{\Gamma(\frac{2}{3})} f(\eta) - \frac{3^{-\frac{1}{3}}}{\Gamma(\frac{1}{3})} g(\eta) \tag{1.129}$$

$$\mathrm{Bi}(-\eta) = \sqrt{3}\left[\frac{3^{-\frac{2}{3}}}{\Gamma(\frac{2}{3})} f(\eta) + \frac{3^{-\frac{1}{3}}}{\Gamma(\frac{1}{3})} g(\eta)\right]. \tag{1.130}$$

The solution of Eq. (1.126) is expressible in terms of the Airy functions as

$$\phi = E\,\mathrm{Ai}(-\eta) + F\,\mathrm{Bi}(-\eta). \tag{1.131}$$

Finally, just as we combined Bessel functions of the first and second kind to form Hankel functions, so we may combine Airy functions to form <u>modified</u> Hankel functions

$$h_1 = 12^{1/6}\, e^{-i\pi/6}\left[\mathrm{Ai}(-\eta) - i\,\mathrm{Bi}(-\eta)\right], \tag{1.132}$$
$$h_2 = 12^{1/6}\, e^{+i\pi/6}\left[\mathrm{Ai}(-\eta) + i\,\mathrm{Bi}(-\eta)\right].$$

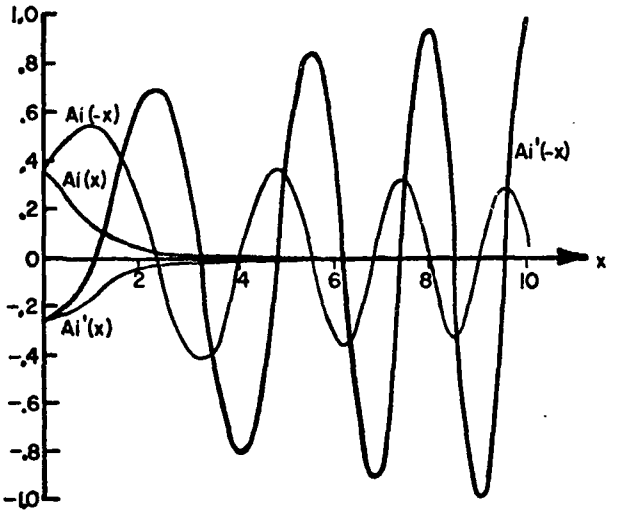

Ai(±x),Ai'(±x)

Airy Functions of First Kind and Derivatives

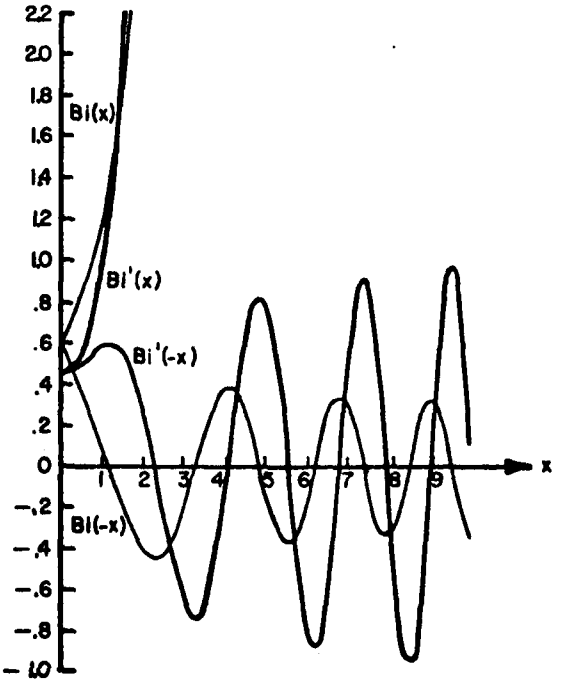

Bi(±x),Bi'(±x)

Airy Functions of Second Kind and Derivatives

Fig. 1.14 and 1.15

Note that when η is positive, the sign in the terms for Ai and Bi alternate giving rise to oscillating functions. When η is negative, which can occur for example when β is negative and z is large, $Ai(-\eta)$ is a monatonically decreasing function with increasing $-\eta$ and $Bi(-\eta)$ is a monatomically increasing function with increasing $-\eta$.

The modified Hankel functions are expressible in terms of z by substituting Eq. (1.125) for η. The expression for ϕ is then

$$\phi = C\, h_1(\eta) + D\, h_2(\eta). \tag{1.133}$$

In contrast to the solution in regular Hankel functions, Eq. (1.123), there are constants as coefficients of h_1 and h_2 as compared to $\gamma(z)$ in the coefficients of $H^1_{\frac{1}{3}}$ and $H^2_{\frac{1}{3}}$. This makes a neater solution.

The Airy functions and their derivatives are plotted in Fig.1.14 and Fig.1.15 taken from Ref. 4.

LAPLACIAN

The wave equation will be derived from physical principles in the treatment of sound propagation. In Cartesian coordinates, it is

$$\nabla^2 \Psi = \frac{1}{c^2} \frac{\partial^2 \Psi}{\partial t}. \tag{1.134}$$

The operator ∇^2 called the Laplacian needs to be defined. The definition will be in terms of Cartesian coordinates and we shall then show how to express it in any coordinate system.

The operator ∇ is defined in vector analysis as

$$\nabla = i \frac{\partial}{\partial x} + j \frac{\partial}{\partial y} + k \frac{\partial}{\partial z} \tag{1.135}$$

in which i, j, and k are unit vectors in the x, y, and z directions respectively. The dot product of ∇ by itself is

$$\nabla^2 = \frac{\partial^2}{\partial x^2} + \frac{\partial^2}{\partial y^2} + \frac{\partial^2}{\partial z^2}. \tag{1.136}$$

The Eq. (1.136) defines ∇^2 in Cartesian coordinates. When ∇^2 operates on a scalar quantity Ψ, we have the left member of the wave equation, Eq. (1.134). Use of Eq. (1.136) in Eq. (1.134) gives the wave equation in Cartesian coordinates.

An expression for ∇^2 in generalized coordinates, q_1, q_2, and q_3, is derivable (e.g. see Ref. 5) and takes the following form:

$$\nabla^2 = h_1 h_2 h_3 \left[\frac{\partial}{\partial q_1} \left(\frac{h_1}{h_2 h_3} \frac{\partial}{\partial q_1} \right) + \frac{\partial}{\partial q_2} \left(\frac{h_2}{h_3 h_1} \frac{\partial}{\partial q_2} \right) + \frac{\partial}{\partial q_3} \left(\frac{h_3}{h_1 h_2} \frac{\partial}{\partial q_3} \right) \right]. \tag{1.137}$$

The h's are given by

$$h_i = \frac{\partial q_i}{\partial n} \tag{1.138}$$

in which n is the normal in the positive direction to the level surface in q_i, i.e., the surface obtained with q_i constant.

In spherical coordinates we have a radial distance r from the origin, the colatitude θ, and the longitude ϕ measured from the positive x axis toward the positive y axis. The level surface in r is a sphere. The normal to this is radial in direction and $\frac{\partial r}{\partial n} = h_1 = 1$.

The level surface in θ is a cone, and the normal to this is a vector normal to the cone giving $\frac{\partial \theta}{\partial n} = h_2 = \frac{1}{r}$. A level surface in ϕ is a plane and

$\frac{\partial\phi}{\partial n} = h_3 = \frac{1}{r \sin\theta}$. Using these h's, Eq. (1.137) for the Laplacian becomes

$$\nabla^2 = \frac{1}{r^2 \sin\theta}\frac{\partial}{\partial r}(r^2 \sin\theta \frac{\partial}{\partial r}) + \frac{\partial}{\partial\theta}(\sin\theta \frac{\partial}{\partial\theta}) + \frac{\partial}{\partial\phi}(\frac{1}{\sin\theta}\frac{\partial}{\partial\phi}). \quad (1.139)$$

For a spherical wave in which spheres are equiphase surfaces of constant amplitude, this reduces to

$$\nabla^2 = \frac{1}{r^2}\frac{\partial}{\partial r} r^2 \frac{\partial}{\partial r} = \frac{\partial^2}{\partial r^2} + \frac{2}{r}\frac{\partial}{\partial r}. \quad (1.140)$$

A third system of coordinates with which we should have familiarity is that of cylindrical coordinates. Here the three coordinates are r, the radial distance from the polar axis; z, the distance from the origin along the polar axis; and θ, the longitude measured from the positive x axis. The level surface in r is a cylinder, the normal is radial and $\frac{\partial r}{\partial n} = h_1 = 1$. The level surface in z is a plane normal to the polar axis, the normal is along the polar (z) axis, and $\frac{\partial z}{\partial n} = h_2 = 1$. The level surface in θ is a plane including the polar axis, the normal is horizontal and tangent to a cylinder of radius r about the polar axis and $\frac{\partial\theta}{\partial n} = h_3 = \frac{1}{r}$.

Applying the general Eq. (1.138) with these h values, we obtain the Laplacian

$$\nabla^2 = \frac{1}{r}\left[\frac{\partial}{\partial r}(r \frac{\partial}{\partial r}) + r \frac{\partial^2}{\partial z^2} + \frac{1}{r}\frac{\partial^2}{\partial\theta^2}\right]$$

$$= \frac{1}{r}\frac{\partial}{\partial r} r \frac{\partial}{\partial r} + \frac{\partial^2}{\partial z^2} + \frac{1}{r^2}\frac{\partial^2}{\partial\theta^2}. \quad (1.141)$$

For cylindrical symmetry in which a sound wave is traveling inward or outward with equiphase surfaces which are infinite cylinders, this reduces to

$$\nabla^2 = \frac{1}{r}\frac{\partial}{\partial r}\, r\, \frac{\partial}{\partial r} = \frac{\partial}{\partial r^2} + \frac{1}{r}\frac{\partial}{\partial r}. \qquad (1.142)$$